

Advanced Studies of Polymer Electrolyte Fuel Cells 10th International Summer School

Shigenori Mitsushima, Takuto Araki, Ken-ichiro Ota, Viktor Hacker (eds.)

Advanced Studies of Polymer Electrolyte Fuel Cells

10th International Summer School

Yokohama, August 20th - 26th, 2017

Impressum

Organization

Shigenori Mitsushima
Takuto Araki
Green Material Innovation Center
Green Hydrogen Center
Division of Material Science and Engineering
Yokohama National University, 79-5 Tokiwadai, Hodogaya-ku; Yokohama
Tel. +81 (0)45-339-4020, Fax +81 (0)45-339-4024
Email: mitsushi@ynu.ac.jp

Viktor Hacker
Brigitte Hammer
Institute of Chemical Engineering and Environmental Technology, NAWI Graz
Graz University of Technology, Inffeldgasse 25c, 8010 Graz, Austria
Tel. +43 (0)316 873-8781, Fax +43 (0)316 873-108781
Email: viktor.hacker@tugraz.at

Editors Shigenori Mitsushima, Takuto Araki, Ken-ichiro Ota, Viktor Hacker

Publisher Verlag der Technischen Universität Graz
www.ub.tugraz.at/Verlag
ISBN (E-Book) 978-3-85125-548-5
DOI 10.3217/978-3-85125-548-5

Copyright © 2017 Verlag der Technischen Universität Graz

Preface

This interdisciplinary training programme for young scientists started as a co-operative project between Graz University of Technology and the Yokohama National University in the year 2008. The training programme grew quickly, both in the number of participants as well as in the number of participating international experts in the field of fuel cell research. This proceeding includes short abstracts along with key slides from the presentation of the lecturers of the 10th International Summer School.

The training programme covers research topics in the fields of basic electrochemistry, thermodynamics, kinetics and catalysis as well as the design and development of the complete fuel cell systems. The goals of the training are to provide the necessary theoretical background to young scientists and to make them more aware of the need to work closely with colleagues from different fields, such as natural sciences and engineering, in order to successfully develop and implement fuel cell technology.

The lectures cover following topics:

- Basic principle of fuel cells
- Basic electrochemistry
- Measurement and Characterisation Techniques
- PEFC Lifetime and Degradation
- PEFC Applications
- Hydrogen as Fuel
- Hydrogen Production and Heterogeneous Catalysis
- Advanced Material Studies

In 1839, Schönbein and Grove described the working principal of a fuel cell. Since then, it was often claimed during a number of fuel cell hypes that fuel cells will soon replace conventional power production technologies. So why don't we use fuel cells nowadays in our daily life? "Economic lifetime" might be the shortest answer. However, the last decade has shown that key industrial players have continued their long-term investment in this technology, even during times of economic stagnation, and research institutions and universities are covering all aspects from basic research to system development in a wide range as never seen before in history. So, this should be the basis to bring this interesting, high efficient and clean technology finally to the market.

Potential applications include portable equipment like laptop computers, tablets and smartphones, mobile applications like hybrid vehicles and stationary power plants ranging from 1 kW to the MW-class. The main advantageous features of fuel cells are the high energy conversion efficiencies, low emissions and hopefully with further development, their long lifespan.

Mobile applications get special priority in fuel cell research and development; however mobile applications are usually tied to a controversial issue: hydrogen as fuel. Within this training programme a discourse covering hydrogen production technologies, transportation

and storage of hydrogen will provide the basis for intensive discussions about advantages and disadvantages of this future fuel. Emphasis will be given to “renewable hydrogen”, i.e. hydrogen produced from renewable energy sources.

The organisers of the training programme would like to express their thanks to the province of Styria for their financial support and the Life Long Learning Team of Graz University of Technology for the organisational support of the training school. We would also like to thank Brigitte Hammer for her professional support in the organisation of the summer programme as well as all lecturers who contributed so much to this effort.

Yokohama, August 20th, 2017



Shigenori Mitsushima
Green Material Innovation Center
Green Hydrogen Research Center
Division of Materials Science and Engineering
Graduate School of Engineering
Yokohama National University



Takuro Araki
Department of Mechanical Engineering
Graduate School of Engineering
Yokohama National University



Ken-ichiro Ota
Green Material Innovation Center
Green Hydrogen Research Center
Division of Materials Science and Engineering
Graduate School of Engineering
Yokohama National University



Viktor Hacker
Institute of Chemical Engineering and
Environmental Technology, NAWI Graz
Graz University of Technology

Contents

1 PROGRAM	7
2 ABSTRACTS AND KEY SLIDES OF LECTURES	9
Basics of fuel cells.....	11
Environmental Impact Factor for Hydrogen Energy.....	19
PEFC Single cell test: setup preparation.....	28
Polymer electrolyte membranes for fuel cells: structure and transport properties	42
Step by step determination of the kinetic parameters on carbon supported nanocatalysts	50
Carbon support corrosion and membrane degradation	58
Synthesis methods of carbon supported nanocatalysts for fuel cell applications	69
Basic of the electrochemical measurements	77
Modeling of fuel cells.....	85
Electrochemical Impedance Spectroscopy and harmonic distortion Analysis	95
Heat and mass transport inside PEFC	118
Basic of thermodynamics for hydrogen production using traditional and membrane reactors..	127
Ultra Pure Hydrogen production using membrane reactor technology	134
Fundamentals of Electrode Processes.....	145
DAFC, DBFC, HTPEM and AFC	153
3 LECTURERS	164

1 Program

Sunday	Monday	Tuesday	Wednesday	Thursday
20.08.2017	21.08.2017	22.08.2017	23.08.2017	24.08.2017
	Fundamentals of electrode processes Prof. Bernhard Gollas	Ultra-pure H₂ production using Pd-based membrane reactors Prof. Angelo Basile	Step by step determination of the kinetic parameters of the ORR on carbon supported nanocatalysts (1) Prof. Boniface Kokoh	Modelling of fuel cell (1) Dr. Uwe Reimer
	Basics of the electrochemical measurements Dr. Teko Napporn	Clean hydrogen production by water electrolysis Dr. Teko Napporn	Step by step determination of the kinetic parameters of the ORR on carbon supported nanocatalysts (2) Prof. Boniface Kokoh	Modelling of fuel cell (2) Dr. Uwe Reimer
	Single cell PEFC testing: MEA preparation Prof. Gaetano Squadrito	EIS and harmonic distortion analysis Prof. Bernd Eichberger	Carbon support corrosion and membrane degradation Prof. Viktor Hacker	Heat and mass transport Prof. Takuto Araki
Welcome	Lunch Break	Lunch Break	Lunch Break	Lunch Break
Basics of fuel cells Prof. Viktor Hacker	Single cell PEFC testing: testing protocol Prof. Gaetano Squadrito	Technical tour Research park of Chiyoda co. Water electrolysis plant (AsahiKASEI) Spera hydrogen plant (Chiyoda)	Workshop (Open session) Lecture of cutting edge Chemical design of nanomaterials for energy and environmental applications Prof. Yoshiyuki Kuroda Yokohama National University HPEM development in South Africa Dr. Cordellia Sita University of the Western Cape	Practical training Prof. Viktor Hacker Prof. Shigenori Mitsushima
Environmental impact factor for hydrogen energy Prof. Ken-Ichiro Ota	Thermodynamics for hydrogen production Prof. Angelo Basile		Experiment	
	Hydrogen storage and transportation Prof. Shigenori Mitsushima		Student poster session Sushi party	Closing Ceremony Group Photograph

2 Abstracts and key slides of lectures

BASICS OF FUEL CELLS

Viktor Hacker

Graz University of Technology, Inffeldgasse 25 C, A-8010 Graz, Austria
viktor.hacker@tugraz.at

Keywords: Fuel Cells, PEFC, thermodynamics, durability, rapid ageing

INTRODUCTION

Electricity is without doubt the most convenient and versatile carrier of energy in our world. Traditionally, electricity is produced in large centralised power plants from fossil fuels. However, nowadays there is an emerging interest of producing electricity in a smaller decentralised way, due to its higher overall efficiency and due to its better compatibility with the usage of renewable resources. These changes in the energy supply chain also require new technologies for storing energy into fuels, for instance in hydrogen through the electrolysis of water. Furthermore, these changes also involve the development of efficient ways to re-convert the fuels into electrical energy.

Fuel cell technology provides all necessary properties for a decentralisation of electricity generation. Fuel cells can be thought of as solid state generators of electricity and heat by combining electrochemically a gaseous fuel and an oxidant gas through electrodes and across an ion conducting electrolyte.

In contrast to batteries, a fuel cell does not require any recharging. As long as a fuel cell is continuously supplied with reactants, it will produce electric energy. In comparison to any conventional thermo-mechanical system, such as internal combustion engines, fuel cells are characterised by their ability to convert the chemically stored energy of a fuel directly into electricity and heat, resulting in much higher conversion efficiencies than any current electricity generators can yield. In other words, fuel cells produce more electricity from the same amount of fuel than any combustion technology. As the conversion of the fuel to electrical energy can be performed also in a very clean way, the fuel cell may represent one fundamental progress towards a sustainable society.

THE POLYMER ELECTROLYTE FUEL CELL - PEFC

Among the most common types of fuel cells, as given in Table 1, the PEFC is especially of interest because it uses a polymeric membrane instead of a liquid electrolyte, which enables compacter systems resulting in a high power density and easy handling. In Figure 1 a schematic drawing illustrates the basic principles of a polymer electrolyte membrane fuel cell (PEFC).

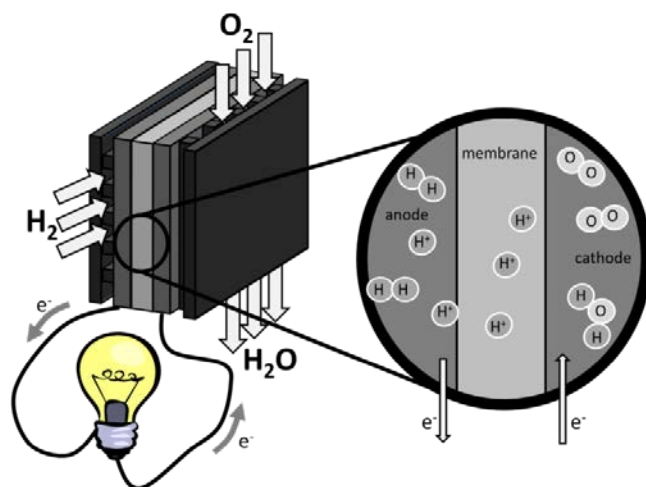


Fig. 1: Principle of a PEFC.

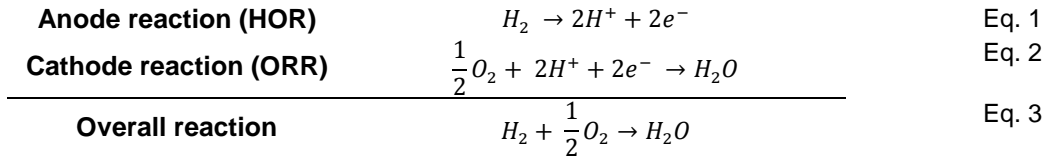
Table 1: Summary of fuel cell types [3].

Fuel cell types	Operating temperature / °C	Applications
Alkaline (AFC)	70-130	Space, military
Proton exchange membrane (PEFC)	60-110	Mobile, portable
Direct methanol (DMFC)	60-120	Portable
High temperature PEMFC	160-200	Small-scale power and CHP
Phosphoric acid (PAFC)	175-210	Medium- to large-scale power and CHP
Molten carbonate (MCFC)	550-650	Large-scale power generation
Solid oxide (SOFC)	500-1000	Medium- to large-scale power and CHP, auxiliary power units, off-grid power and μ -CHP

The most interesting part of a PEM fuel cell is the so-called membrane electrode assembly (MEA). The MEA resembles the heart or the central part of a PEM fuel cell and consists of two electrodes, i.e. anode and cathode, and the electrolyte. The electrolyte is as mentioned above a quasi-solid polymeric film. The required properties of this polymer electrolyte vary with the working condition of the fuel cell and the particular application [29]. Nevertheless, these polymer electrolytes should offer high proton conductivity and high chemical, mechanical and thermal stability in order to sustain a high lifetime of the PEFC. Most commonly perfluorinated polymers (similar to polytetrafluoroethylene, PTFE) containing $-\text{SO}_3\text{H}$ groups (perfluorosulphonic acid, PFSA) are employed. The PTFE-like backbone provides the membrane with chemical inertness, high mechanical and good thermal stability, whereas the $-\text{SO}_3\text{H}$ groups are superacid and protogenic in hydrated state, and provide the necessary proton conductivity. To maintain a high proton conductivity, these PFSA membranes must be hydrated at all times during operation. Usually this is achieved by leading the fuel and oxidant gases through water before introducing them into the fuel cell.

The two electrodes (anode and cathode) which are located on either side of the membrane usually consist of three layers, a carbon gas diffusion paper/cloth (Figure 15a), a highly porous gas diffusion layer and the active or catalyst layer. The gas diffusion layer is generally made out of high surface area carbon (HSAC), in order to provide a fine structured porous network in which the reactant gases can be transported to the active layer, and PTFE, which renders the gas diffusion layer hydrophobic, thus disabling a wetting and blocking of the pores with water. The active layer usually contains an active catalyst supported on HSAC, which enables the oxidation of hydrogen at the anode (HOR, hydrogen oxidation reaction) and the reduction of oxygen at the cathode (ORR, oxygen reduction reaction).

Hydrogen (H_2) is introduced into the PEM fuel cell from the anode side, where it is converted into protons (H^+) and electrons (e^-) through the HOR. The electrons are transferred through the electrical conductive gas diffusion layer and are collected at an external circuit, providing electrical energy. The protons are transported through the polymer electrolyte membrane to the cathode. Once protons reach the cathode side, they react with oxygen (O_2) and electrons producing water (H_2O) via the ORR. The reactions which occur at the anode and the cathode are summarised below.



Considering both reactions, HOR and ORR, the thermodynamical theoretical cell voltage of a H₂/O₂ fuel cell can be described by a combination of the two Nernst equations for the anode and cathode and would be 1.229 V at standard conditions [34,35].

$$V_{theory} = E_{O_2/H_2O}^0 - E_{H_2/H^+}^0 + \frac{2.303 RT}{zF} \cdot \log \left(\frac{p_{O_2}^{\frac{1}{2}} p_{H_2}}{p_{H_2O}} \right) \quad \text{Eq. 4}$$

with the two standard electrode potentials at 1.0 atm and 25 °C

$$E_{H_2/H^+}^0 = 0.000 \text{ V} \quad \text{Eq. 5}$$

$$E_{O_2/H_2O}^0 = 1.229 \text{ V} \quad \text{Eq. 6}$$

Where R is the universal gas constant (8.314 J K⁻¹mol⁻¹), F the Faraday constant (96,485 C mol⁻¹), T the temperature and p the corresponding partial pressures of the reactant gases and the product water.

However, the real cell voltage, i.e. the performance of a fuel cell is affected by several significant voltage losses, which lower the power output dramatically (see **Fehler! Verweisquelle konnte nicht gefunden werden.**). For instance, the partial pressure of oxygen is reduced when air is supplied to the cathode.

$$V_{cell} = E_{rev} - \Delta E_{ohmic} - \eta_{ORR} - \eta_{mt} \quad \text{Eq. 7}$$

The reversible cell voltage E_{rev} describes the reduced theoretical OCV by considering the real partial pressures of the reactant gases and the operating temperature of the fuel cell. The ohmic losses E_{ohmic} result from the contact resistances between flow-fields and the gas diffusion layers as well as from proton conduction through the electrolyte membrane. The slow transport of oxygen (usually hydrogen transportation is negligible) causes mass-transport losses η_{mt} . But the most significant loss is due to overpotential losses η_{ORR} of the slow reaction kinetics of the oxygen reduction reaction.

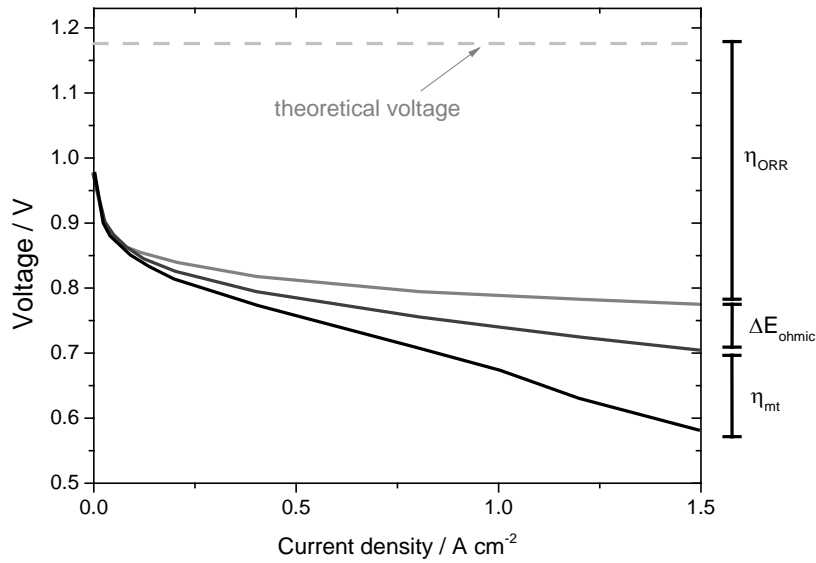


Figure 2: Influence of different loss mechanisms on the VI-characteristic of a PEM fuel cell. Figure adapted from [10].

The electrical efficiency of a PEFC can be given as the ratio of electrical energy output to energy input. However, there is no general definition of efficiency since the energy value of hydrogen varies in dependence of the aggregation state of the product water. When the product water is obtained in liquid form, the so-called higher heating value ($\Delta H_{HHV}^0 = -285.6 \text{ kJ mol}^{-1}$) defines the overall reaction enthalpy (heat energy), while the so-called lower heating value ($\Delta H_{LHV}^0 = -241.2 \text{ kJ mol}^{-1}$) is obtained when product water is in gaseous state [34].

Since there are also irreversible losses in form of heat ($T\Delta S$) the maximum electrical work that the fuel cell can generate (Gibbs free energy) is reduced to $\Delta G^0 = -237.4 \text{ kJ mol}^{-1}$, using Fehler! Verweisquelle konnte nicht gefunden werden..

$$\Delta G^0 = \Delta H^0 - T\Delta S \quad \text{Eq. 8}$$

Table 2: The theoretical cell voltage depending on the total reaction enthalpy.

	kJ mol^{-1}	E_{th} / V
ΔH_{HHV}	-285.6	1.48 ($E_{th,l}$)
ΔH_{LHV}	-241.2	1.25 ($E_{th,g}$)
$\Delta G = \Delta H - T\Delta S$	-237.4	1.23 (E_{rev})

The theoretical electrical energy efficiency (η_{id}) of a fuel cell can be defined as

$$\eta_{id} = \frac{\Delta G}{\Delta H_{HHV}} = \frac{E_{rev}}{E_{th,l}} = 0.83 \quad \text{Eq. 9}$$

which results in a value of 83% in the case of HHV and liquid product water.

The electric efficiency of an operated fuel cell can be given by

$$\eta_{el} = \frac{E}{E_{rev}} \quad \text{Eq. 10}$$

and varies for a PEMFC in a range of 35 – 70%.

REFERENCES

- [1] A. Schenk, *“The oxygen reduction reaction in high temperature proton exchange membrane fuel cells: Long term behaviour of platinum-cobalt catalysts under ex-situ and in-situ conditions”*, Dissertation, Nov. 2014, Graz University of Technology
- [2] A. Schenk, C. Grimmer, M. Perchthaler, S. Weinberger, B. Pichler, C. Heinzl, C. Scheu, F.-A. Mautner, B. Bitschnau, V. Hacker, *J. Power Sources* 266 (2014) 313.
- [3] P.P. Edwards, V.L. Kuznetsov, W.I.F. David, N.P. Brandon, *Energy Policy* 36 (2008) 4356.
- [4] J. Garche, *“Encyclopedia of Electrochemical Power Sources”*, Elsevier, Amsterdam, 2009.
- [5] A. Rabis, P. Rodriguez, T.J. Schmidt, *ACS Catal.* 2 (2012) 864.
- [6] A.B. Stambouli, *Renew. Sustain. Energy Rev.* 15 (2011) 4507.
- [7] P. Malacrida, *“Alloys of Pt and Rare Earths for the Oxygen Electroreduction Reaction”*, PhD thesis, 2014, Technical University of Denmark
- [8] J. Zhang, H. Zhang, J. Wu, J. Zhang, *“Pem Fuel Cell Test. Diagnosis”*, Elsevier B.V., Amsterdam, 2013, pp. 1–42.
- [9] C.H. Hamann, W. Vielstich, *“Elektrochemie”*, Wiley-VCH, Weinheim, 2005.
- [10] H.A. Gasteiger, S.S. Kocha, B. Sompalli, F.T. Wagner, *Appl. Catal. B Environ.* 56 (2005) 9.

Historical Overview



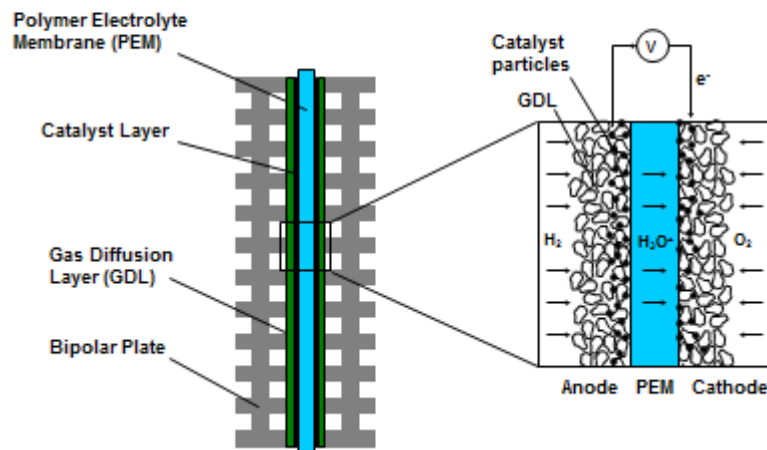
Sir W. Grove



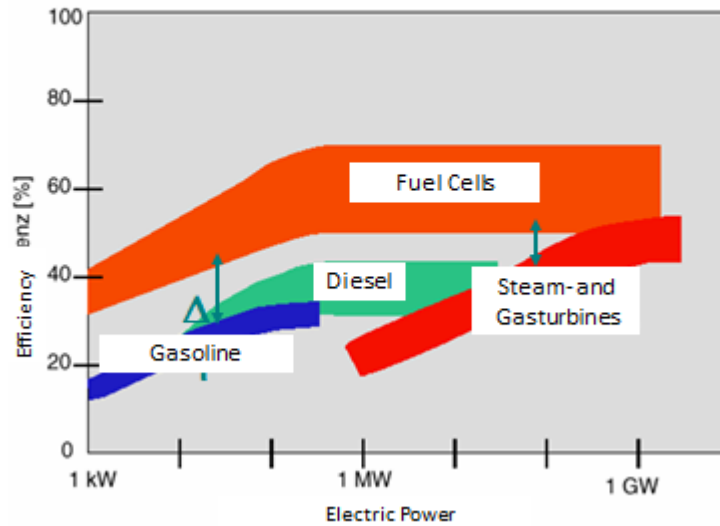
Pre-batch production

- 1838/39 Discovery of the fuel cell effect
1838 C.F. Schönbein "On the Voltaic Polarization of Certain Solid and Fluid Substances".
1839 Sir W. Grove "On the Voltaic Series and the Combination of Gasses by Platinum".
- 1843 Construction of a "gas battery" by Grove.
- 1889 Work by L. Mond and C. Langer led to the first alkaline fuel cell. They also discovered the high polarization losses at the oxygen electrode.
- 1896 W.W. Jaques used molten sodium hydroxide as an electrolyte in order to directly convert coal into electricity.
- 1900 W. Nernst carried out conceptual work on solid electrolyte fuel cells (SOFC).
- 1905 F. Haber carried out systematic thermodynamic investigations regarding hydrogen consuming fuel cells.
- 1932 F.T. Bacon started a long term fuel cell development program.
- 1935 W. Schottky developed the theoretical fundamentals of the SOFC.
- 1938 E. Baur and H. Preis first reported on experimental SOFC work.
- 1959 F.T. Bacon constructed the first working 5 kW alkaline fuel cell stack.
- 1964 Diaphragm gas cell supplied in Gemini spacecraft.
- 1967 Concept of the phosphorus-sour gas cell by UTC.
- 60/80ies alkaline fuel cells are used for Apollo and space shuttle missions.
- 1984 "Rediscovery" of the Polymer.

PEFC Principle



Efficiencies in the real world!



Polarisation curve (V/I curve)

- Low current density (see Butler-Volmer Equation)

$$j = j_c \left\{ \exp\left(\frac{\alpha \cdot z \cdot F \cdot \eta_a}{R \cdot T}\right) - \exp\left(-\frac{(1-\alpha) \cdot z \cdot F \cdot \eta_c}{R \cdot T}\right) \right\}$$

Charge transfer overpotential
charge transfer through double layer is limited, highly non-linear loss of voltage

Reaction overpotential
kinetic limitation of a reaction step

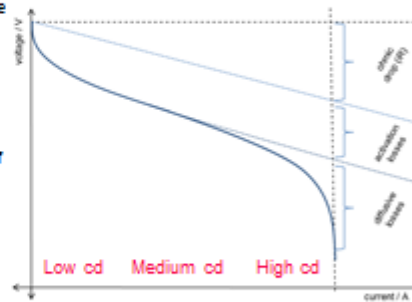
- Medium current density (see Ohm's law)

$$\eta_{Ohm} = j \cdot r_i$$

Ohmic region
Linear loss due to internal resistance of the cell (good conductivity of all parts minimize these losses)

- High current density (see Fick's law)

Diffusion limiting region
The limiting factor in this region is the diffusion (gas transport) of reactants, non-linear loss



Polarisation curve (V/I curve)

Power $P_D = E \cdot j$
 $P = E \cdot i$

P power [W]
 P_D power density [W cm⁻²]
 E voltage [V]
 i current [A]

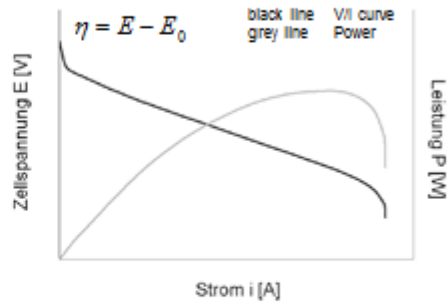
Work $W = z \cdot F \cdot E$
 $W_{max} = z \cdot F \cdot E_0$

W work [J mol⁻¹]
 W_{max} Maximum Work [J mol⁻¹]
 z number of exchanged electrons
 F Faraday constant

Efficiency (under load)

$$\xi_L = \frac{W}{W_{max}} = \frac{E}{E_{M0}} = \frac{E_0 - \eta}{E_{M0}}$$

E_{M0} thermoneutral cell voltage [V]
 η Overpotential [V]

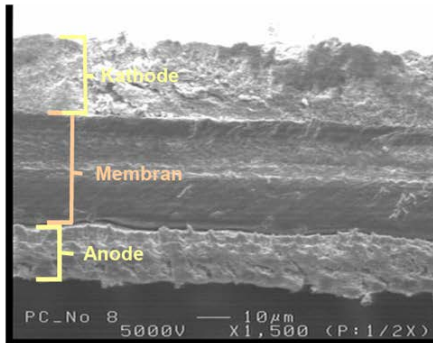


@ theoretic efficiency:

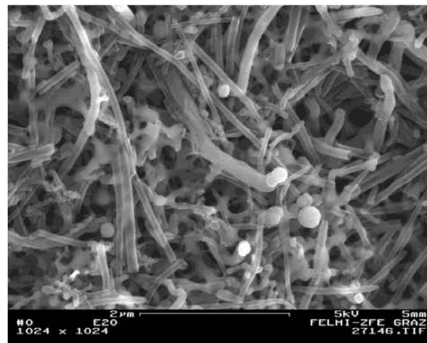
With: $\Delta H_0 = -z \cdot F \cdot E_{H0}$ $\Delta G_0 = \Delta H_0 - T \cdot \Delta S_0$
 $\Delta G_0 = -z \cdot F \cdot E_{00}$ *all activities = 1*

$$\xi_{th} = \frac{\Delta G}{\Delta H} = 1 - \frac{T \cdot \Delta S}{\Delta H} = \frac{E_{00}}{E_{M0}}$$

Electrodes



Membrane-Electrode-Assembly (MEA)



Gas diffusion layer - GDL (carbon nanotubes)

ENVIRONMENTAL IMPACT FACTOR FOR HYDROGEN ENERGY

Ken-ichiro Ota

Green Hydrogen Research Center
Yokohama National University
79-5 Tokiwadai, Hodogaya-ku, Yokohama 240-8501 Japan
ken-ota@ynu.ac.jp

Keywords: hydrogen energy, impact factor, water circulation

INTRODUCTION

A viewpoint of entropy is very important when energy and environment are discussed, because all activities on the Earth including the human beings cause entropy production according to the second law of thermodynamics with the conservation law of materials and energy. Entropy governs a direction of all changes, so that the entropy production should be considered in order to sustain the activity of human society. Several studies in consideration of entropy were performed when a desirable energy system of the civilization was planned [1,2].

IDEAL ENERGY SYSTEM CONSISTED ON MATERIALS CIRCULATION

A human society is one of the typical self-organizing systems. Therefore, in order to sustain the steady state of human society included its energy system, materials should be permanently circulated, and the produced entropy should always be disposed of as a long-wave thermal radiation to space.

Here, it is assumed that the primary energy of the ideal energy system can be supplied with the renewable energy. Therefore, the problem is that what kind of material is selected as a secondary energy. From the viewpoint of entropy, the ideal energy supply system must be based on the materials circulation. When hydrogen is chosen

as a secondary energy, the circulation of water, which is oxidative state of hydrogen, is used. On the other hand, when hydrocarbon is chosen as secondary energy, the circulations of carbon as well as water are utilized. Then, a water cycle is compared with a carbon cycle as a material circulation which mankind can utilize for the energy system.

Table 1 shows the comparison of carbon and water on the Earth [4, 5, 6]. The total abundance of water is much greater than that of carbon. 27,000 times are different in the weight ratio. The water abundance in the atmosphere is also more plentiful than the carbon

Table 1: Comparison of the cycle quantity of carbon and water.

	Carbon	Water
Total amount	54Tt Carbon	1,460,000 Tt Water
Atmosphere abundance	750 Gt Carbon	15.5 Tt Water
Annual Movement form atmosphere	152 Gt Carbon	496 Tt Water
Average retention period in atmosphere	5 year	10 day
Ratio of energy consumption of mankind to atmosphere abundance	0.7 %	0.3 %
Environmental impact factor	0.036	0.0001

abundance in the weight ratio about 21 times. Circulation with much abundance in the nature is difficult to be affected by human activity. The annual movement from the atmosphere of water is 3160 times larger than that of carbon, so that a large difference occurs in the mean residence time in the atmosphere. In comparison with the carbon cycle, the water cycle is difficult to receive the effect of the mankind activity. Here, the effect of the energy consumption of mankind on the carbon and the water cycles are concretely compared. For that purpose a new parameter named "Environmental Impact Factor" was introduced. The environmental impact factor (EIF) was defined as the ratio of annual quantity of materials produced by energy consumption of mankind to a natural movement on earth. The influence of human activities on the global environment could be evaluated quantitatively by this environmental impact factor.

On the other hand, the combustion heat of hydrogen is 143kJ/g to calculate the effect on the water cycle. Because the annual energy consumption of mankind is $6.0-8.2 \times 10^{17}$ kJ (2000), the production quantity of water due to this consumption is calculated to be 38-52 G ton. This water production is about 0.3% of vapor in atmosphere and the same order as carbon. However, it becomes very small value of 0.01% against the annual movement from atmosphere, that is, the environmental impact factor of water was 0.0001. The environmental impact factor of hydrogen is more than two orders of magnitude less than that of carbon.

EVALUATION OF LOCAL EFFECT USING ENVIRONMENTAL IMPACT FACTOR

Table 2 shows the comparison of the environmental impact factor of carbon on the earth, Japan and Tokyo [7]. The environmental impact factor of carbon in Japan was 24 times larger than that in earth. In particular, the environmental impact factor of carbon in Tokyo metropolitan area was estimated to be 35351 since the natural carbon release in Tokyo is much smaller than that in other areas as well as the density of energy consumption was one order of magnitude larger. This means that human activity affects strongly natural carbon flow in Tokyo area.

Table 2: Comparison of Environmental impact factor of carbon on the Earth, Japan and Tokyo Metropolitan area.

	Earth	Japan	Tokyo Metropolitan area
Natural carbon release	61.1 Gt/y	0.37 Gt/y	576.5 t/y
Carbon (CO ₂) Emission by Energy Consumption	5.5 Gt/y	0.32 Gt/y	0.02 Gt/y
Environmental impact factor (Carbon)	0.036	0.86	35351

Table 3 shows the comparison of the environmental impact factor of hydrogen on the earth, Japan and Tokyo (Fujii, 2004). The environmental impact factor of water in Japan was 60 times larger than that in the earth. The environmental impact factor of water in Tokyo was also estimated to be 0.118. This value might not be neglected. The climate in Tokyo would be affected even if the hydrogen-based energy system was introduced, although the effect might be far small compared to that of carbon. Too much energy is consumed in Tokyo. In comparison of Tables 2 and 3, the environmental impact factor of water was always smaller than that of carbon in all areas. That means hydrogen energy is friendly to the environment.

Table 3: Comparison of Environmental impact factor of hydrogen on the Earth, Japan and Tokyo wards.

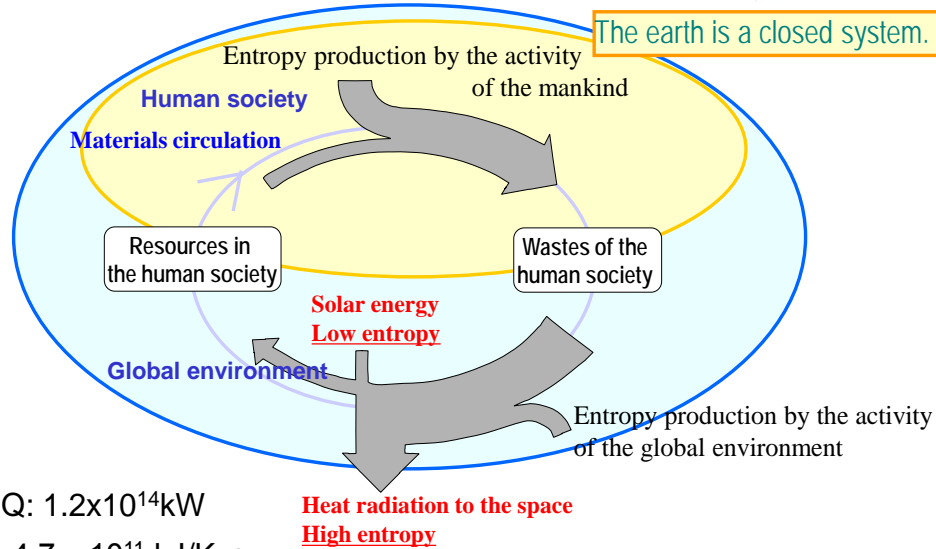
	Earth	Japan	Tokyo Metropolitan area
Annual Evaporation	4.96×10^{14} t/y	2.3×10^{11} t/y	2.5×10^8 t/y
H ₂ O through H ₂ Energy System	$3.8-5.2 \times 10^{10}$ t/y	1.4×10^9 t/y	2.9×10^7 t/y
Environmental impact factor (Hydrogen)	~0.0001	0.006	0.118

REFERENCES

- [1] Rosen MA, Scott DS. Entropy production and exergy destruction: Part I-hierarchy of Earth's major constituencies. *Int. J. Hydrogen Energy* 2003;28:1307-1313.
- [2] Rosen MA, Scott DS. Entropy production and exergy destruction: Part II- illustrative technologies *Int. J. Hydrogen Energy* 2003;28:1315-1323.
- [3] Ota K, Ishihara A, Mitsushima S, Kamiya N. Environmental impact factor for hydrogen energy, Abst 112, WHEC 2006.
- [4] Baumgartner, Reichel E., *The World Water Balance*, Elsevier Scientific Pub.co. 1975.
- [5] Berner EK, Berner RA. *Global water cycle, Geochemistry and Environment*, Prentice-Hall, Inc., Englewood Cliffs, New Jersey 1987.
- [6] Wigley TML. and Schimel DS. Ed., *The carbon cycle*. Cambridge University Press, 2000.
- [7] Fujii M. Doctoral thesis, Yokohama National University, 2004.

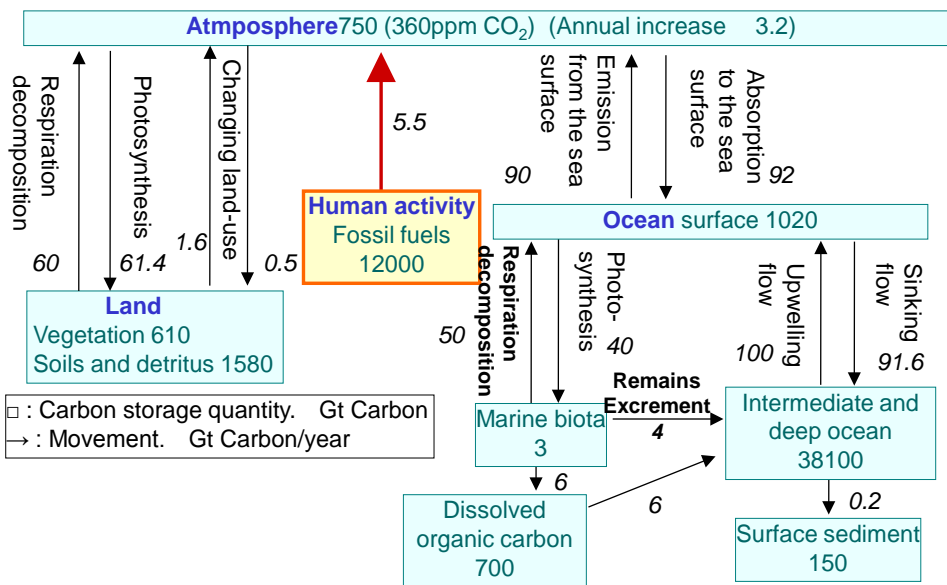
Global entropy flow for sustainable growth

Chemical Energy Laboratory, Y.N.U.



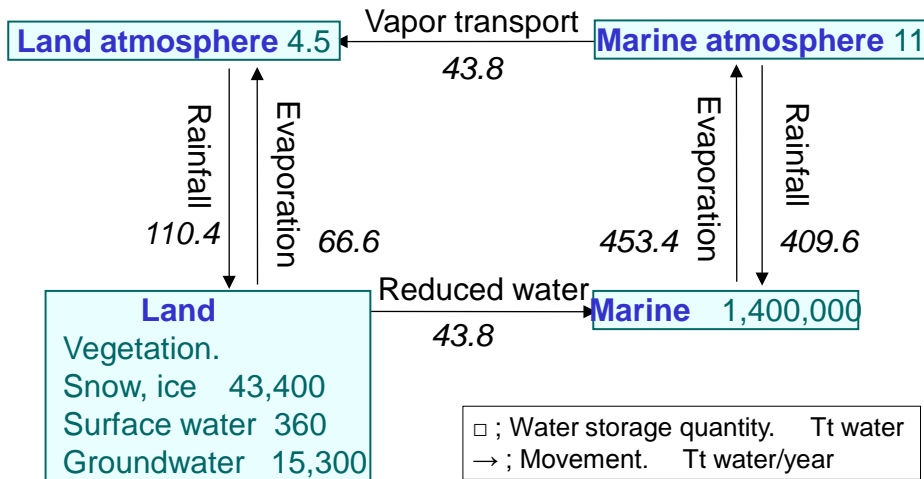
Carbon cycle on the earth

Chemical Energy Laboratory, Y.N.U.



Water cycle on the earth

Chemical Energy Laboratory, Y.N.U.



Comparison between water cycle and carbon cycle

Chemical Energy Laboratory, Y.N.U.



	carbon		water
Total amount	54Tt	27000 Times	1,460,000Tt
Atmosphere abundance	750Gt	21Times	15.5Tt
Annual movement from atmosphere	152Gt/yr	3160 Times	496Tt/yr
Average retention period in atmosphere	5 yaer	180 Times	10 day

Environmental Impact Factor of Carbon

Chemical Energy Laboratory, Y.N.U.



EIF (Environmental Impact Factor) of Carbon

Carbon (CO₂) Emission by Energy Consumption
/ Natural Carbon Circulation

	Earth	Japan
Natural Carbon Cycle	150Gt/y	0.37Gt/y
Carbon (CO ₂) Emission by Energy Consumption	5.5Gt/y	0.32Gt/y
EIF of Carbon	0.036	0.86

D.S.Shimel; Terrestrial ecosystems and the carbon cycle, global change biology(1995)

EIF of H₂ Energy

Chemical Energy Laboratory, Y.N.U.



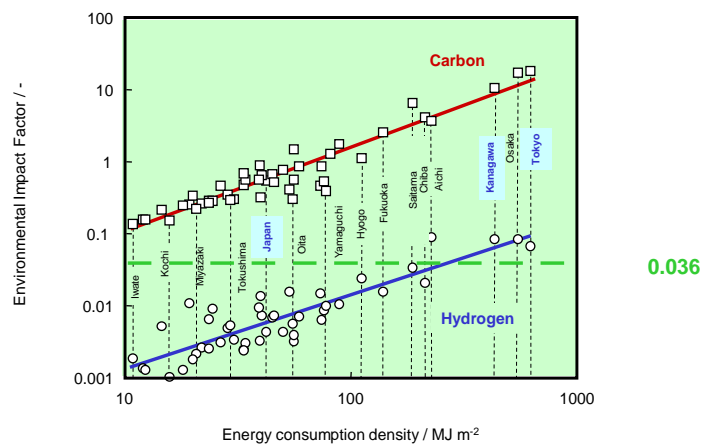
EIF (Environmental Impact Factor) of Hydrogen

= (H₂O through H₂ Energy System) / (Natural Water Vaporization)

	Earth	Japan
Annual Vaporization	4.96×10 ¹⁴ t/y	2.3×10 ¹¹ t/y
H ₂ O through H ₂ Energy System	3.8~5.2×10 ¹⁰ t/y	1.4×10 ⁹ t/y
EIF of H ₂	~0.0001	0.006

Local EIFs of Prefectures in Japan

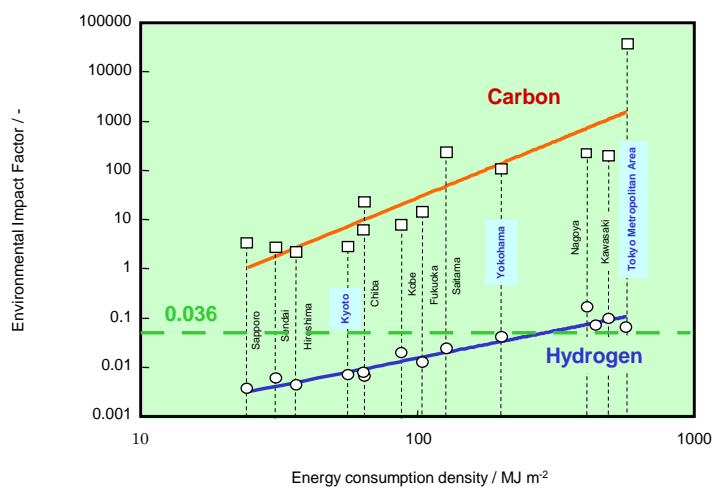
Chemical Energy Laboratory, Y.N.U.



Local Environmental Impact Factor (EIF) vs. Energy Consumption of Prefectures in Japan.

Local EIFs of Cities in Japan

Chemical Energy Laboratory, Y.N.U.



Local Environmental Impact factor (EIF) of Cities in Japan

Comparison of EIF of Carbon and Hydrogen

Chemical Energy Laboratory, Y.N.U.



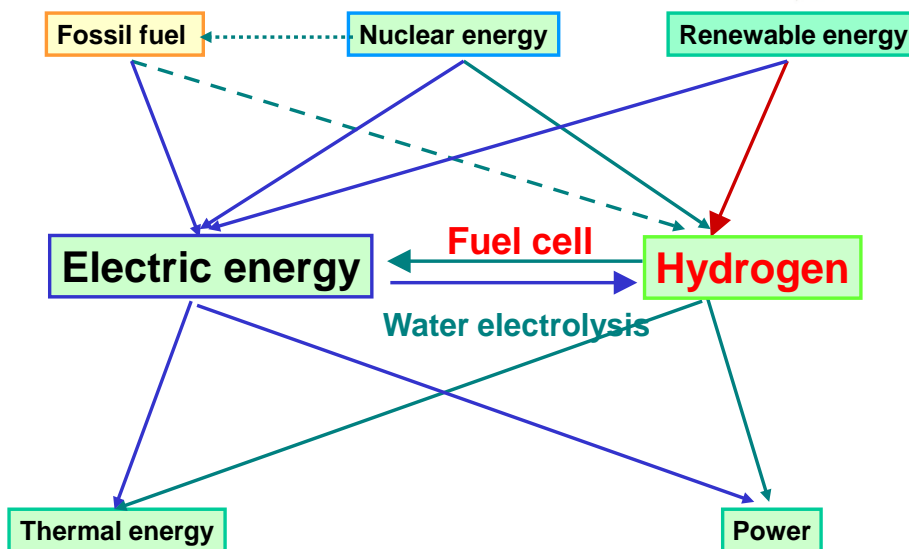
	EIF of Carbon		EIF of H ₂
Earth	0.036	1/360	~0.0001
Japan	0.88	1/150	0.006
Tokyo Metrop.	35000	1/300000	0.12

Hydrogen Energy is friendly to the environment.

Hydrogen Energy is more suitable to a huge energy consumption area.

Hydrogen energy system

Chemical Energy Laboratory, Y.N.U.



Hydrogen for Energy System

Chemical Energy Laboratory, Y.N.U.



By-product Hydrogen (Feasibility study)



Reformed Hydrogen from Natural gas or MeOH



Reformed Hydrogen from Oil or Coal



Hydrogen from Water using Renewable Energy
(Ultimate Clean Energy System)

“I believe that water will one day be employed as fuel, that hydrogen and oxygen which constitute it, used singly or together, will furnish an inexhaustible source of heat and light.”

Jules Verne “Mysterious Island”, 1874



PEFC SINGLE CELL TEST: SETUP PREPARATION

Gaetano Squadrito

CNR-ITAE, salita per S. Lucia sopra Contesse 5, 98126 Messina, Italy
e-mail: gaetano.squadrito@itae.cnr.it

Keywords: PEFC, single cell testing, experimental protocol, MEA, MEA preparation.

INTRODUCTION

For their characteristics, low temperature operation, solid electrolyte, compactness and lightness, scalability, Polymer Electrolyte Fuel Cells (PEFCs) could be considered the most “user friendly” within fuel cells technologies. Today, the PEFCs are in the early stage of commercialisation both for stationary and portable power and in the next few years large scale commercialisation will start [1-7]. The Cogeneration Heat and Power (CHP) systems for home application are a reality in Japan and will be available in Europe in the next years. Car manufacturers like Daimler, Toyota, Nissan and Hyundai announced the started regular commercialisation of their hydrogen fuelled FC cars in 2015-2017 [4-6]. But this don't means that the research on PEFC could be considered concluded, further efforts are required for a progressive cost reduction, the efficiency increase, the endurance implementation and the safety assurance.

Independently by the application, a further cost reduction is the main request, followed by an increase in durability. For this purpose further basic research efforts on materials and components, modelling, new applicative studies and tests are necessary for supplying industries with all the information for assuring to the customer good products with certified quality standards, and according to the market necessities [7].

Usually, new concepts, materials, components and design are firstly tested in laboratory before their application to large scale systems and the preparation of an appropriate testing set up will be one of the most important activities in our laboratory everyday practice.

In this chapter we will focus mainly on preparation of Membrane Electrode Assembly (MEA), the heart of the PEFC, for testing it. We will use hydrogen fuelled cells as reference, taking into account that PEFC could be fuelled with alcohols and other fuels also.

Laboratory scale MEA, and its components, preparation is different by the large scale production and strongly depends on the research group experience and available facilities. Consequently only the general approach and the main recommendation will be treated, the students must be able to apply these general indications according to the facilities availability in their laboratories.

SINGLE CELL TEST SETUP

According to the IEC-62282-1 Terminology the Membrane Electrodes Assembly is a component of a fuel cell, usually PEFC / DMFC, consisting of an electrolyte membrane with gas diffusion electrodes on either side.

The MEA structure is reported in Figure 1, but the MEA cannot work alone, hydrogen and oxygen (or air) must be supplied to anode and cathode, respectively, produced water must be removed, electric connections must be established and operative conditions maintained. For this purpose an appropriate MEA's test-holder is necessary, usually a single MEA per time is characterised and the test holder is

usually called “single cell”. Usually this single cell consist of two plates on each side of MEA: a plate, usually graphite made, having channels for gas distribution (flow field) hollowed on the face in contact with the gas diffusion layer of the MEA, and a metallic compression plate working also as current collector. Tie bolt with insulating washes to avoid short circuits are used for clamping the cell, and a couple of gaskets avoiding gas leakage from cell. Other configuration are also possible, but the basic concept is the same.

MEA PREPARATION

Membrane Electrode Assembly (MEA) is composed by different parts; depending on the material or component to be tested you will need to prepare a single part or all of them. Consequently the preparation procedure will depends on the component to be tested, and we must take into account that after experimentation and validation our product (know-how, new material or component, other) could be useful for community only if it can be applied in practice at a reasonable cost. We must remember that some production methods very useful in laboratory scale could be not applicable at industrial level, and some industrial approach can't be easily reproduced in laboratory scale. This situation could introduce some limits that must be taking into account. These aspects are out of the purpose of this chapter and will be not considered.

In figure 1 is reported a schematic of MEA section, starting from anode side (Up-down in figure) there is the Gas Diffusion Layer (GDL) that could be composed of two sub-layers, the catalyst layer where hydrogen is separated into protons and electrons, the electrolytic membrane allowing the transport of protons to cathode, the cathode catalyst layer where water formation occurs, and the cathode gas diffusion layer.

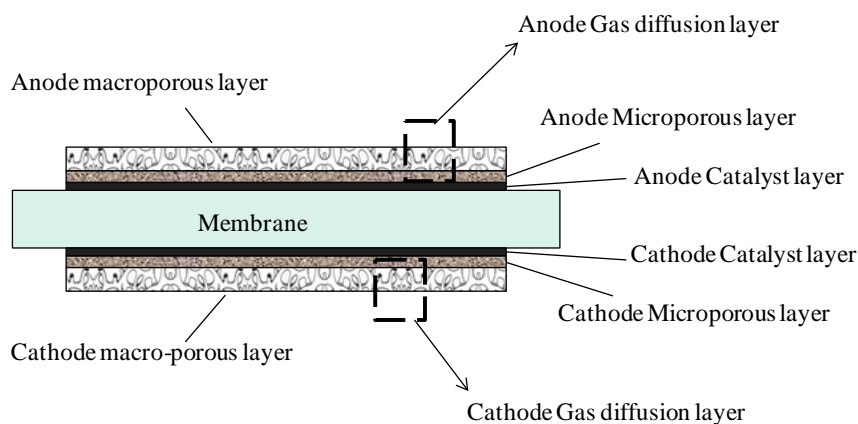


Figure 1: schematic of MEA structure. Membrane is in direct contact with the catalyst layer, membrane and catalyst layer are sandwiched by two gas diffusion layer. Each diffusion layer is usually composed of two layers with different porosity called micro-porous and macro-porous layer respectively.

The MEA manufacturing is a complex matter; we will limit our discussion to standard laboratory procedures giving an overview to possible drawback and to industrial production processes. For a more wide and detailed description, the reader is invited to read the references [7-10]. The membranes, catalyst, carbons and other materials for MEA preparation are considered as well characterised materials coming from a material

preparation laboratory of our institute/university or from any other third party provider. Then, starting from standard composition, we will consider the preparations of gas diffusion layer, catalyst layer and MEA assembling.

Membrane

The solid polymer electrolyte membrane is the inner part of the cell and its properties define large part of the cell operative limits and performances. The membrane we have to use will come from another lab of our institution, or will be acquired on the market, or will be delivered by a collaborating institution or company. The membrane preparation and properties have been treated in previous chapter 3, paragraph 3.1, for MEA preparation we have just to cut it with the correct shape and dimension and, if needed, to perform a pre-treatment according to the supplier instruction or to literature information. Will be our care asking the supplier all possible information about the characteristics of the membrane, like conductivity, water uptake, swelling, operating temperature, glass transition temperature and so on. These data could be useful both for MEA preparation and experimental results analysis.

Gas diffusion Layer

The GDL is the intermediate between the catalyst layer and the flow field. Consequently, it plays an important role in PEFC performance and has several functions: transport and distribution of reactant and liquid water, conduction of electron, mechanical interface, and heat conduction.

To be compliant to these requests the GDL must be:

- prepared using materials that are electric and thermal conductors and stable in the electrochemical environment, like carbon based materials or some metallic materials;
- porous to allow gas transport and produced water removing, to and from all the electrode area respectively, not only close to gas channels;
- mechanically stable under compression and thermal fluctuations.

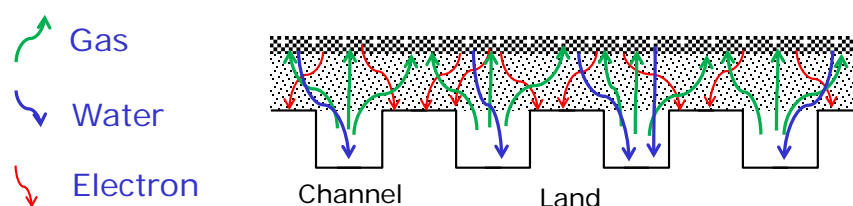


Figure 2: schematic of the GDL function, anode side scheme.

Usually GDL is composed of two sub-layers: the macro-porous or support layer (SL) and the micro-porous layer (MPL). Historically macro porous backing was used since the first time, while micro-porous layer was introduced in a second time [11-13]. The MPL has the functions to allow a better gas distribution, to optimise the GDL hydrophobic properties close to the catalyst layer, to assure a better electric contact between the GDL and the catalyst layer, to avoid dispersion of the small catalyst particles. Today GDL prepared with the dual layer structure with a macro-porous substrate as SL and a thin micro-porous layer coated on SL is considered the standard for PEFC, direct methanol fuel cells (DMFC) and other direct fuelled PEFC.

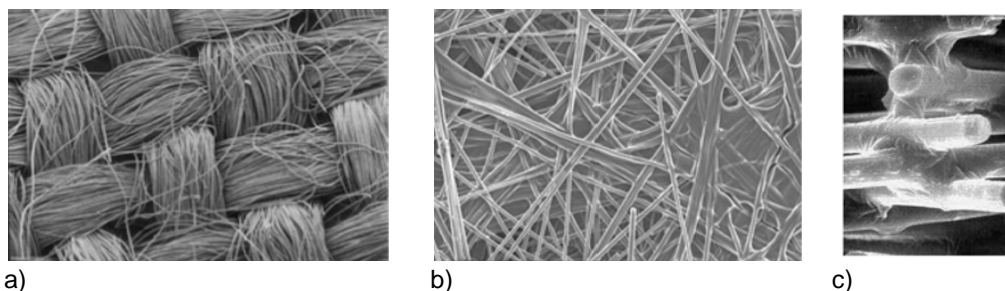
A high quality SL should have excellent gas permeability, high electron and heat conductivity, relatively smooth surface, good mechanical strength, appropriate wet ability, stable chemical and thermal properties, and low cost. The most common SL materials used in PEFC are carbon fibre based products, such as woven carbon cloth and not woven carbon paper and carbon felt. This is due mainly to their high porosity (> 70%) and good electrical conductivity. These carbon based materials are not really low cost, but are more light and stable in PEFC environment in respect to metal based materials. Moreover they allow a low interface resistance with catalyst layer.

Carbon cloth has a woven structure and is obtained by carbonisation and graphitisation of a polymer tissue. The base polymer, the thickness of polymeric fibres and the thermal treatments to transform it into carbon defines the carbon cloth's electric, thermal and mechanical properties. Due to its structure it has two main pores classes [14]: large pores are present close to the fibres intersection, while small pores are present on the remaining area. Moreover fibres are ordered, these characteristics conduct to preferential path for electron, water and gas transport. Carbon cloth offer very interesting mechanical properties and offer a very good adaptability under compression.

Carbon paper is obtained by gluing together carbon fibres; this conducts to a less ordered structure giving to material more homogeneous properties. The surface is more flat in comparison with that of carbon cloth. In front of this, also for carbon paper preferential path for water transport have been observed [15-16].

Carbon felt is composed by carbon fibres like carbon paper, but in this case the fibres are very long and flexible, this allows obtaining a felt like structure where no binder is necessary to maintain the structure.

All these carbon based materials have hydrophobic characteristic, but usually are wet proofed by adding a polymer like polytetrafluoroethylene (PTFE). Please, note that, also the addition of a thin MPL is sometime considered as GDL wet proofing. Commercial supplier usually give few indication about the wet proofing, this results in the possibility that materials of the same type and with the same porosity distribution coming from different suppliers, and some time from the same supplier but coming from different production batch, will have different hydrophobic characteristics. Moreover, must be highlighted that hydrophobic properties of the GDL can change in time due to operative conditions.



a) b) c)
Figure 3: Scanning Electron Microscope images of a) Carbon cloth; b) Carbon paper; c) Carbon paper section.

As can be seen in Figure 3, the surface of Carbon Cloth is largely irregular due to the texture, while carbon paper presents irregular large pores. In both cases the contact between SL and catalyst layer cannot be really effective.

The addition of a MPL surface layer onto the SL improves both the SL surface flatness and water/gas management of the whole GDL. The MPL provides a reduction of the electrical

contact resistance between SL and catalyst layer and a control of water removing from cathode catalyst layer thanks to the micro-porous structure that increase the contact surface and limits the liquid water transport.

Usually, the MPL consists of carbon based (carbons, graphite, carbon nanotubes, carbon nanofibres, carbon felt, carbon foams) particles mixed with a binder acting as hydrophobic agent also, usually PTFE. Typical pore size of MPL is the order of the carbon agglomerates, 100-500 nm, with a layer thickness of 5-50 μm , while SL have a thickness of 100-300 μm and a pore size of 10-30 μm . For a liquid, the pressure necessary to enter a pore increase as pore section decrease [14, 15] as a consequence the MPL structure is more favourable to water vapour diffusion than to liquid water transport. Recent studies [15-17] demonstrate that the pore distribution in SL has as consequence the creation of preferential path for liquid water transport, and that MPL define the liquid water pressure necessary in the catalyst layer to push out the produced water. A deeper discussion of water transport is out of scope for this chapter. For chapter purposes is sufficient to remember that the properties of the GDL will be defined by:

- porosity, material and applied wet proofing for the support layer;
- porosity, material and hydrophobic binder for MPL.

A review about the influence of materials on GDL properties can be found in publication [18-19] reported in reference list.

In laboratory practice the GDL can be:

1. acquired from outer sources;
2. produced in our laboratory according to necessities.

The first case is the simpler one, no work is needed for its realisation. Usually the supplier will supply also the GDL characteristics, if it is not the case and if necessary a GDL characterisation is needed to define, for example, porosity and pore distribution, permeability to gasses, hydrophobic properties. Due to the double layer structure all these characterisations are not simple to be performed.

In the second case, usually the starting point is the selection of the SL. Production of carbon cloth, carbon paper and other supports is not simple. In common practice, the SL is acquired with the requested wet proofing, but if necessary wet proofing could be applied according to experimental necessities.

The MPL is obtained by deposition of an ink or paste containing the appropriate balance of carbon and PTFE on the SL. After drying, a thermal treatment is carried out to allow the PTFE sintering. The ink must have the correct density according to the deposition method; the density can be adjusted changing the solvent/dispersion agent percentage. More dense inks are requested for doctor blade or spatula deposition, while lower densities are requested for serigraphy, brushing, air brushing, spray and ink jet deposition.

The MPL porosity is defined mainly by the carbon particles size and binder concentration, while the deposition technique has less influence. To manage the porosity pore former materials can be added to the ink.

The choice of the deposition techniques will influence the minimum thickness that can be uniformly deposited and the possibility to design the MPL. For example spray techniques allow very thin layer deposition and the possibility to create multi layer MPL where each layer have a different composition, while ink jet some spray techniques allow to create 3D design also.

Catalyst layer

The catalyst layer (CL) is the location where electrochemical reaction takes place, so that it is a key component of the MEA. The catalyst particles must be in contact with both electronic and proton conducting materials and must be accessible to the reactants. Moreover path for product water removal must be available in the CL [20]. This leads to an architecture resulting by the co-penetration of three percolating network: one for electron conduction, one for ion conduction and a pore network for gas transport and water removal, Fig. 4. The presence of the percolating paths is necessary not only in the catalyst layer but also in the other components of the MEA, but only in the catalyst layer the three percolating paths must be all present. Looking at Fig. 4, that represents the cathode side of the MEA, the reaction of water formation can occur only on catalyst grains where protons, oxygen and electrons are simultaneously present. Protons will arrive through ion conducting polymer paths. The ionomer inserted in catalyst layer forms ion conducting bridges between the membrane and the catalyst grains. Electrons run along the fibres of the support layer (SL) first and along percolating paths of carbon particles of the microporous layer to reach the reaction site. Oxygen pass through percolating path of wet proofed pores or not water full pores of the GDL and catalyst layer (CL). Finally water produced during reaction can be absorbed by the membrane or can be removed by percolating path of pores. In Fig. 4 the circle “npp” indicate a section of the MPL without percolating path for the electrons. If this arise the catalyst layer close to this area will be less effective. Actually, this can arise in any part of the MEA both for electron, oxygen, protons and water paths. In all these cases there will be a reduction of the MEA performances and, in some cases, destructive processes can be triggered. The described structure is the result of a long research on electrode development that starting from Teflon bonded catalyst layer applied on GDL arrived to the “Catalyst Coated Membrane” (CCM) configuration [8-9, 20].

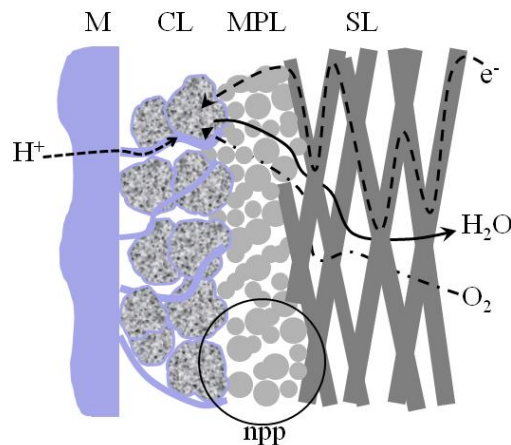


Figure 4: Scheme of the interaction between GDL, CL and Membrane (cathode side).

PEFC catalysts usually consist of a powder of Platinum (Pt) based nano-particles deposited on carbon support [21-22], but for some applications unsupported Pt particles can be used. Catalysts have been treated in section 3.1 of this book, for the scope of this chapter metal on carbon catalyst is used as reference. Catalyst will be used for the catalyst

layer preparation as it is or by applying pre-treatments according to indication of the supplier. Although direct deposition/formation methods on membrane or GDL of the metal used as catalyst by sputtering and physical-chemical deposition have been proposed, these methods are not treated here because considered special case and not common practice.

Starting from catalyst powder, CL could be realised onto the MPL of GDL or on the membrane, the first approach give the so called "gas diffusion electrode" (GDE) and is the basic preparation technique, the second the CCM.

Also in this case the starting point is the catalyst ink, usually consisting in a suspension of catalyst particles in a solution containing the solid electrolyte ionomer that will act both as ion conductor and binder. Pore formers and other additives could be added to manage the CL architecture, to increase the durability and to ameliorate the water management, just as example. The deposition techniques are the same techniques used for the MPL and the ink could be applied to GDL or to the membrane. The deposition of the CL on the membrane is more complex but allows a reduced contact resistance between membrane and CL and could increase the MEA endurance reducing delaminating problems. The Pt load and the composition of the catalyst layer can be different for anode and cathode side depending on the operative condition of the PEFC and on the performance targets.

For applying the catalyst layer onto membrane there is also an alternate technique, the "decal". In this case the CL is realised on a support, usually PTFE, and then hot pressed onto membrane for transferring the catalyst layer from the support to the membrane.

Each deposition method and substrate of application requires a specific ink, especially referring to its density and used solvents. But the components of the ink are essentially the same: catalyst (Pt on carbon), ionomer, solvent (usually water and alcohols).

The CL preparation can follow the solution method or the colloidal method. In the solution method, the traditional one, the catalyst particles are suspended in a solution of ionomer. As reported by M. Uchida et al. [23], which also introduced the colloidal method, the perfluorosulfonic ionomer assume solution form when the dielectric constant of the solvent is over 10, while undergo to precipitation for solvent dielectric constant less than 3, and colloid is obtained for dielectric constant in a range around 5.

Consequently solution method need of solvents like water, glycerol and alcohols for preparing the ink. In colloidal method solvents of the family of Esters and Ethers are largely used to obtain a colloidal solution of ionomer to which the catalyst is added.

In few words, in solution method is expected that the CL structure will be defined mainly by the catalyst particles, while in colloidal method are the ionomer clusters that define the CL architecture. In both cases to increase the CL porosity pore former could be added to the ink. The addition of pore former has been reported with the aims of obtaining greater porosity. Pore formers are materials that after their removal live void space for gas and water transport. Both water soluble and thermal decomposable pore formers have been tested, these could be removed both by an electrode or MEA treatment before the use or directly inside the single cell or the stack in the start up and activation phase. Also plasticizer and stabilizer could be added to improve manufacturing and reduce ink sedimentation respectively. All these additives must be not poisoning for the catalyst, not dangerous for the MEA performances, and easy to be removed after MEA preparation.

Usually after the CL ink deposition a thermal treatment is carried out for removing all solvents, both with and without the application of a mechanical compression. Must be underlined that the application of a mechanical compression on the MEA could change the structures previously formed and, if this compression is too hard, it can also destroy the electrode. Other treatment like washing or chemical treatments could be used if necessary.

Moreover, in case of pore formers use, applying the thermal and washing treatments the pore former characteristics must be taken into account to avoid the pore former misusing. In Fig. 5 a scheme of the catalyst layer preparation is reported for resuming.

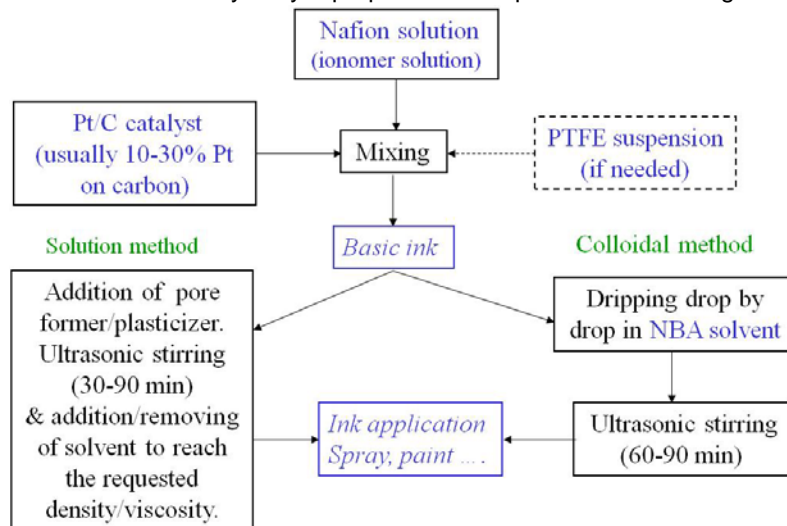


Figure 5: Resuming scheme of catalyst layer preparation procedure.

MEA assembling

When all components are ready to use, the last step is the MEA preparation. The MEA is obtained by sandwiching the membrane between two GDE, or sandwiching the CCM between two GDL. Before this, the application of a pre-gasket on the membrane area outside the active area to reinforce and protect the membrane is considered a good practice.

Hot pressing is then used to link together the components. Sometimes the assembling can be done directly inside the cell shell if requested by the membrane characteristics or by the specific test to be performed, but this is not a standard practice. In fact hot pressing reduce contact resistances between the layers composing the MEA, and allow to handling the MEA as a single piece allowing a more practice, precise and simple mounting of the experimental set up, in laboratory, and stack assembling in industrial production.

In laboratory, hot pressing is made by a press with heated plates. Press with digital control are easily available on the market, also manual press can be used but only if equipped with a good pressure gauge and a high quality temperature control. It is recommended to periodically verify the planarity and the parallelism of the plates. The MEA is very thin and small defects can totally destroy the previous work. The use of a template mould could be useful both for the correct coupling of the different pieces and for granting a uniform compression.

It is to be underlined that usually the hot pressing is carried out at temperature close to the glass transition of the ion conducting polymer composing the membrane and used as ionomer in the catalyst layer. Using GDE hot pressing allows a better matching between the CL and the membrane, while using CCM it allows a better arrangement of the CL and MPL contact surface.

It is advisable to cool the MEA between two cooling plates and applying light pressure to reduce creasing and warping.

After cooling the MEA is ready for the insertion in the single cell fixture or in the stack, if necessary it may be stored in plastic bags, preferably hermetic.

The MEA preparation steps are resumed in Fig. 6; MEA testing is discussed in chapter 4.

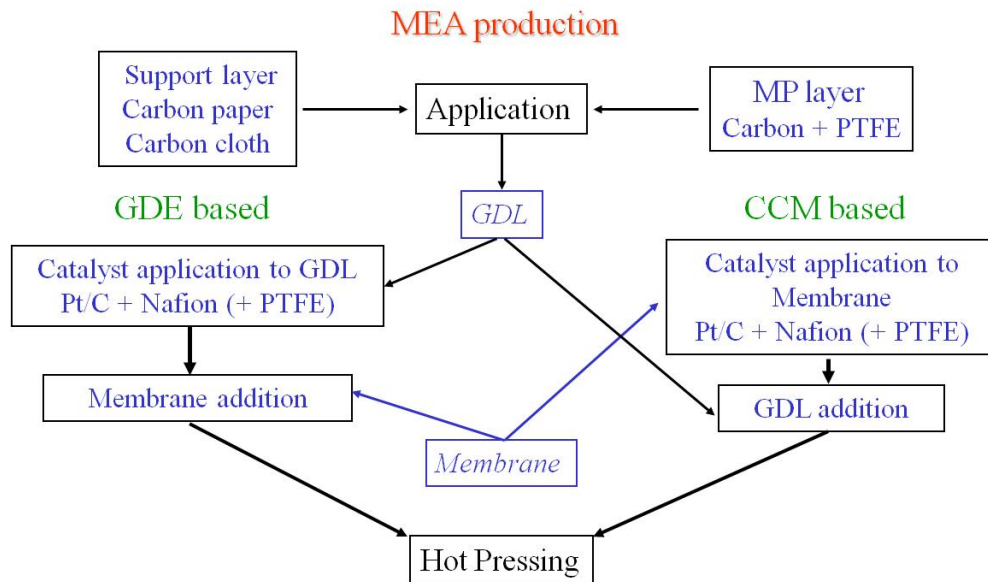


Figure 6: Resuming scheme of MEA preparation process.

REFERENCES

- [1] G. Squadrito, L. Andaloro, M. Ferraro and V. Antonucci, "Chapter 16 – Hydrogen Fuel cell technology", in "Advances in Hydrogen Production, Storage and Distribution", A. Basile and A. Iulianelli editors, Woodhead Publishing, 2014 (ISBN – 978-0-85709-768-2).
- [2] "The Fuel Cell Industry Review 2015", E4Tech, December 2014; free download <http://www.fuelcellindustryreview.com/archive/TheFuelCellIndustryReview2015.pdf>, (last availability check 30/6/2017).
- [3] 4th Energy Wave, "The fuel cell and hydrogen annual review 2016" - free download from <https://www.4thenergywave.com/fuelcellannualreview>; (last availability check 30/6/2017).
- [4] <http://www.hngn.com/articles/33584/20140612/toyota-hydrogen-fuel-cell-vehicles-to-be-available-in-2016.htm>, published on June 12, 2014. – last access June 11, 2015.
- [5] "Fuel Cell Electric Vehicles: The road ahead", published by Fuel Cell Today, available on www.fuelcelltoday.com – (last availability check 30/6/2017).
- [6] Hyundai UK web site: <http://www.hyundai.co.uk/about-us/environment/hydrogen-fuel-cell> - last access June 11, 2015.
- [7] Y. Wang, K. S. Chen, J. Mishler, S. C. Cho, X. C. Adroher, "A review of polymer electrolyte membrane fuel cells: technology, applications, and needs on fundamental research"; Appl. En. 88 (2011) 981-1007.
- [8] S. Lister, G. McLean, "PEM fuel cell electrodes", J. Pow. Sources 130 (2004) 61-76.
- [9] V. Mehta, J.S. Cooper, "Review and analysis of PEM fuel cell design and manufacturing", J. Pow. Sources 114, (2003), 32-53.
- [10] D. Wheeler, G. Sverdrup, "2007 status of manufacturing: Polymer Electrolyte Membrane (PEM) fuel cells", Technical report NREL/TP-560-41655, march 2008; <http://www.nrel.gov/docs/fy08osti/41655.pdf>

- [11] D. Bevers, N. Wagner, M. Bradke, "Innovative production procedure for low cost PEFC electrodes and electrode membrane structures", *Int. J. Hydrogen Energy* 23 (1998) 57-63
- [12] E. Passalacqua, G. Squadrito, F. Lufrano, A. Patti, L. Giorgi, "Influence of the structure in low-Pt loading electrodes for polymer electrolyte fuel cells", *Electrochimica Acta* 43 (1998) 3665-3673.
- [13] F. Lufrano, E. Passalacqua, G. Squadrito, A. Patti, L. Giorgi, "Improvement in the diffusion characteristics of low Pt-loaded electrodes for PEFCs", *J. Appl. Electrochem.* 29 (1999) 445-448.
- [14] J. Benziger, J. Nehlsen, D. Blackwell, T. Brennan, J. Itescu, "Water flow in the gas diffusion layer of PEM fuel cells", *J. Membrane Science* 261 (2005) 98-106.
- [15] S. Lister, D. Sinton, N. Djilali, "Ex situ visualization of liquid water transport in PEM fuel cell gas diffusion layers", *J. Pow. Sources* 154 (2006) 95-105.
- [16] B. Auvity, G. Giacoppo, G. Squadrito, E. Passalacqua, "Visualisation study of water flooding in a model fuel cell", Second International conference on Hydrogen Energy (ICHE'10) May 9-11 2010 Hammamet (Tunisia).
- [17] O. Chapuis, M. Prat, M. Quintard, E. Chane-Kane, O. Guillot, N. Mayer, "Two-phase flow and evaporation in model fibrous media. Application to the gas diffusion layer of PEM fuel cells", *J. Pow. Sources* 178 (2008) 258-268.
- [18] K. T. Cho, M. M. Mench, "Effect of material properties on evaporative water removal from polymer electrolyte fuel cell diffusion media", *J. Pow. Sources* 195 (2010) 6748-6757.
- [19] S. Park, J.-W. Lee, B. N. Popov, "A review of gas diffusion layer in PEM fuel cells: Materials and designs", *Int. J. Hydrogen Energy* 37 (2012) 5850-5865.
- [20] E. Passalacqua, F. Lufrano, G. Squadrito, A. Patti, L. Giorgi, "Nafion content in the catalyst layer of polymer electrolyte fuel cells: effects on structure and performance"; *Electrochimica Acta* 46 (2001) 799-805.
- [21] E. Antolini, "Formation of carbon-supported PtM alloys for low temperature fuel cells: a review", *Mat. Chem. Phys.* 78 (2003) 563-573.
- [22] H.A. Gasteiger, S.S. Kocha, B. Sompalli, F.T. Wagner, "Activity benchmarks and requirements for Pt, Pt-alloy, and non-Pt oxygen reduction catalysts for PEMFCs", *Appl. Catalysis B: Environ.* 56 (2005) 9-35.
- [23] M. Uchida, Y. Aoyama, N. Eda, A. Ohta, "New preparation method for polymer-electrolyte fuel cells", *J. Electrochem. Soc.* 142 (1995) 463-468.

PEFC SINGLE CELL TEST: COMMON EXPERIMENT PROCEDURES

Gaetano Squadrito

CNR-ITAE, salita per S. Lucia sopra Contesse 5, 98126 Messina, Italy
e-mail: gaetano.squadrito@itae.cnr.it

Keywords: PEFC, single cell testing, experimental protocol.

INTRODUCTION

In previous chapter the materials and components of a PEFC have been introduced and their basic characterisation discussed, now testing is necessary to verify if the developed materials and components are useful. In fact catalysts or other components must demonstrate their utility and performances in real operative condition. Single cell testing is a simple and low cost system for testing materials and components in conditions close to real operation.

What must be done in laboratory for characterising a PEFC?

- 1) Defining the testing protocol according to the experimental finalities;
- 2) Preparing the appropriate test rig;
- 3) Preparing the MEA for testing;
- 4) Testing and reporting.

Point 3) has been already treated; this chapter will be focused on the set up of a simple protocol for single cell testing of Membrane Electrode Assembly (MEA), the heart of the PEFC. Hydrogen fuelled cells will be used as reference, taking into account that PEFC could be fuelled with alcohols and other fuels also.

WHAT IS A PROTOCOL

A researcher usually doesn't only work alone, he has to publish his research results, he needs to remember what he has to do, and he has to analyse the results.

The simple way to face front all these necessities is writing an experiment protocol.

In the follow starting from the definition of the experimental protocol, a trace for experimental planning and standard reference test will be introduced with the aims of supplying the basic concepts about good practice in PEFC testing.

The experimental protocol is a recipe, or a project, of the experimental work to be carried out for investigating a specific material, component, model, behaviour or other object under investigation. It is composed of few fundamental parts but could be enriched on necessity:

- **Purpose:** a statement of what question we are trying to answer and, when applicable, what hypothesis we wish to test.
- **Materials:** List of all major items needed to carry out your experiment. This list need not be lengthy if a part of its contents has been already published, but it should include all the essentials. Literature references could be useful.
- **Methods:** experimental set up, how many experimental sets, how will be measured the effects of the object under study, how long will the experiment last, operative sequences, list of data to be acquired. Methods should be explicitly stated or referenced so that a reader has all the information they need to know to be able to repeat the experiment and verify its results without talking with the protocol writer(s).

- **Controls:** Identify the relevant control(s) to be performed before, during and after the experiment. Think about the variable(s) we are manipulating. On line controls need to be carried out under conditions not affecting the test results.
- **Data Interpretation:** What will be done with the data once it is collected? Data must be organized and summarized so that the scientist himself and other researchers can determine if the hypothesis has been supported or negated. Results are usually shown in tables and graphs; it is a good practice to define the standard for data representation. Statistical analyses are often made to compare experimental result, also for this is useful to define the analysis to be carried out and the output structure.
- **Report template (optional):** A standard for report template could be useful for reporting measurement results. This approach is really effective when we work in community, this allow having results coming from different stations and researchers reported in the same way and easily comparable. Moreover it could be a check table for the person that carry out the experiment avoiding that important data could be missed.

Looking at the structure of the protocol could be noted that it has the same structure of a scientific publication. The purpose is what has to be reported in the introduction of the paper, "materials and methods" compose the second part of the paper sometime named "experimental". The part of the paper normally named "results" cannot be present in the protocol obviously, but the section "controls" is necessary to validate the acquired data, and figure and graph planned in "data interpretation" will be helpful. Finally "result discussion", the heart of the publication will be based on the previous prepared "data interpretation". In summary all the scientific paper could be already wrote in the protocol if it is well constructed.

PEFC SINGLE CELL TEST PROTOCOL

It is expected that the research after the laboratory step will be transferred to industry for application and commercialisation. At this point the industries and the consumers need some kind of reference for quality and safety of the new product. Consequently it is necessary to develop "reference test protocols" aimed at assuring the quality, safety and interchange-ability (is applicable) of products and their components.

Since year 2000, a number of projects to develop standard testing procedures for fuel cells have been made by USFCC (United State Fuel Cell Council) [1, 2], by EU with the FCTESTNET and FCTESqa [3] projects, by JARI (Japan Automobile Research Institute) [4], and other national and international projects. The Technical Committee 105 of the International Electrotechnical Commission (IEC) assembled all these experience in a series of normative and technical specification documents regarding the fuel cells systems, from single cell to the full power module. Single cell testing is the object of Technical Specifications "Fuel cell technologies – part 7.1: Single cell test methods for polymer electrolyte fuel cell (PEFC)" [5], the first revision of this document was started in 2014. In this document the minimum instrumentation requirements and reference procedures for testing methods are reported. In the new version, publication planned in August 2016, a number of new testing specifications will be added.

These technical specifications are a reference for the testing methods to be used in experimental planning, especially working in project supported by industries.

The IEC document in its first edition was wrote specifically for industries, the new edition, will introduce a number of tests not previously considered because one of the requests was the possibility to compare results, both published and reserved, without

misunderstanding. An action that is impossible if the results have been not obtained using the same procedure and parameters.

In general the researcher is free to develop its own approach, but if his target is to develop something that in the future could be produced and commercialised for the community, he need to refer to the standards. Then, in research the IEC recommendation could be adapted to specific necessity but the quality and reproducibility of the test results must be maintained and the adopted testing procedure well publicized.

TESTING HARDWARE

Usually are considered test hardware the test station (or test bench) and the single cell fixture. But in PEFC the performance of the single component (catalyst layer, electrode, membrane, gas diffusion layer, flow field) is strictly related to the efficiency and structure of the other components and to the interaction between these and the tested component. Consequently could be useful to redefine the meaning of “test hardware”.

A possibility is to define “hardware” all the systems and accessories necessary to test the PEFC component under study, Fig. 1. This means that if we have to test a new catalyst layer all the other part of the MEA and single cell will be the “test hardware”, i.e. the presence of laboratory reference materials and components is of basic importance to reach correct results and simplifying their analysis and interpretation. To differentiate the test bench hardware from the reference materials and components could be practical to refer to the test bench as the “main hardware” and to reference materials and components as “secondary hardware”. A periodic check of both primary and secondary hardware is needed to avoid false results and misunderstandings.

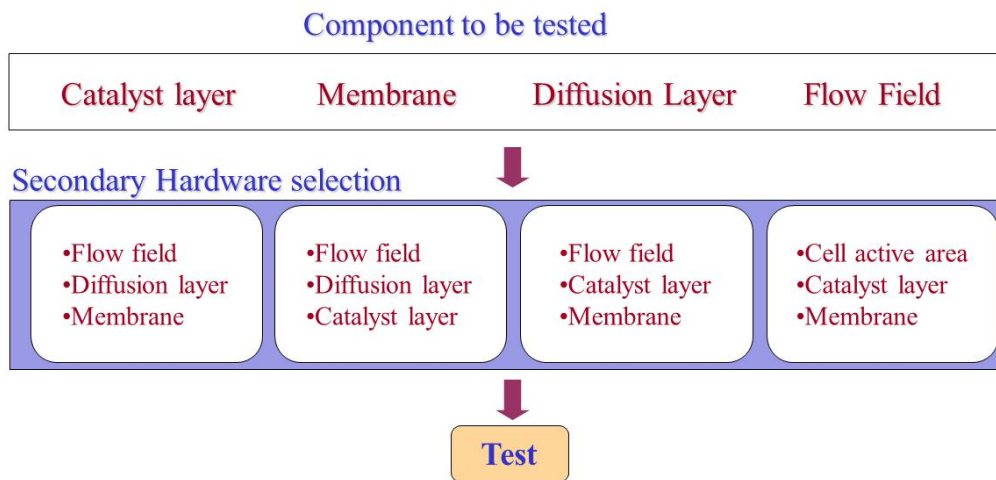


Figure 1 – For each PEFC component we can define the secondary hardware as the reference components we will use to test the experiment object.

The main hardware have a standard form, the basic test station is composed by gas flow controllers, gas conditioning system (for controlling gas inlet humidity and temperature), electronic load, data acquisition system, single cell embodiment. More recently is common to have also a Frequency Response Analyser for impedance spectroscopy, and a voltammetry system for studying PEFC ageing. These test stations are commercially available, or can be built in home by assembling different instruments. In the second case the major difficulties are encountered in calibrating the instrument, in controlling the test

station (mainly regarding the safety), and in data acquisition software development. Indications about the test station configuration and requirements are easily available in literature [6-7]. In the follow of this chapter the availability of a basic fuel cell test station is considered.

Preparing the single cell embodiment, the first point to be defined is the cell active surface area. Today graphite based flow filed plates with 25 cm² active area are largely used as standard. For studying new catalysts 5 cm² area cell are also used for reducing experimental cost and avoiding the necessity of preparing large batch of catalyst. While for studying components for stack application is preferable a single cell having the same flow filed and active area of the stack cell. The flow field could have different geometries, serpentine like geometry is largely used, parallel channels, interdigitated and pin geometries are also considered for laboratory cells.

Plain polymeric fabric gaskets having a thickness close to that of gas diffusion layer are normally used to avoid excess MEA stress of contact resistance. Copper current collectors and aluminium end plates are placed on both sides to complete the assembly. The cell hardware is clamped by tie-bolts through the end plates. The bolts are tightened in a diagonal pattern using incremental torque up to reach the requested medium pressure on MEA. The warm up is assured by heater placed in or onto the end plates. The use of distributed heaters (such as the adhesive heater pads) is recommended to assure a good temperature distribution on the cell active area.

The reference cell built according to these indications will be the shell for testing the MEA. It will be coupled to a test station able to control all the operative condition and to acquire the requested data.

Finally a protocol for testing the gastight, start-up / reconditioning the cell, obtain I-V curves and other data, switching of the cell, and the result report template must be defined before the test start. About this, the recommendation of IEC will be illustrated and discussed considering the most important test to be conducted on the PEFC: I-V curve acquisition, time testing in steady conditions, cycling test for applicative performance evaluation..

REFERENCES

- [1] "Fuel cell test station requirements and verification procedure", USFCC document n. 04-011B, 2006 – available on www.usfcc.com
- [2] "Single Cell test protocol", USFCC document n. 05-014B.2, 2006 – available on www.usfcc.com
- [3] FCTESTqa - <http://iet.jrc.ec.europa.eu/fuel-cells/about-fctesqa-project>
- [4] Y. Ashimasa, T. Numata, K. Moriya, S. Watanabe, "Study of fuel cell structure and heating method – Development of JARI's standard single cell", J. Pow. Sources 155, (2006), 182-189
- [5] IEC 105/241/DTS*IEC/TS 62282-7-1 the "Fuel cell technologies – part 7.1: Single cell test methods for polymer electrolyte fuel cell (PEFC)"
- [6] USFCC, document number USFCC 04-011 Rev B "Fuel Cell test station requirements and Verification procedure", USFCC 2006.
- [7] E. Guelzow, S. Weisshaar, R. Reissner, W. Schroeder, "Fully automatic test facilities for the characterisation of DMFC and PEFC MEAs", J. Pow. Sources 118 82003) 405-410

POLYMER ELECTROLYTE MEMBRANES FOR FUEL CELLS: STRUCTURE AND TRANSPORT PROPERTIES

KARPENKO-JEREB Larisa

Graz University of Technology, 8010 Graz Stremayrgasse 9/I, Austria,
larisa.karpenko-jereb@tugraz.at

Keywords: doped polymer, ion-exchange membrane, water sorption isotherm, conductivity, percolation theory, electro-osmosis, membrane over-potential, AVL FIRE

INTRODUCTION

The contribution presents the chemical classification and commercial types of the PEMs; the physico-chemical and transport properties of ion-exchange membranes (IEMs) and some experimental methods for their testing, as well as a description of an algorithm estimating the membrane over-potential in the FC performance.

CLASSIFICATION OF PEMS

Currently the available commercial PEMs can be divided into two main groups: I. non-charged polymers doped by strong inorganic acids; II. polymers containing ion-exchange groups.

I. Polymers doped with inorganic acids, mainly with H_3PO_3

- Polybenzimidazole (PBI) membranes (FuMA-Tech, Celanese)
- Pyridine type TPS membrane (Advent Technologies)

II. Sulfonated Membranes = Ion-exchange membranes

- Perfluorinated ion-exchange membranes (DuPont, GEFC and FuMA-Tech)
- Hybrid perfluorinated ion-exchange membranes (GEFT and FuMA-Tech)
- Sulfonated hydrocarbon membranes (FuMA-Tech)
- Sulfonated poly-trifluorostyrene (TFS) (Ballard Power Systems)

The first group of the membranes based on aromatic polymers contains the nitrogen atoms. This type of the polymers possesses high absorption capacity for inorganic acids (up to 300%), after the sorption the polymers become ion-conductors: the protons can be transported through the polymer. The advantages: the PEMs has a high thermal stability and can be used at $T=150-200^{\circ}C$ and do not need any humidification. The disadvantages: lower conductivity than ion-exchange polymers, during the FC operating the membranes loose the absorbed acid.

The second group is the ion-exchange polymers. At present mainly sulfo-cationic polymers are used in FCs. In dry conditions the ion-exchange polymer is a non-conductor ($\sigma=10^{-6}S/m$). After the water sorption the IEMs begin to conduct the electric current and the conductivity grows dramatically (up to $\sigma=10^{-1}S/m$). The advantage of the membranes is a higher conductivity than of the doped polymers. The disadvantage is that the water is transported by electro-osmosis through PEM to cathode catalyst layer, and it can lead to water flooding and drop of the FC potential.

IMPORTANT PROPERTIES

The most important characteristics of the ion-exchange membranes are listed below.

The physico-chemical properties: 1) Thickness; 2) Density, 3) Tensile strength; 4) Swelling factor; 5) Equivalent weight; 6) Ion-Exchange Capacity; 6) Water uptake; 7) Hydration number - number of water molecules per one ion-exchange group; 8) Water Sorption Isotherm describes the dependence of membrane hydration number on the water vapour humidity.

The transport properties: 1) diffusion permeability; 2) electro-osmotic permeability; 3) conductivity.

TEST METHODS

Very often the membrane conductivity is determined by the impedance spectroscopy method directly in PEMFC. This method allows measuring the dependence of the membrane conductivity on the water vapour humidity [1]. The conductivity of the completely hydrated membrane can be measured by the differential method. In the first step the resistance of the test cell is determined with the electrolyte solution and membrane. In the second step the resistance of the cell is detected with the same solution but without the membrane. The difference between these two measurements is the membrane resistance (Eq.1), which does not include the electrode/solution transient interfaces [2]. The value of the specific conductivity is calculated from Eq.2.

$$R_{mem} = R_{sol+mem} - R_{sol} \quad (1)$$

$$\sigma_{mem} = \frac{L_{mem}}{R_{mem} \cdot S_{mem}} \quad (2)$$

where R_{mem} – membrane resistance, $R_{sol+mem}$ – resistance of the test cell with the electrolyte solution and the membrane, R_{sol} – resistance of the test cell with the electrolyte solution, σ_{mem} – specific membrane conductivity, L_{mem} – membrane thickness, S_{mem} – the active area of the membrane in the test cell.

The electro-osmotic coefficient (C_{drag}) is usually determined by volumetric method: the test cell consist of two chambers, separated by the membrane and equipped with the electrodes and measuring capillaries. The electric current (I) is passing through the cell, the changes of the volumes of the electrolyte solution in the both capillaries (ΔV_1 , ΔV_2) are detected after a time interval (τ). The electro-osmotic coefficient is found using Eq.3.

$$C_{drag} = (\Delta V_1 + \Delta V_2) \cdot d_w \cdot F / (2 \cdot M_w \cdot \tau \cdot I) \quad (3)$$

where F – Faraday constant; d_w – water density; M_w – molar mass of the water.

INFLUENCE OF MEMBRANE PROPERTIES ON PEMFC POTENTIAL

The potential losses in PEMFC are caused mainly by over-potentials in catalyst layers and by ohmic resistance of the polymer electrolyte membrane. The estimation of the over-potential of the ion-exchange membranes can be done in the following way: 1) calculation of the hydration number of the membrane from water sorption isotherm; 2) calculation of the membrane conductivity from hydration number using the equation of the percolation

theory [3]; 3) finally the membrane over-potential is found from the current density and the membrane conductivity.

Detailed investigations about an influence of ion-exchange membrane characteristics on the PEMFC performance can be carried out using CFD Code AVL FIRE [4].

REFERENCES

- [1] T.V. Reshetenko, G. Bender, K. Bethune, R. Rocheleau: *Electrochimica Acta*. Vol. 69 (2012), p.220
- [2] L. V. Karpenko, O. A. Dyomina, G. A. Dvorkina, S. B. Parshikov, C.Larchet, B.Auclair, N. P. Berezina: *Russian J. Electrochem.* Vol. 37 (3) (2001), p. 287
- [3] W.Y. Hsu, T. D. Gierke: *J. Membr. Sci.* Vol. 13 (1983), p. 307
- [4] AVL FIRE®.VERSION 2010. General Purpose Modules: AST AVL, 2010, 91 pp

Polymer electrolyte membranes for FCs: structure and transport properties

Dr. Karpenko-Jereb Larisa

Outline

1. PEMs classification
2. Chemical compositions
3. Properties of ion-exchange membranes
4. Test methods
5. Estimation of membrane over-potential

1. PEMs Classification

I. Polymers doped with acids, mainly with H_3PO_3

- Polybenzimidazole (PBI) membranes (FuMA-Tech, Celanese)
- Pyridine type TPS membrane (Advent Technologies)

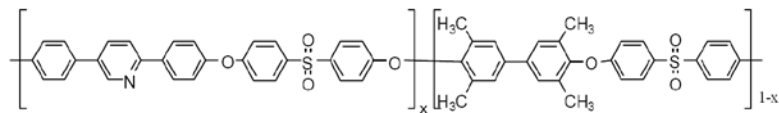
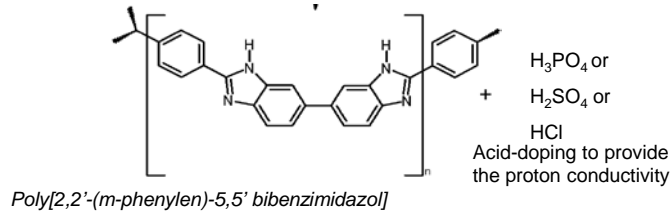
II. Sulfonated Membranes = Ion-exchange membranes

- Perfluorinated ion-exchange membranes (DuPont, GEFC and FuMA-Tech)
- Hybrid perfluorinated ion-exchange membranes (GEFT and FuMA-Tech)
- Sulfonated hydrocarbon membranes (FuMA-Tech)
- Sulfonated poly-trifluorostyrene (TFS) (Ballard Power Systems)

2. Chemical Compositions

I. Polymers doped with acids, mainly with H₃PO₄

Polybenzimidazole (PBI) membranes



Doped with H₃PO₄ to provide proton conductivity

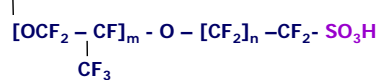
II. Sulfonated Membranes = Ion-exchange membranes

Perfluorinated membranes: $-(\text{CF}_2 - \text{CF}_2)_x - (\text{CF}_2 - \text{CF})_y -$

Nafion: $m \geq 1, n=2, x=5-13.5$

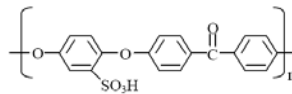
Flemion: $m=0, 1, n=1-5$

Aciplex: $m=0, n=2-5, x=1.5-14$

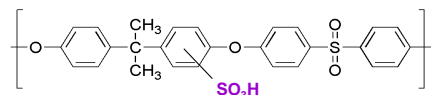


Hybrid perfluorinated ion-exchange membranes: **modified with SO₂ or ZrP**

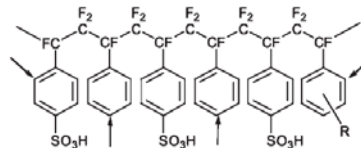
Sulfonated hydrocarbon membranes:



Sulfonated polysulfone, SPSU



Sulfonated poly-trifluorostyrene (TFS):

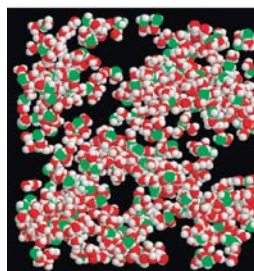
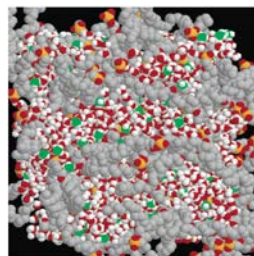
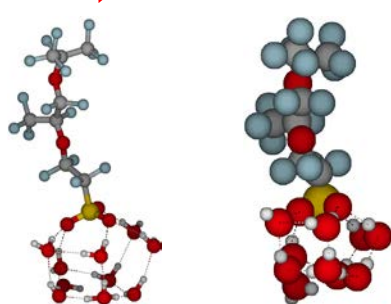
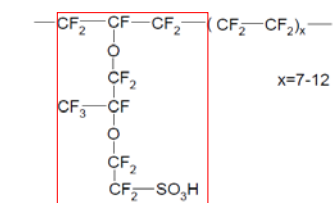


Comparison of the membranes

Operating characteristics of commercial membranes for PEMFC

	Membrane type	Temperature, °C		Humidif., RH%		K, 10 ⁻³ Ohm ⁻¹ cm ⁻¹
		Max	Opt	Max-Min	Opt	
1	^a Perfluorinated ion-exchange	100	65-80	30-100	50-100	90-100
2	Hybrid perfluorinated ion-exchange					
	^a ZrP	120	---	---	50	75-85
	^b SiO ₂	150	≤150	---	---	100
3	^a Sulfonated hydrocarbon	110	65-80	30	100	120
4	Sulfonated poly-trifluorostyrene	---	---	---	0	---
5	^a Polybenzimidazole	200	160	---	0	40 (120°C)
6	^c Pyridine type TPS	150-200	180	---		7,0 [*] (120°C, 70%RH)

Data for ^aFumatech-membranes, ^bGEFC, ^cAdvent Technologies
 Conductivity for the membrane types 1, 2 and 3 were measured for H⁺-form H₂O



elvan M. et al. J. Phys. Chem. C 112 (2008) 1975

3. Properties of ion-exchange membranes

The physico-chemical properties:

1. Thickness
2. Density
3. Tensile strength
4. Swelling factor
5. Equivalent weight
6. Ion-Exchange Capacity
7. Water uptake
8. Hydration number
9. Water Sorption Isotherm

The transport properties:

1. Diffusion permeability
2. Electro-osmotic permeability
3. Conductivity

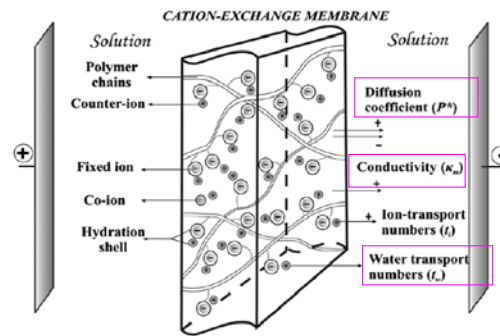
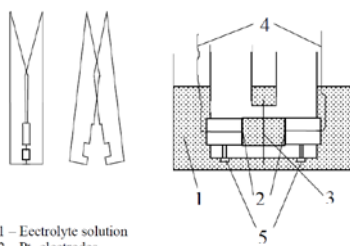
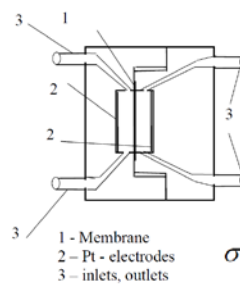


Fig. 1. Schematic diagram of an electromembrane system.

Determination of PEM conductivity by differential methods



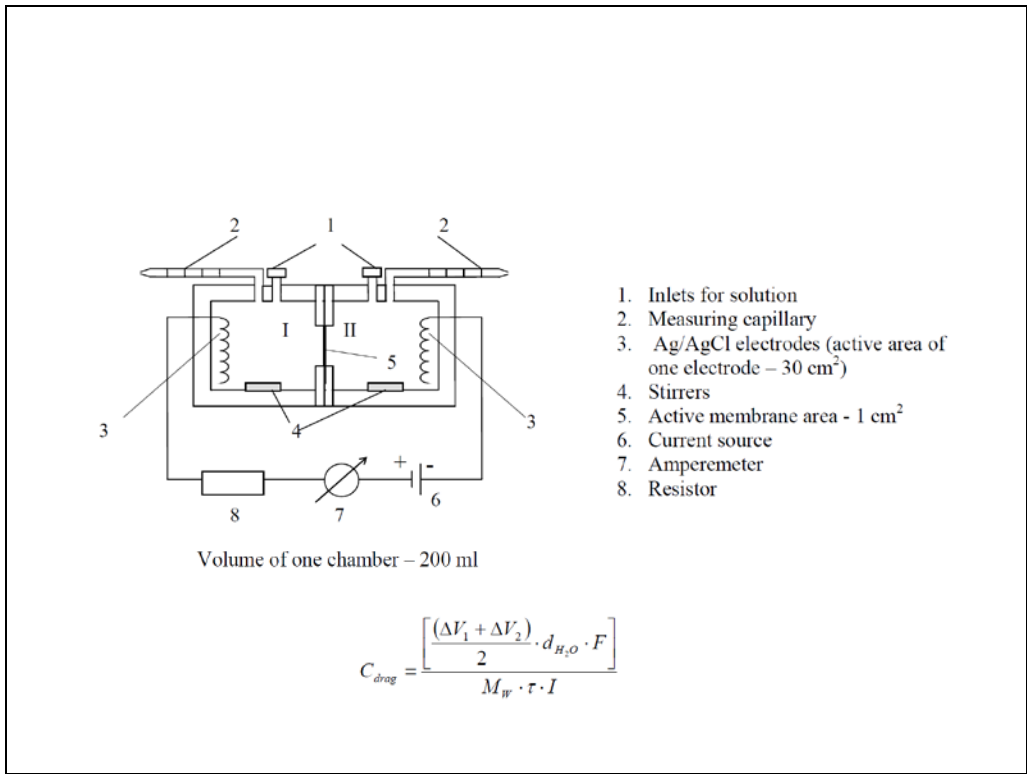
- 1 - Electrolyte solution
- 2 - Pt- electrodes
- 3 - Membrane
- 4 - Insulated conductors
- 5 - screws



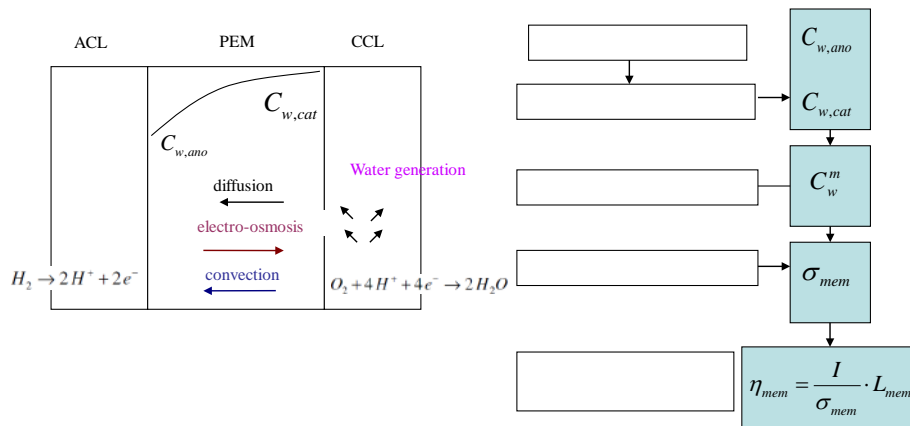
- 1 - Membrane
- 2 - Pt - electrodes
- 3 - inlets, outlets

$$\sigma_{mem} = \frac{\Delta R}{l \cdot S}$$

Allows measuring without destroying the samples



5. Estimation of membrane over-potential



STEP BY STEP DETERMINATION OF THE KINETIC PARAMETERS ON CARBON SUPPORTED NANOCATALYSTS

K. Boniface Kokoh

Université de Poitiers, UMR CNRS 7285, IC2MP, 4 rue Michel Brunet, B27 - 86022
Poitiers cedex, France
e-mail: boniface.kokoh@univ-poitiers.fr

Keywords: Proton Exchange Membrane Fuel Cell; Oxygen Reduction Reaction.

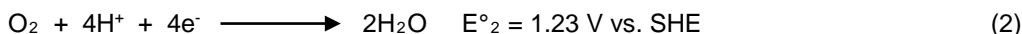
INTRODUCTION

From the various fuel cells investigated in the Electrocatalysis Group at the University of Poitiers (*Proton Exchange Membrane Fuel Cell* and *Direct Alcohol Fuel Cell*), the Oxygen Reduction Reaction (ORR) constitutes the similar process encountered in the cathodic event. It is proposed in this course to show how we determine the kinetic parameters of O₂ reduction at electrode nanomaterials. We will use Butler-Volmer and Koutecky-Levich equations to assess the main factors such as the exchange current density (*j*₀) the apparent number of electrons, the associated kinetic current (*j*_k) and Tafel slopes.

An electrochemical cell converts directly the Gibbs energy change Δ*G* in oxygen of a fuel such as hydrogen into electricity. At the anode of a PEMFC the electrooxidation of hydrogen takes place:

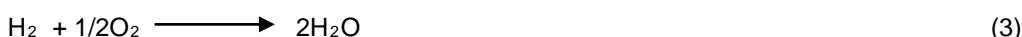


whereas the cathode undergoes the electroreduction of the oxidant O₂ *i.e.*:



where *E*^{°1} and *E*^{°2} are the electrode potentials *versus* the Standard Hydrogen Electrode (SHE)

This corresponds to the overall combustion reaction of H₂ in O₂:



with the thermodynamic data under standard conditions, Δ*G* = - 237 kJ mole⁻¹

If one considers that the standard electromotive force (EMF), *E*[°]_{eq} at equilibrium is:

$$E^\circ_{\text{eq}} = -\frac{\Delta G}{nF} = \frac{237 \cdot 10^3}{2 \times 96485} = E^\circ_2 - E^\circ_1 = 1.23 \text{ V} \quad (4)$$

The development of a fuel cell requires the control of three parameters:

- The largest EMF that is possible. Assuming that the couple H⁺/H₂ has an electrode potential at 0 V vs. SHE, the scientific challenge must be focused on the oxygen electroreduction which may be done with a low overpotential.

- Active catalysts capable of performing a 4-electron oxygen reduction *i.e.* a direct conversion of O₂ to H₂O. Another pathway can occur with a 2-electron reduction route which proceeds through the production of intermediate species such as hydrogen peroxide. The occurrence of H₂O₂ not only decreases the electrical performances of the fuel cell but provokes the degradation of the mechanical properties of the membrane in the Membrane Electrode Assembly (MEA).
- In the durability test the cathode which runs at high potential must be stable for a long lifetime and fuel tolerant because of the crossover of the latter molecule through the membrane.

ORR kinetics is generally a very slow process. It can be speeded up according to the nature of the cathode material. The rate determining steps of the ORR will be discussed during this session of summer school according to the values that will be found from the following j-E equation:

$$\frac{1}{j} = \frac{1}{j_l^{\text{diff}}} + \frac{1}{j_l^{\text{film}}} + \frac{1}{j_l^{\text{ads}}} + \frac{1}{j_0 \left(\frac{\theta}{\theta_{eq}} \right) e^{(anF/RT)\eta}} \quad (5)$$

REFERENCES

- [1] A. Damjanovic, J. Electrochem. Soc., vol. 138 (1991), p. 2315
- [2] A. Damjanovic, V.I. Birss, D.S. Boudreaux, J. Electrochem. Soc., 138 (1991), p. 2549
- [3] A. Damjanovic, V. Brusić, Electrochim. Acta, vol. 12 (1967), p. 1171.
- [4] C. Coutanceau, M.J. Croissant, T. Napporn, C. Lamy, Electrochim. Acta, vol. 46 (2000), p. 579
- [5] J.X. Wang, N.M. Markovic, R.R. Adzic, J. Phys. Chem. B, vol. 108 (2004), p. 4127

E³

IC2MP - UMR CNRS 7285



SAM^{CAT}

DU SITE ACTIF AU MATÉRIAU CATALYTIQUE

Conception de matériaux catalytiques pour l'énergie et la dépollution de l'air et de l'eau

Step by Step Determination of Kinetic Parameters of the Oxygen Reduction Reaction on Carbon supported nanocatalysts

Boniface KOKOH, Professor



To keep the contact: boniface.kokoh@univ-poitiers.fr



Bulmer-Volmer current-potential relationship

$$j = j_0 \left[\exp \left(\frac{(1 - \alpha)nF}{RT} (E - E_{eq}) \right) - \exp \left(\frac{-\alpha nF}{RT} (E - E_{eq}) \right) \right]$$

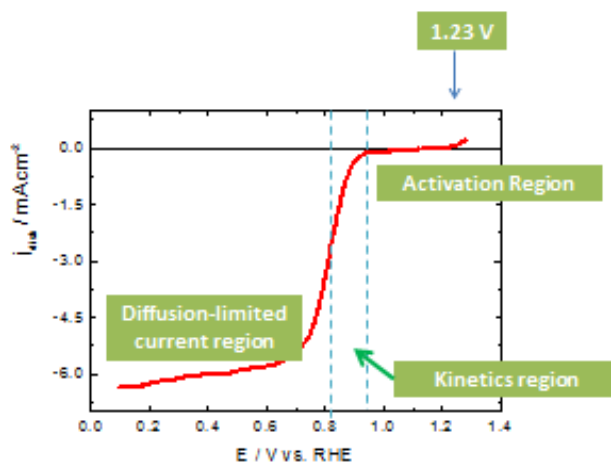
$$\eta = E - E_{eq}$$

E and E_{eq} : the applied and equilibrium potentials
n: the number of electrons transferred
F: Faraday's constant

R: the gas constant
T: the absolute temperature
j₀: exchange current density
α: the transfer coefficient (0 < α < 1) ≈ 0.5

Diffusion-limited current density

The Koutecky-Levich equation: $\frac{1}{j} = \frac{1}{j_k} + \frac{1}{j_L}$



Diffusion-limited current density

The Koutecky-Levich equation: $\frac{1}{j} = \frac{1}{j_k} + \frac{1}{j_L}$

$$\frac{1}{j_L} = \frac{1}{j_1^{\text{film}}} + \frac{1}{j_1^{\text{ads}}}$$

j_L is the Levich current density given by:

$$j_L = 0.201 n F C_{O_2} D_{O_2}^{2/3} \nu^{-1/6} \Omega^{1/2} = B \Omega^{1/2}$$

Ω is the rotation rate in rpm

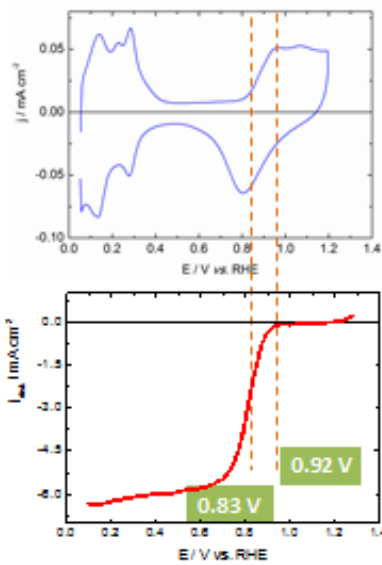
To minimise j_1^{film} at the preparation of the electrode :

film thickness $< 5 \mu\text{m}$:

F. Gloaguen et al., *Appl. Electrochem.*, 24 (1994) 863

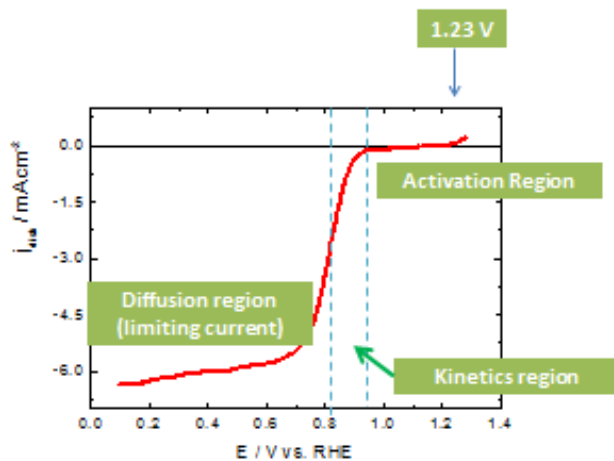
K.B. Kokoh et al., *J. Electrochem. Soc.*, 160 (2013) H302

Oxygen reduction reaction: potential domains



Pt/PtO contribution

Oxygen reduction reaction: mechanism and kinetics



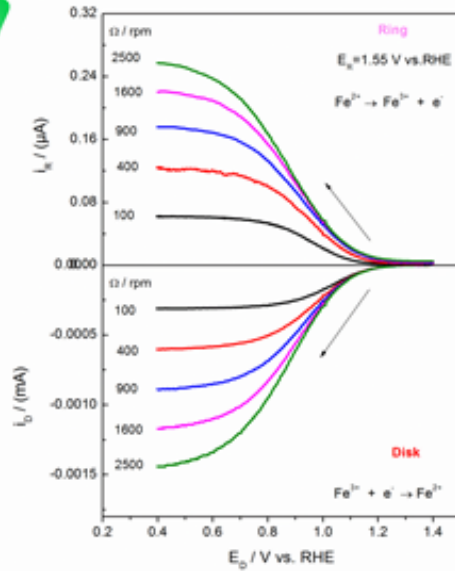
At a low current density range (high potential : $0.83 \text{ V} < E < 0.92 \text{ V}$) a Tafel slope is 60 mV/dec

On Pt/PtO surface: 2-electron procedure

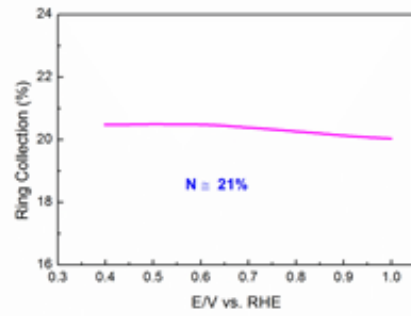
At a high current density range (low potential : $E < 0.83 \text{ V}$) a Tafel slope is 120 mV/dec

On pure Pt surface: the first electron transfer is the rds

Determination of collection efficiency (N) - RRDE



$$N = \frac{I_R}{I_D}$$



$E_R = 1.55 \text{ V vs. RHE}$

$0.1 \text{ mol L}^{-1} \text{ NaOH} + 0.01 \text{ mol L}^{-1} [\text{Fe}(\text{CN})_6]^{3-} \cdot 3\text{K}^+$

ORR Measurements with the RDE

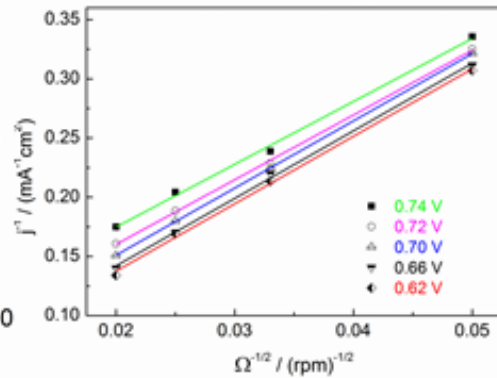
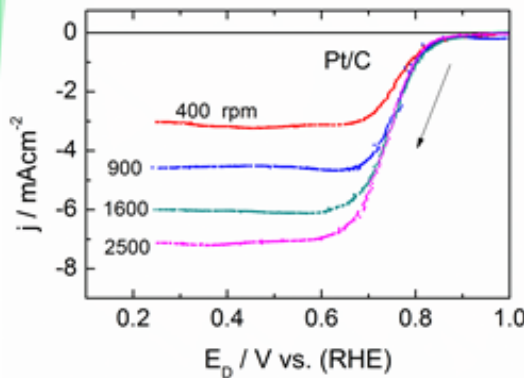
Levich Equation

$$j_L = 0.201nFC_{O_2}D_{O_2}^{2/3}v^{-1/6}\Omega^{1/2} = B\Omega^{1/2}$$

$0.1 \text{ mol L}^{-1} \text{ HClO}_4$

Ω in rpm

5 mV s^{-1}



Kinetic current measurement: j'_k

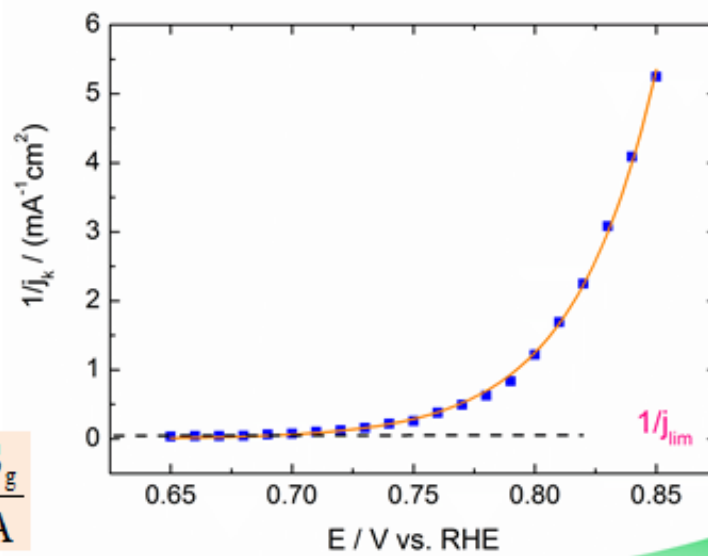
$$\frac{1}{j_k} = \frac{1}{j_L} + \frac{1}{j_0 \exp(\alpha n F / RT) \eta}$$

0.1 mol L⁻¹ HClO₄

S_g : geometric surface

A : active surface area

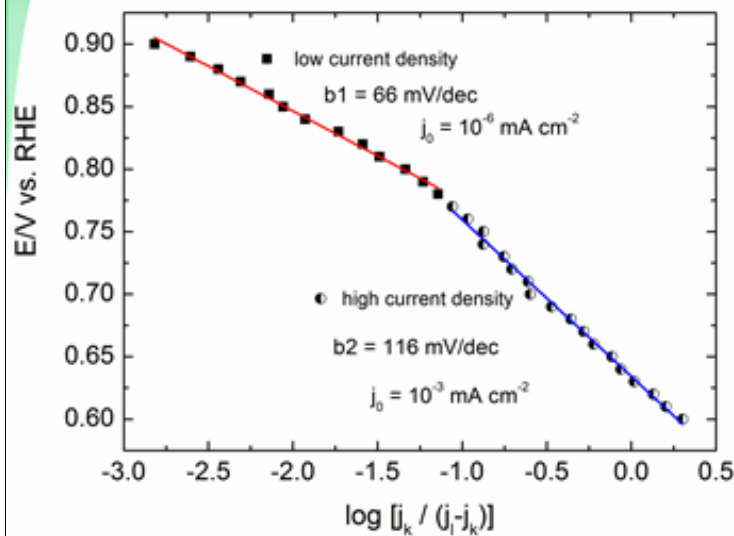
$$j'_k = j_k \times \frac{S_g}{A}$$



Measurements of Exchange current density (j_0) and b

$$\eta = E - E_{eq} = -b \left[\ln \frac{j_L}{j_0} + \ln \left| \frac{j_k}{j_L - j_k} \right| \right]$$

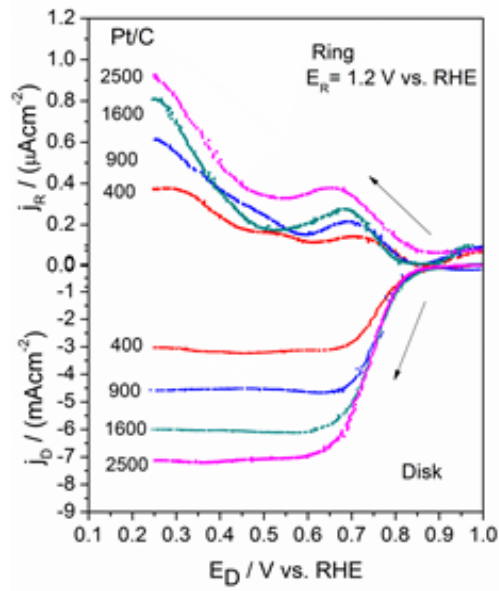
0.1 mol L⁻¹ HClO₄



$$b = 2.303 \times \frac{RT}{\alpha n F}$$

Kinetic parameters of the O₂ Reduction Reaction

0.1 mol L⁻¹ HClO₂



Rotating Ring Disk Electrode

Ring : Pt

Disk : herein Pt/C

$$n_e = \frac{4I_D}{I_D + I_R/N} = 3.9$$

CARBON SUPPORT CORROSION AND MEMBRANE DEGRADATION

Viktor Hacker, Alexander Schenk, Merit Bodner

Graz University of Technology, Inffeldgasse 25 C, A-8010 Graz, Austria
viktor.hacker@tugraz.at

Keywords: PEFC, lifetime, durability, rapid ageing

INTRODUCTION

Polymer electrolyte fuel cells (PEFCs) generate electrical power at very high efficiencies and are considered to play a major role in a future sustainable society. In particular, there is a high interest for using PEFC technology in automotive applications and combined heat and power (CHP) units in residential applications. The required lifetime for PEFCs ranges from 5,000 hours for mobile applications to 80,000 hours for stationary applications. However, commercial systems do not fully live up to the expectations yet. Limitations in lifetime and performance of PEFCs are mainly caused by the degradation of the materials contained in the membrane electrode assembly (MEA). In general, the degradation of the MEA can be distinguished into either membrane or electrode degradation. Both events are closely related to undesirable operating conditions in PEFCs. Impurities in the fuel and the oxidant, poor water management, agglomeration and migration of Pt, chemical reactions of cell components, carbon-support degradation, and hydrogen and air starvation strongly affect the integral stability of the MEA.

In order to improve the operational life of PEFCs, it is necessary to gain a deeper understanding of each PEFC degradation failure mode and their mechanisms.

DEGRADATION IN FUEL CELLS

• MEMBRANE DEGRADATION AND PINHOLE FORMATION

Besides being the proton conducting electrolyte, the membrane also separates anode and cathode, thus blocking the crossover of the corresponding reactant gases. Such a crossover of the reactants would result in lower potentials and therefore a lower efficiency of the fuel cell. During fuel cell operation the membrane is exposed to thermal, mechanical and chemical stress. Undesirable operating conditions, such as operation at open circuit potential or low humidity can further lead to chemical degradation of the polymeric

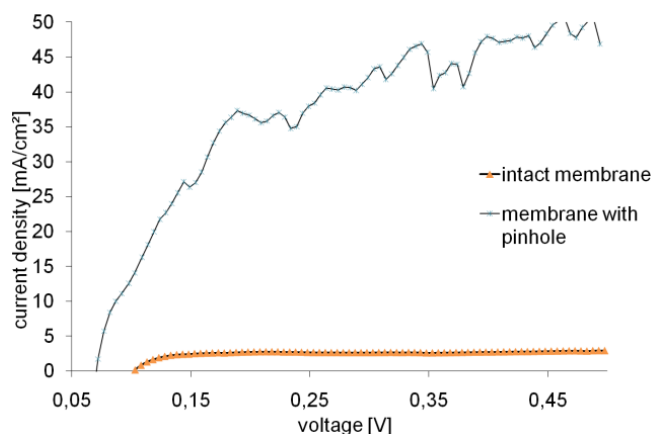


Fig1: Hydrogen diffusion current measurements

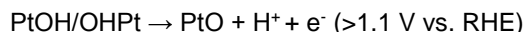
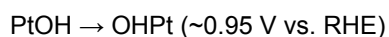
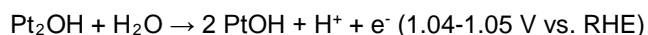
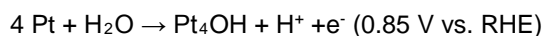
membrane, resulting in a thinning that can ultimately evolve into pinholes signing the end-of-lifetime of the cell. Furthermore, pinholes and cracks can be introduced to the membrane by mechanical stressors either within the fuel cell, during membrane manufacturing or during implementation in the fuel cell.

Areas of membrane thinning and pinholes result in a local increase of hydrogen crossover, which can be detected by measuring the hydrogen-crossover current density and by thermographic measurements.

- **ELECTROCATALYST DEGRADATION**

The dissolution and redistribution of the platinum electrocatalyst leads to particle growth and agglomeration and thus a loss of active catalyst surface area. Agglomeration is considered the most dominant mechanism of catalyst degradation and is driven by the reduction of the high surface energy of the catalyst particles.

Platinum dissolution is triggered by intermediate to high potentials in the range of 0.85 to 1 V. At potentials exceeding 1.1 V, a highly stable PtO phase is formed.



If dissolved, platinum ions from the cathode catalyst may also be transported through the membrane, where they are reduced in the presence of hydrogen, forming metallic aggregates. There, platinum can no longer contribute to the electrochemical conversion of the gases.

- **CARBON SUPPORT CORROSION**

The catalyst carbon support corrosion is a critical issue in PEFC system operation. At higher operating temperature like in the PAFC (200°C), it is necessary to use highly corrosion resistant graphitized carbon support. For ideally operated PEFCs, the carbon support corrosion is negligible in the normal operation mode and at normal cathode potentials.

Damaging operating conditions including high water content, acidic environment and high potentials exceeding 1 V, lead to carbon corrosion, resulting in a decreasing active area of the active catalyst surface.

In the absence of fuel or during fuel starvation following reactions take place on the anode side:



The reaction at the cathode side is not influenced by fuel starvation on the anode side:



In order to determine damaging influences on the PEFC it is necessary to know the local operating conditions in the cell. Since most damages occur local (e.g. carbon corrosion), these conditions have to be investigated spatially resolved.

MEASUREMENT TECHNIQUES

- Hydrogen-crossover measurement

In order to determine membrane thinning and the formation of pinholes or cracks in the membrane, typically the anode is fueled with hydrogen while the cathode is fueled with nitrogen or any other inert gas instead of air. The potential of cathode is then varied in the potential window of 100-450 mV and the corresponding hydrogen oxidation current density is recorded. In a fully functioning fuel cell, the current density in a hydrogen-crossover measurement is limited by the diffusion of the hydrogen through the (intact) membrane, i.e. higher cathode potentials do not result in a higher current density. However, after the events of membrane thinning or pinhole formation, the hydrogen is directly transported through the defects to the cathode resulting in an increasing current density with increasing voltage (see Fig 1).

- Accelerated stress test

Accelerated stress tests (ASTs) are a powerful tool for determining the influence of different failure modes on the overall PEFC lifetime. Depending on the applied AST protocol specific defective modes can be provoked in the MEA and subjected to characterization. For example, the applied electrode potentials, especially at the cathode, the operating temperature and the water content in the fuel cell have strong impacts on integral stability of the catalyst nanoparticles and the high surface area carbon support material. Additionally to the above mentioned factors, which influence the electrode stability, the availability of reactant gases at the catalyst layer in the MEA is of high importance. Fuel starvation, i.e. insufficient supply of reactant gases, can occur during high current density operation and leads to a severe degradation of the carbon support material. During periods of fuel starvation, all hydrogen fed to the fuel cell is oxidized near the anode inlet. To maintain the current, the carbon support is oxidized instead. This phenomenon is called carbon corrosion. Carbon corrosion further occurs during start-up events, where oxygen is purged from the anode side. This transient fuel starvation induces severe carbon corrosion. Typically, carbon corrosion is detected by measuring the CO and CO₂ content in the anode and cathode outlets.

- CURRENT DENSITY DISTRIBUTION - SEGMENTED CELL

A uniform degradation of the active area increases the life expectancy of fuel cells considerably and is therefore an important parameter with respect to the future utilization in commercial applications. Fig. 2 shows a segmented polymer electrolyte fuel cell for local analyses of cell degradation phenomena.

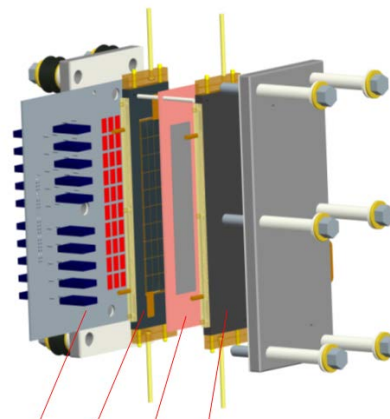


Fig. 2: Design of a 25 cm² segmented fuel cell: 1) current collector with resistors, 2) segmented cathode plate, 3) MEA, 4) anode plate.

- Infrared thermography

Infrared thermography is a convenient method to investigate membrane defects. One side of the membrane-electrode-assembly is exposed to hydrogen diluted in nitrogen, while the other side is open and exposed to ambient air. When hydrogen crosses over through pinholes or areas of membrane thinning, it reacts with oxygen on the platinum catalyst surface, thus producing water and heat. The locally increased temperature can then be detected by infrared thermography (see Fig 4).

EXPERIMENTAL INVESTIGATIONS

- Membrane degradation

A pinhole was introduced in the membrane at the cathode inlet using a 0.8 mm needle. The effect was determined by electrochemical characterisation and infrared thermography. While there was only a small effect noted under normal operation conditions (Fig. 3,1), the hydrogen diffusion current was clearly raised locally for the perforated MEA (Fig.3,2).

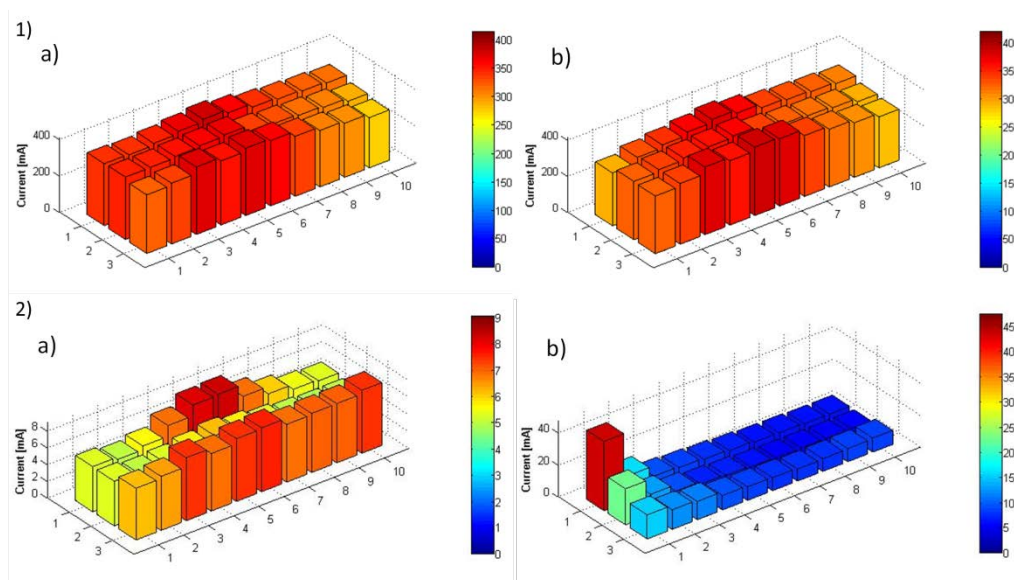


Fig. 3: Current distribution 1) at 400 mA/cm² and 2) hydrogen diffusion measurement at 430 mV for a) a pristine MEA and b) a MEA perforated at segment 1.

It was possible to localise the perforated area by both segmented cell and infrared thermography. Latter further has the advantage, that it is possible to make better assumptions on the exact location and the size of the pinhole. Also, a distinction between pinholes and areas of membrane thinning is possible. The pinhole is easily distinguishable in Fig. 4 b.

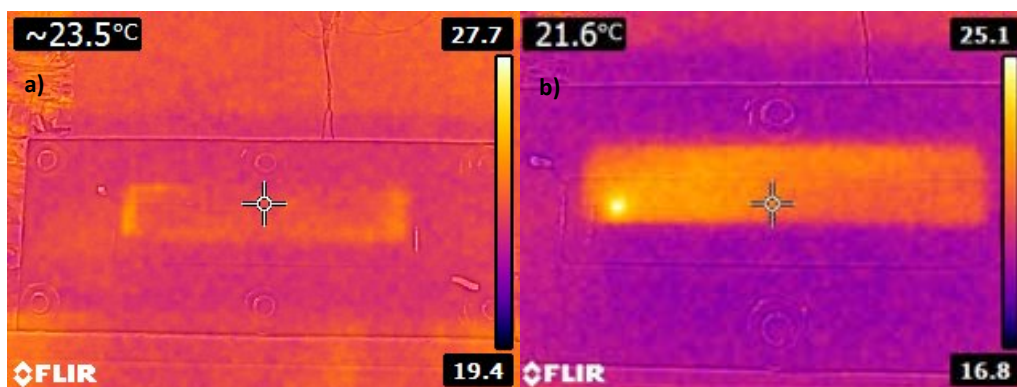


Fig. 4: Infrared thermography for a) a pristine MEA and b) a MEA perforated at segment 1.

• PLATINUM CATALYST DEGRADATION

In order to determine the stability of platinum catalysts electrochemical studies were carried out by using the thin-film method on a rotating disk electrode (RDE) in a standard electrochemical 3-electrode glass cell set-up. A commercial Pt/C catalyst sample was subjected to potential cycling according to a standard AST protocol (Fig 5). For this purpose, the electrodes were cycled 1665 times between 0.5 and 1.4 V_{RHE} in deaerated 0.1 M HClO₄ at a scan rate of 500 mV s⁻¹. Every 555th cycle the electrochemical active surface area (ECSA) was determined. The loss of ECSA gives information on the stability of the electrocatalysts. Fig 5 shows representative results from catalyst degradation testing. Typically, the Pt/C catalysts lost approx. the half of their electrochemical active surface area, indicating the need for further catalyst stabilization measures.

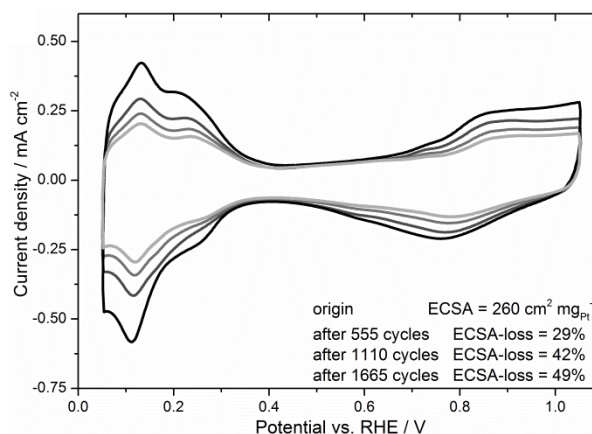


Fig.5: Degradation of a standard Pt/C catalyst during AST cycling [3]

• CARBON CORROSION

A MEA was perforated five times near the cathode inlet and the middle section with a 0.45 mm needle and underwent five 10 s cycles of fuel starvation, during which the anode off-gas was analysed.

During fuel starvation, the CO₂ content is increased due to carbon corrosion (Fig.6). However, more carbon support is oxidised during starvation in the defective MEA than in the pristine MEA, thus the carbon corrosion, evident from the carbon emission rate, was clearly increased after perforation of the membrane.

The increasing reactant cross over was also evident from the gas analysis. The oxygen content in the anode off-gas was significantly raised after perforation of the membrane.

This could be a phenomenon due to the excessive cross over after the perforation of the membrane, or could be due to electrolysis caused by cell reversal during fuel starvation.

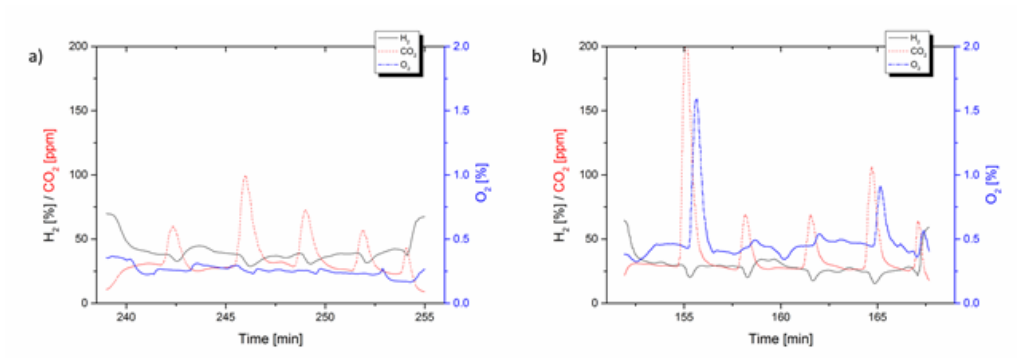


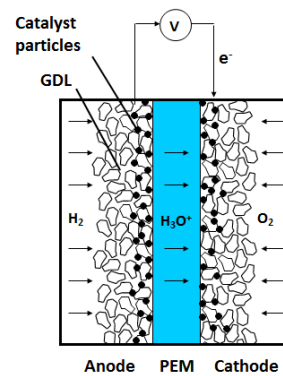
Fig. 6: Anode off-gas analysis of a) a pristine MEA and b) a MEA perforated five times.

REFERENCES

- [1] M. Bodner, C. Hohennauer, V. Hacker, "Effect of Pinhole Location on Degradation in Polymer Electrolyte Fuel Cells", submitted in Journal of Power Sources, June 2015
- [2] L. Dubau, L. Castanheira, M. Chatenet, F. Maillard, J. Dillet, G. Maranzana, S. Abbou, O. Lottin, G. De Moor, A. El Kaddouri, C. Bas, L. Flandin, E. Rossinot, N. Caque, "Carbon corrosion induced by membrane failure: the weak link of PEMFC long-term performance" in International Journal of Hydrogen Energy 39 (2014) 21902-21914
- [3] A. Schenk, C. Grimmer, M. Perchthaler, S. Weinberger, B. Pichler, C. Heinzl, C. Scheu, F.-A. Mautner, B. Bitschnau, V. Hacker, "Platinum-Cobalt Catalysts for the Oxygen Reduction Reaction in High Temperature Proton Exchange Membrane Fuel Cells – Long Term Behavior Under Ex-situ and In-situ Conditions" in Journal of Power Sources 266 (2014) 313-322

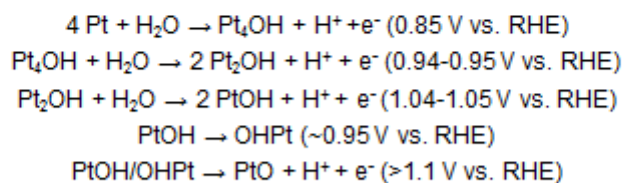
Degradation in PEFCs

- Contamination
 - Ionomer
 - Catalyst
- Electrode Degradation
 - Loss of active catalyst surface area
 - Degradation of PTFE and ionomer in the electrode
 - **Carbon corrosion**
- Membrane Degradation
 - Loss of the ion conductive moieties
 - **Membrane thinning**
 - **Pinhole formation**



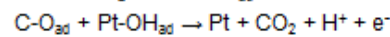
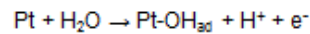
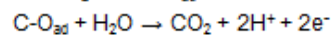
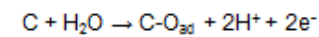
Loss of Catalyst Active Area

- Ostwald ripening (agglomeration of the Pt nanoparticles)
- Reduction of dissolved Pt in the membrane
- Accelerated by high temperatures and humidity
- Potential dependent

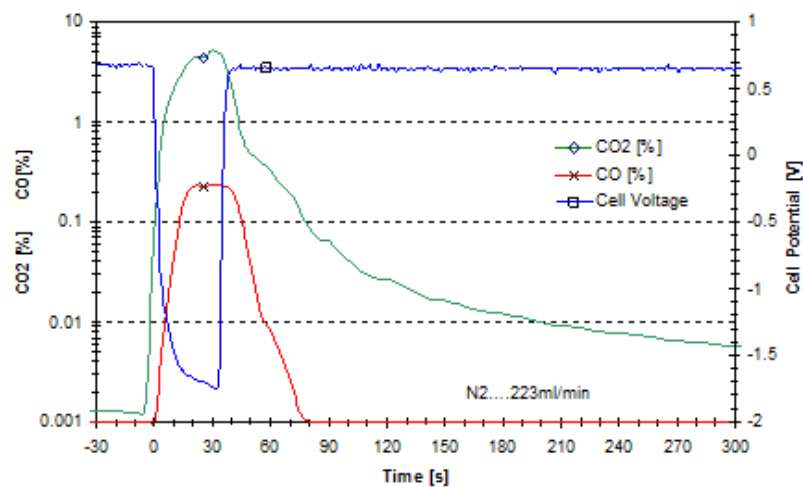


Carbon Corrosion

- Carbon support of the catalyst, carbon backing layer and carbon based bipolar plates
- This is accelerated by high temperatures, low pH-values and high humidity
- Potential dependent

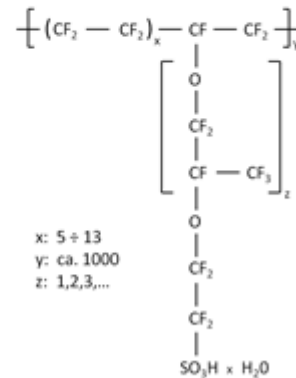


CO₂/CO Emissions at the Anode Side



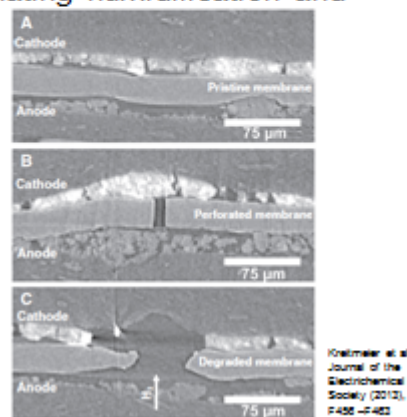
Membrane Thinning

- A result of chemical degradation
- PTFE backbone is degraded at high temperatures
- Accelerated by the formation of H_2O_2 and HNO_3



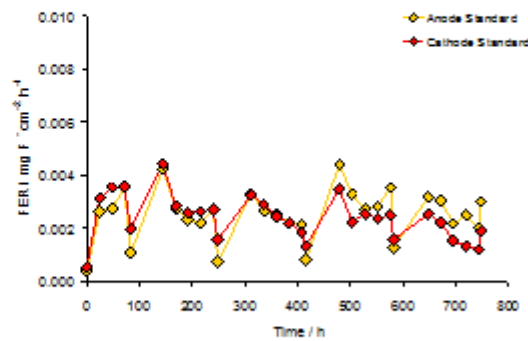
Pinhole Formation

- Due to mechanical tension, especially in thin membranes
- Accelerated by low and alternating humidification and high temperatures

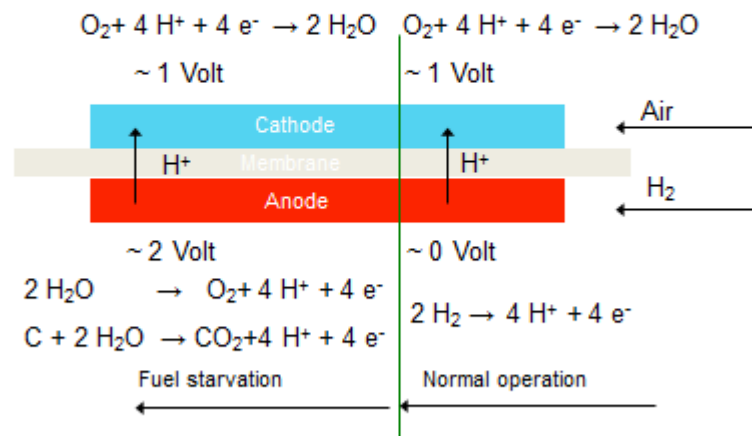


Fluoride Emission Rate

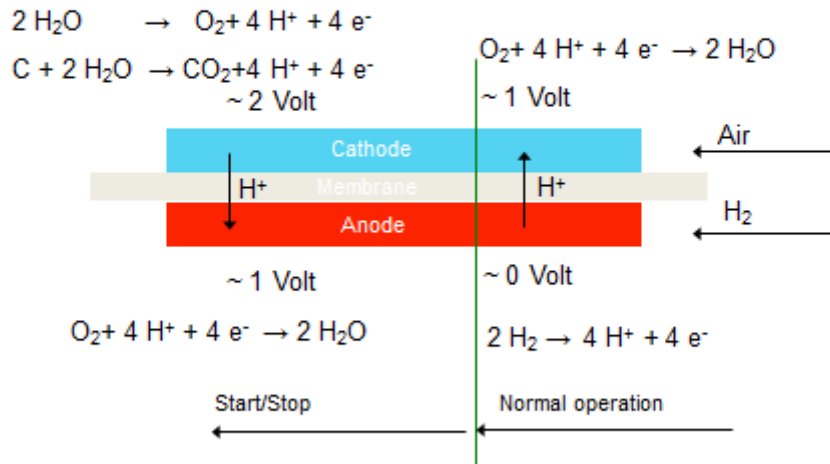
- Fluoride emission rate measured in the anode and cathode exhaust water
- Analysis with a fluoride selective electrode
- FER in the anode and cathode exhaust water nearly the same
- FER slightly decreasing with operating time



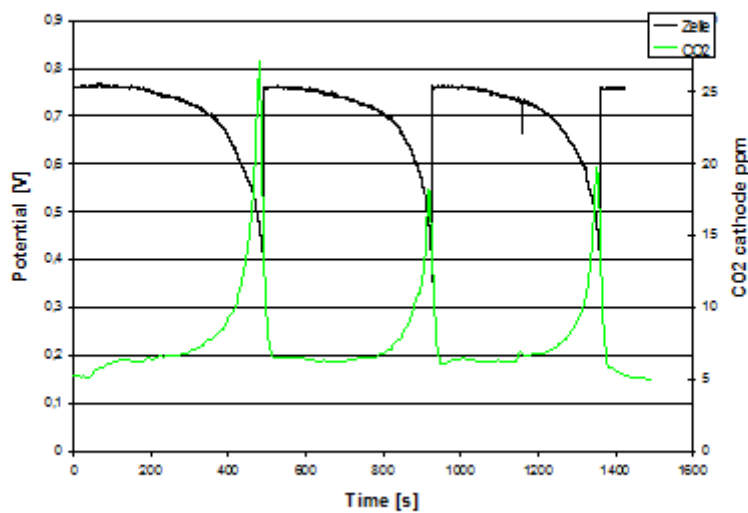
Operation under low Anode Stoichiometry



Start/Stop Operation



Cell Potential at Dead End Operation



SYNTHESIS METHODS OF CARBON SUPPORTED NANOCATALYSTS FOR FUEL CELL APPLICATIONS

Teko W. Napporn

IC2MP, UMR CNRS 7285, Université de Poitiers, 4 rue Michel Brunet, B27 - 86022 Poitiers cedex, France

e-mail: teko.napporn@univ-poitiers.fr

Keywords: Synthesis methods; colloidal synthesis; nanoelectrocatalysts; Proton Exchange Membrane Fuel Cell

INTRODUCTION

During the last twenty years, a significant improvement in performance has been observed for Proton Exchange Membrane Fuel Cells (PEMFC) systems, because of the extensive research development on efficient electrodes materials. From this development, the methods proposed by different research groups are expected to produce metallic-nano-sized particles with a controlled size distribution. Consequently, the noble metal loading has considerably decreased [1] and the active surface area increased.

Most of the synthesis methods proposed are based on wet chemistry mainly on colloidal synthesis. In order to control the particles size, structure and/or morphology, the germination process and the particles growth become important steps which need to be carefully managed.

In the present lecture, various electrocatalysts synthesis methods such as Bönemann method [2, 3], water-in-oil microemulsion [4-6], polyol methods with thermal [7] or microwave activation [8], instant method [9], bromide anions exchange method [10] will be presented. Step by step, the methodology for performing these syntheses is also described. The influence of the material structure and morphology will be discussed based on the physical, chemical and electrochemical characterizations measurements. The correlation between the activity and the selectivity of the nano-scale supported electrocatalysts e.g. Pt/C catalysts to their morphology and structure is an objective which should drive the development of fuel cells systems [11]

REFERENCES

- [1] M. Cavarroc, A. Ennadjaoui, M. Mougnot, P. Brault, R. Escalier, Y. Tessier, J. Durand, S. Roualdes, T. Sauvage, C. Coutanceau, *Electrochem. Commun.*, 11 (4) (2009) 859-861
- [2] L. Dubau, F. Hahn, C. Coutanceau, J.-M. Léger, C. Lamy, *J. Electroanal. Chem.* 554-555 (2003) 407-415.
- [3] R. Sellin, C. Grolleau, C. Coutanceau, J.-M. Leger, S. Arrii-Clacens, S. Pronier, J.-M. Clacens, *J. Phys. Chem. C* 113 (2009) 21735-21744.
- [4] Capek I., *Adv. Colloid Interface Sci.*, 110 (2004) 49
- [5] S. Brimaud, C. Coutanceau, E. Garnier, J.-M. Léger, F. Gérard, S. Pronier, M. Leoni, *J. Electroanal. Chem.* 602 (2007) 226-236.
- [6] D. Diabaté, T. W. Napporn, K. Servat, A. Habrioux, S. Arrii-Clacens, A. Trokourey and K. B. Kokoh, *J. Electrochem. Soc.* 160(6) (2013) H302-H308

- [7] C. Grolleau, C. Coutanceau, F. Pierre, J.M. Leger, J. Power Sources 195 (2010) 1569-1576.
- [8] E. Lebegue, S. Baranton, C. Coutanceau, J. Power Sources 196 (3) (2011) 920-927
- [9] Reetz, M. T. Schulenburg, H. Lopez, M. Splinthoff, B. Tesche, B. Chimia, 58, N°12, (2004) 896-899
- [10] P. Tonda-Mikiela, T. W. Napporn, C. Morais, K. Servat, A. Chen and K. B. Kokoh, J. Electrochem. Soc. 159(11) (2012) H828-H833.
- [11] C. Coutanceau, S. Baranton, T. W. Napporn, "The Delivery of nanoparticles", Chap. 19, p.401 in edited by Abbass A. Hashim, InTech Publisher 2012, Rijeka, Croatia. ISBN 978-953-51-0615-9.

Electrocatalysts preparation methods

Dr. Têko W. Napporn

CNRS' Research Scientist
French National Center for Scientific Research (CNRS)
University of Poitiers, France

Adjunct Prof. Chemistry of Hydrogen Energy conversion Unit
Institute of Advanced Sciences, Yokohama National University, Japan
teko-napporn@ynu.ac.jp

Permanent contact: teko.napporn@univ-poitiers.fr



Electrocatalysis and Fuel Cells

- Reactions at the fuel cells electrodes are controlled by electrocatalytic processes.
- The behavior of catalytic sites is determined by the surface **morphology, structure and composition**

Challenge is to control these parameters

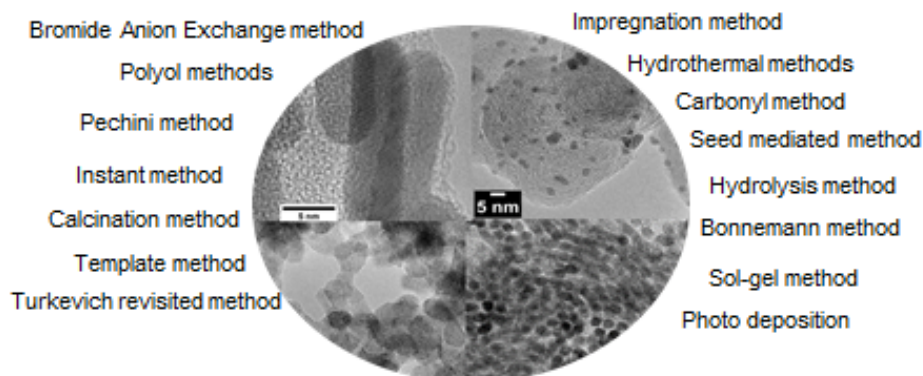
- Increase the active surface area
- Decrease or avoid noble metals contents

Find the adapted synthesis method for the desired electrodes

Several methods are proposed in the literature but all are not adapted for preparing active and suitable supported electrocatalysts for fuel cells and electrolyzers.



Some synthesis methods for electrocatalysts preparation

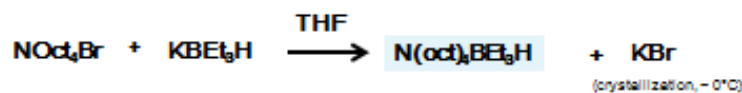


Design of nanomaterials

Bonnemann Synthesis Methods

3 different steps in **Anhydrous atmosphere**

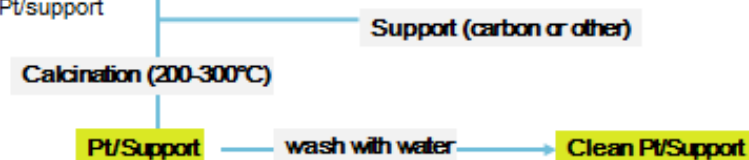
1 - Preparation of the reducing agent



2 - Preparation of the colloid precursor (example : reduction of the Pt salt)

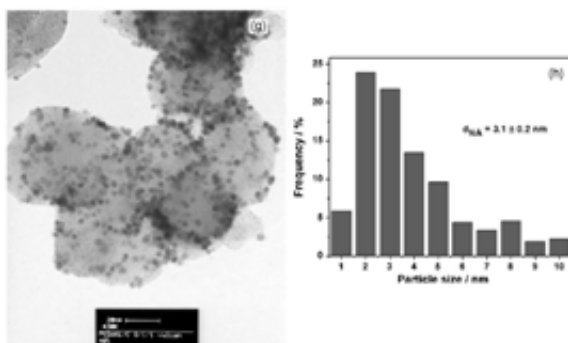


3 - Preparation of Pt/support



Bonnemann Synthesis Methods

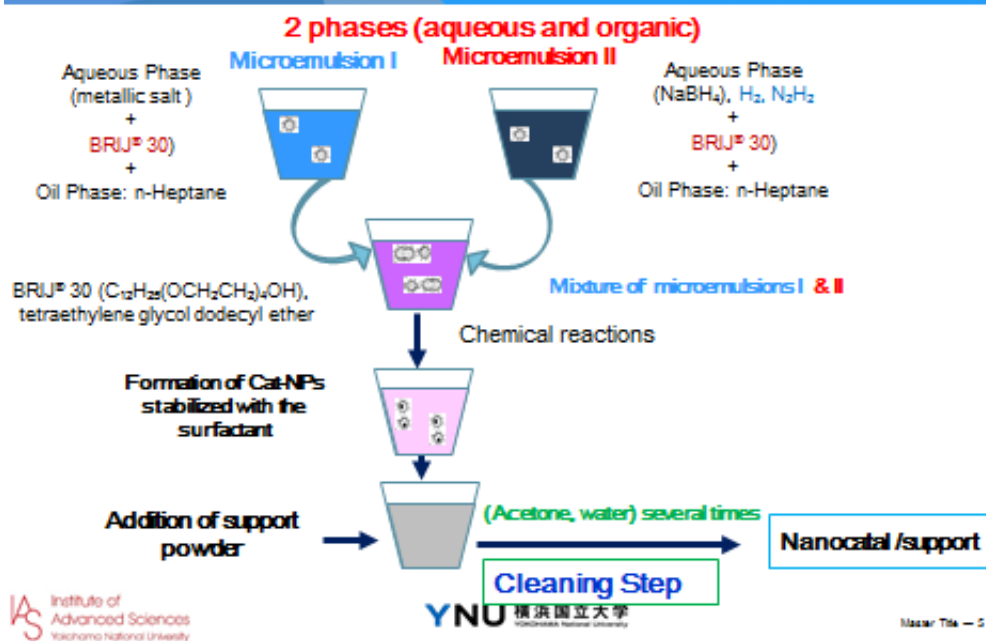
Possibility of multimetallic catalysts preparation



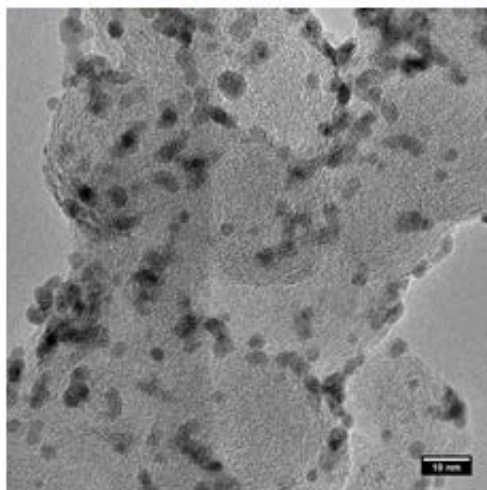
Pt₈₀Sn₁₀Ni₁₀/C as anode for direct ethanol fuel cell

from Bayhan S. et al. Appl. Catal. B: Environmental 130-1031(2013) 305-313

Water-in-oil Microemulsion Method (W/O)



Water-in-oil Microemulsion Method (W/O)



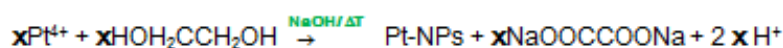
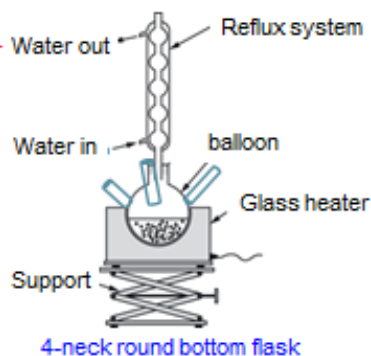
HRTEM micrograph of a Pd₇₀Ni₃₀ (20 wt. %)/C by the microemulsion route

from D. Diabate et al., J. Electrochem. Soc. 160(6) (2013) H302-H308

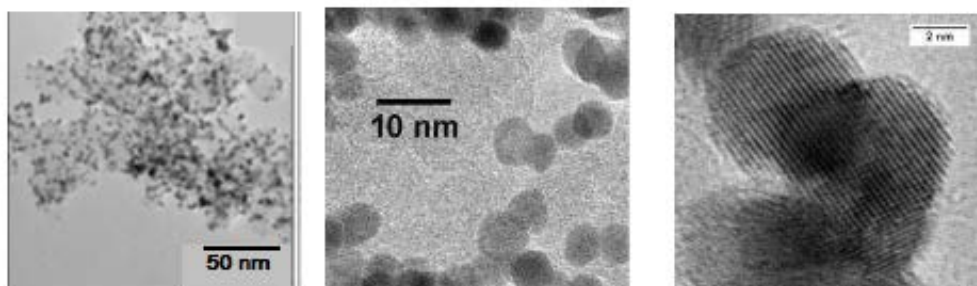
Polyol Synthesis Method

- 1 phase (organic, ethylene glycol or related compounds)
- Avoid the presence of water or control the ratio EG/Water
- pH is also important parameter
- Control of the temperature

- Critical step: seed growth
(pH, atmosphere, other surfactant...)
- Microwave assisted ...

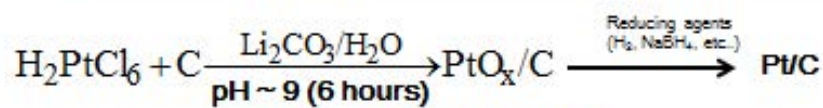


Polyol Synthesis Method

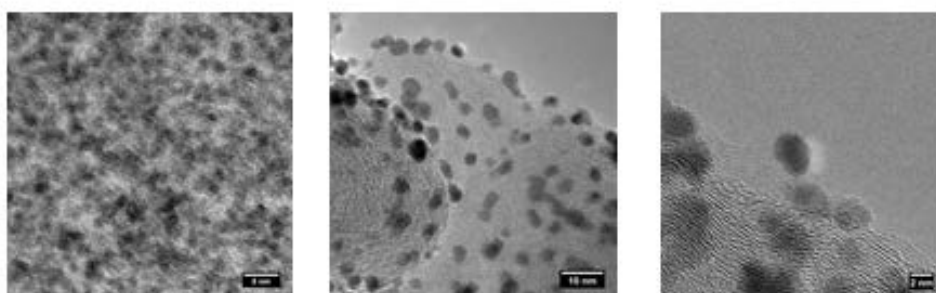


(a) and (b) TEM images at different magnifications, and (c) HRTEM micrograph for a Pt(40 % w/w)/C prepared from the polyol method at 200 °C for 2 hours.

Instant Method

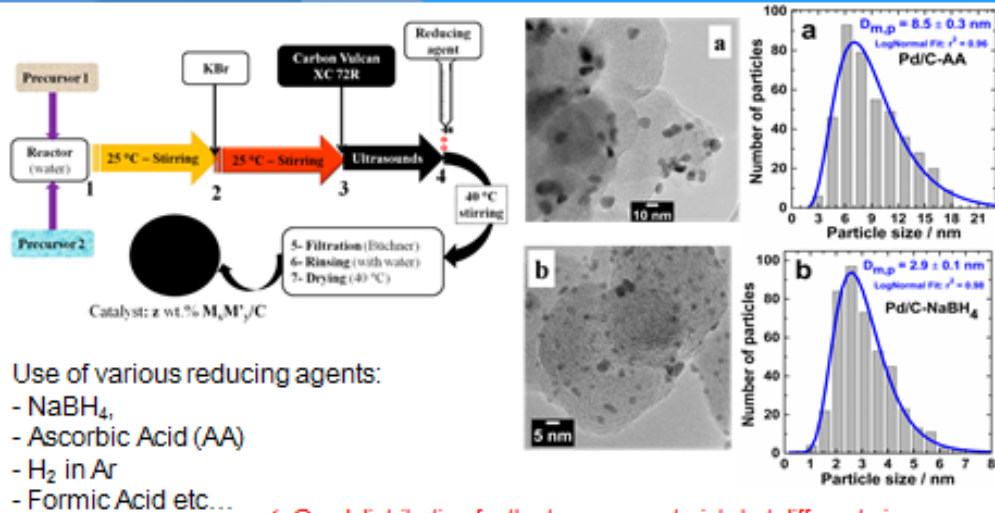


Surfactant free, clean catalysts



(a) TEM image of PtOx, TEM image (b) and HRTEM image (c) of Pt/C catalysts obtained from "instant method" at 40 °C, metal loading 40% w/w

Bromide Ion Exchange Method



✓ Good distribution for the two nanomaterials but different sizes

✓ How to make the good choice of the reducing agent ?

BASIC OF THE ELECTROCHEMICAL MEASUREMENTS

Shigenori Mitsushima

79 – 5 Tokiwadai, Hodogaya-ku, Yokohama 240-8501 JAPAN, mitsushi@ynu.ac.jp,

Keywords: fuel cells, electrochemical measurements, electrocatalyst, electrode

INTRODUCTION

Electrochemical measurements are very strong tool to evaluate fuel cells and their components such as electrocatalysts, catalyst layers, and gas diffusion electrodes. An electrochemical system consists of two electrodes that are electronic conductor and an electrolyte which connect two electrodes by ionic conduction. In general, the two electrodes were named an anode that oxidizes the reduced form and a cathode that reduces the oxidized form.

In the electrochemical measurements, a reaction polarization, such as a charge transfer polarization at an interface between an electrode and an electrolyte, a mass transfer polarization near an electrode surface, or an ionic resistance polarization of electrolyte, is wanted to be determined separately. In addition, the polarizations are time functions because of poison, degradation, and others. Electrochemical measurements are also applied to the determination of performance related parameters such as effective electrochemical surface area, hydrogen crossover through the electrolyte membrane, and others.

For the correct determination, basic of electrochemical measurements is important. In this chapter, basic equipment's of electrochemical measurements and basic technique of half-cell measurements is introduced.

BASIC EQUIPMENT

In half-cell measurement, the electrodes are named a working electrode that is determined by the measurement and a counter electrode that flows opposite current to the working electrode. Figure 1 shows the schematic drawing of 3-electrodes electrochemical cell with their potential profile image. Using 2-electrode system that has no reference electrode can measure current and cell voltage that is potential difference between the working and the counter electrodes. The relationship between current and cell voltage is affected by interfaces between the working electrode and the electrolyte, another interface between the counter electrode and the electrolyte, and the ionic resistance between the working and the counter electrodes. The 2-electrode system cannot determine polarization of the interface between the working electrode and the electrolyte that is what you want to know, individually. For 3-electrode system, the current is loaded between the working and the counter electrodes. In this case, a voltage between the reference electrode and the working electrode, which is affected by

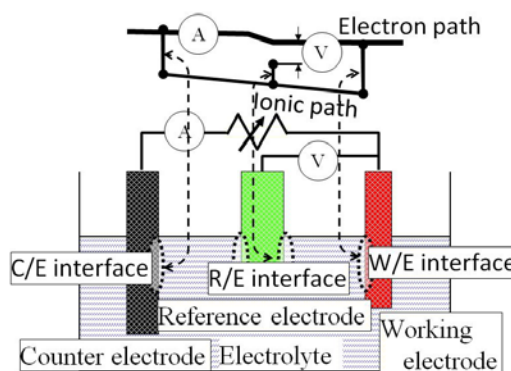


Fig. 1 Schematic drawing of 3-electrode electrochemical cell with their potential profile image.

an interface between the working electrode and the electrolyte, can be measured. Here, the polarization of the interface between the reference electrode and the electrolyte are constant value, because the current of this interface is controlled small enough to be free from change of polarization. Therefore, voltage measurement technique that is free from electrolyte resistance is needed.

Figure 2 shows the schematic drawing of the Luggin capillary, which minimize iR drop between the reference electrode and the working electrode. It can put around $2d$ distance from the working electrode. Here, d is diameter of a top of the Luggin capillary and $2d$ is the nearest distance without the effect of the Luggin capillary on the current flow of the working electrode. In the Luggin capillary, there is no current, so it is free from iR drop. Therefore, iR is affected by the resistance of only $2d$ distance. The iR corresponded to $2d$ distance is usually negligible, but some large current measurement is affected by the iR . Resistance of electrode itself, for example surface oxide, also affects measurements. These resistances, which cannot be removed by Luggin capillary, is called as uncompensated resistance, and shall be determined by another transient response measurements.

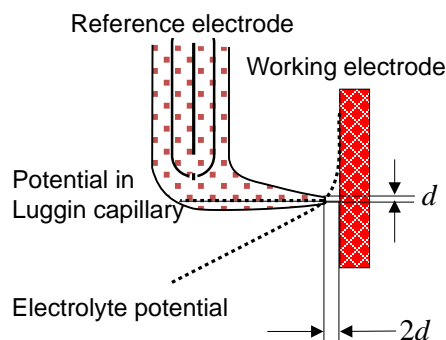


Fig. 2 Schematic drawing of the Luggin capillary.

The reference electrode must have ionic contact to the electrolyte, but the ionic resistance is usually very large to separate electrolyte between the chambers for the reference electrode and the working electrode. In order to accurate measurement, internal resistance of voltmeter must be huge. Figure 3 shows the equivalent circuit of voltage measurements. Now, you want to measure E_s with a voltage meter which internal resistance is R_x . Does R_s , which is internal resistance of the sample, affect to E_x which the voltmeter indicates? Here, the R_s may be corresponded to the resistance of the Luggin capillary, glass electrode of pH meter or something. If the R_s is equal to the R_x , the $E_s = 2E_x$. To make accurate measurement, $R_x \gg R_s$, and equipments for electrochemical measurements has large internal resistance. How can you determine the internal resistance of the equipments? Figure 3 has an answer of this problem. Put a primary battery to E_s which voltage was already measured by your voltmeter, and use R_s that has large resistant to decrease of the E_x more than 10% of E_s . Here, the R_x is given by

$$R_x = \frac{R_s}{E_s/E_x - 1} \quad [1]$$

The potentiostat, which is an electrochemical equipment, satisfy all these requirements and control the potential between the reference and the working electrodes.

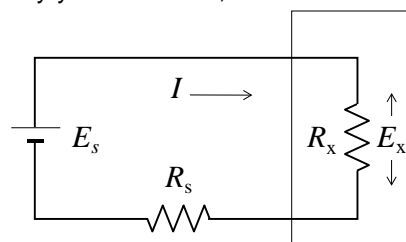


Fig. 3 Equivalent circuit of voltage measurements.

BASIC TECHIQUE FOR HALF CELL MEASUREMENTS

Figure 4 shows various potential patterns for electrochemical measurements. Here, a), b), c), and d) are used for cyclic voltammetry, linear sweep voltammetry,

chronoamperometry, and electrochemical impedance spectroscopy, respectively. These methods shall be selected by the subject of the measurements using nature of electrochemical system. The detail is written many textbooks of electrochemical measurements [1].

Figure 5 shows the cyclic voltammogram of poly-crystalline Pt in sulfuric acid, and the behavior of the surface during the cyclic voltammetry in inert atmosphere. Below 0 V, hydrogen evolution reaction occurs. During positive sweep from 0.05 V, a monolayer of the adsorbed H is oxidized to H⁺, and desorbs with oxidation current up to 0.4 V. From 0.4 to 0.8V, only charge current of double layer is observed. From 0.9 to 1.5V, the Pt surface is oxidized. This behavior is not fully understood, because there are many oxide forms, such as PtOH, PtO, and PtO₂. Above 1.5 V, oxygen evolution reaction occurs. During negative scan, opposite reaction occurs, but reduction of Pt surface is concentrate around 0.8 V. This behavior is a characteristic of Pt. The H adsorption / desorption current is used for the measurement of the real surface area of Pt.

Usually, lower limit potential is selected at 0.05 V vs. RHE, and roughness factor (*R.F.*), which is the real surface area per the geometrical surface area, is determined with following equation with 100% of H coverage.

$$R.F. = \frac{(Q_H^a)_{geom} / \text{mC cm}^{-2}}{(0.21)_{real} / \text{mC cm}^{-2}} \quad [2]$$

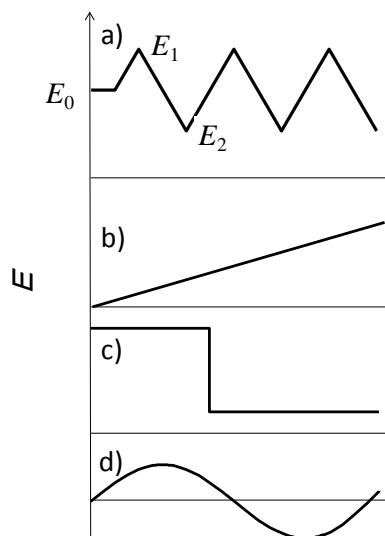


Fig. 4 Potential patterns in measurements.

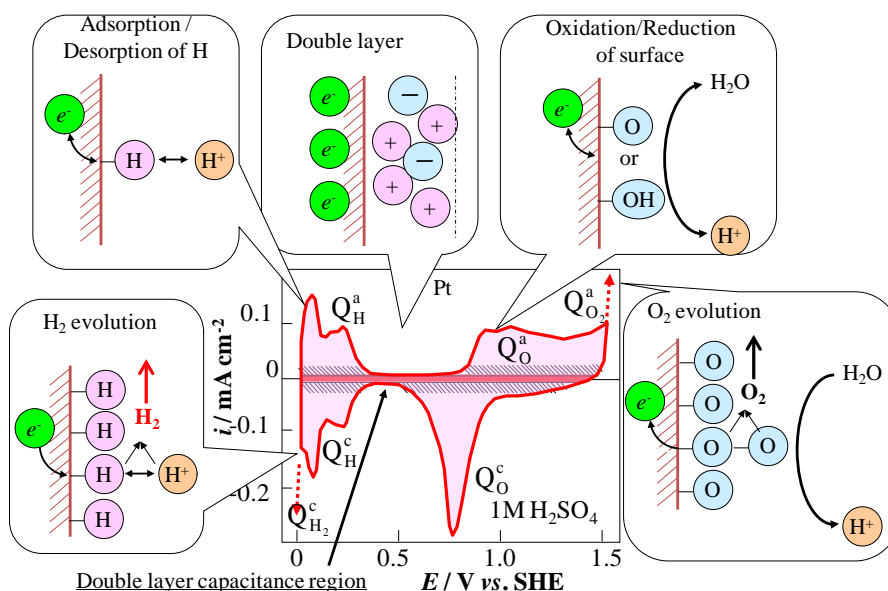


Fig. 5 Cyclic voltammogram of Pt and the behavior of the surface.

Here, $(Q_H^a)_{geom}$ and $(0.21)_{real}$ are hydrogen desorption charge per geometrical surface area for the sample and real surface area for platinum, respectively. In order to be free from hydrogen evolution reaction, lower limit potential is selected at 0.08 V vs. RHE, and the *R.F.* is determined with following equation with 77% of H coverage [2].

$$R.F. = \frac{(Q_H^a)_{geom} / \text{mC cm}^{-2}}{0.7 \times (0.21)_{real} / \text{mC cm}^{-2}} \quad [3]$$

The relationship between H coverage and potential depend on material; therefore, in order to determine the *R.F.* of Pt alloys, eq. [2] and [3] are not accurate. As alternative methods of the *R. F.* measurement, CO stripping and Cu under potential deposition are sometimes employed. These techniques are selected with nature of samples.

In order to evaluate the catalytic activity of oxygen reduction reaction, slow scan voltammetry with a rotating disk electrode (RDE) is usually performed. Catalytic activity is a function of time, and then it is difficult to get steady state polarization curve for ORR because of adsorption of poison species. The slow scan voltammetry gives the ORR current as a function of potential with good reproductively. Figure 6 shows the slow scan voltammogram of $12 \mu\text{g cm}^{-2}$ -Pt of Pt/C on a glassy carbon disk electrode at 25°C in O_2 . Sweep rate and rotating speed were 0.05 Vs^{-1} and 900 rpm, respectively. The dashed dot line shows the diffusion limit current for ORR. The current increased with the decrease of potential in the potential region from 0.8 to 1.0 V vs. RHE. The ORR current is the current difference between in O_2 and N_2 . The onset potential of negative scan for the ORR is lower than that of positive scan. In the negative scan, the onset potential is the reduction potential of surface oxide that forms higher potential region. In the positive scan, Pt surface is not oxidized at the onset potential in the negative scan. Therefore, the catalytic activity of the positive scan seems to be higher than that of the negative scan. Recently, most of researchers use the positive scan to determine the catalytic activity of the ORR.

In order to evaluate catalytic activity, kinetic current, which is free from mass transfer, must be determined. RDE method is one of hydrodynamic voltammetry to evaluate kinetic

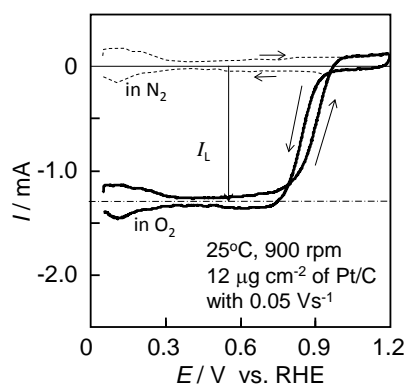


Fig. 6 Slow scan voltammogram of Pt/C for oxygen reduction reaction using rotating disk electrode.

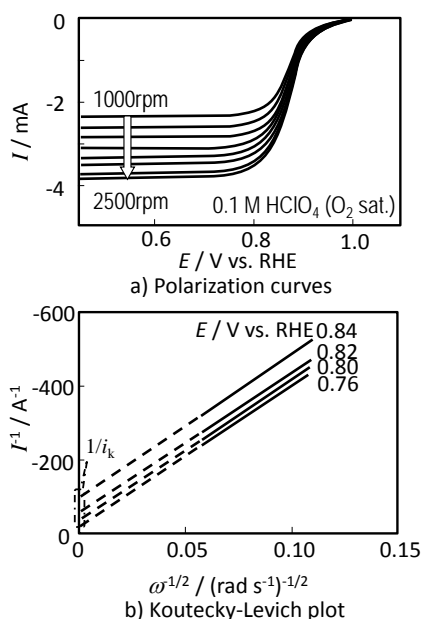


Fig. 7 Polarization curves and Koutecky-Levich plot for oxygen reduction reaction using rotating disk electrode.

current. A simple equation to obtain kinetic current is as follows

$$I_k = (I I_L) / (I_L - I) \quad [4]$$

Here, I , I_L and I_k are faraday current, diffusion limit current and kinetic current, respectively. Formal method may use Koutecky-Levich plot from RDE measurements. The theory of the RDE measurement is based on planer disk electrode. Therefore, catalyst layer on a glassy carbon must be thin and uniform, and catalyst loading is usually in the range from 10 to 30 $\mu\text{g cm}^{-2}$ -Pt. Figure 7 shows polarization curves and Koutecky-Levich plot for ORR. Diffusion limit current increased with rotating speed. Relationship between faraday current and rotating speed is expressed as follows

$$1/I = 1/I_k + 1/0.320nFAcD^{2/3} \nu^{-1/6} \omega^{1/2} \quad [5]$$

Here, n , F , A , c , D , ν , and ω are number of electron for the reaction, Faraday's constant, electrode area, concentration of the reactant, diffusion coefficient of the reactant, viscosity of the electrolyte, and rotating speed, respectively. Therefore, the intercept of $\omega^{1/2}$ axis is inverse of the kinetic current in Koutecky-Levich plot.

Figure 8 shows a chronoamperogram of Pt/C for ethanol electrooxidation reaction. The oxidation reaction current slightly decreases with time. Complete ethanol oxidation reaction produces CO_2 and H_2O with a 12-electron reaction; however, there are by-products such as CH_3CHO , CH_3COOH , and others. During these reactions, the surface of electrocatalyst is poisoned by intermediates, for example CO . In order to evaluate oxidation of hydrocarbons or alcohols, both catalytic activity and anti-poison property are needed, and shall be determined separately. Determination of products is also important. Potential sweep method is easy to get current – potential property, but it is difficult to separate activity and anti-poison property and to analyze reaction products at a potential. Therefore, chronoamperometry is useful in these subjects.

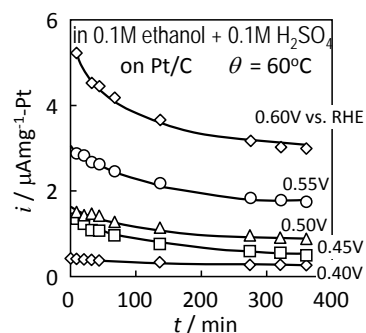


Fig. 8 Chronoamperogram of Pt/C for ethanol oxidation reaction.

APPLICATION TECHNIQUES FOR FUEL CELL MEASUREMENTS

In order to determine a membrane electrode assembly (MEA) of polymer electrolyte fuel cells (PEFCs), there are some specific techniques. In this section, some application techniques will be introduced. Generally, cell voltage (U) is described following equation.

$$U = U_{eq} - \eta_a - \eta_c - iR \quad [6]$$

Here, U_{eq} , η_a , η_c , i and R are equilibrium cell voltage, anode overpotential, cathode overpotential, current, and summation of ionic and electronic resistance. A three-electrode MEA is sometimes used to analyze the performance; however, a conventional two-electrode MEA is usually used because of difficulty of accurate potential measurement with a reference electrode of the three-electrode MEA places beside the cathode or anode. In order to determine the η_a and η_c , the R must be divided to the anode and cathode sides; however, it is difficult that the determination of actual position of the reference electrode between the anode and cathode. Furthermore, the η_a is much smaller than the η_c if pure hydrogen is used as fuel. In this case, the η_a is negligible from the eq. [4], and the R is measured with current interact method or AC impedance spectroscopy. Then, the η_c can be evaluated independently.

In the determination of the membrane electrodes assembly (MEA) of polymer electrolyte fuel cells, the real surface area of the cathode is determined with anode that works as the counter and the reference electrode. Humidified N_2 and H_2 are fed to cathode and anode, respectively. Schematic image of cyclic voltammograms for polycrystalline Pt in $1M H_2SO_4$ and Pt/C of MEAs is shown in Fig. 9. The potential region of scanning for polycrystalline Pt is usually between 0.05 to 1.5 V vs. RHE, and no significantly hydrogen and oxygen evolution reactions occur in this potential region (line (a)). The upper limit of MEAs is blow 1.2 V vs. RHE, because carbon support of Pt/C is oxidized higher potential region. (Line (b)). In this case, the oxidation and reduction charge above 0.5 V vs. RHE for the (b) is smaller than that for the (a), but hydrogen adsorption and desorption peaks below 0.4 V vs. RHE are almost the same for the (a) and (b). To determine cyclic voltammograms for MEAs, the feed of N_2 shall be stopped, otherwise hydrogen evolution reaction proceeds at higher potential, and the charges of hydrogen adsorption and desorption increase like line (c). Cyclic voltammogram can also determine hydrogen crossover through the membrane. If hydrogen reaches cathode, hydrogen oxidized and the cyclic voltammogram is observed as line (d), and the baseline of the cyclic voltammogram, which is line (e), is hydrogen oxidation current. The current around 0.5 V vs. RHE corresponds to the hydrogen crossover. In the lower potential region, hydrogen cannot be oxidized because of electrode potential. In the higher potential region, hydrogen cannot be oxidized because of catalytic activity of oxidized Pt surface, too. The surface area determined with cyclic voltammogram is called as electrochemical active surface area (ECSA), because this area has ionic conduction with ionomer to the counter electrode. Sometimes ECSA of MEA per ECSA of Pt/C in acid solution is called Pt utilization, which is an important parameter to evaluate catalyst layer.

In order to determine the internal resistance R in eq. [4], AC impedance spectroscopy or current interrupt method is applied. They use time response difference among transportation of electrons ($\ll ms$) and ions ($\ll ms$), charge separation at electrode – electrolyte interface ($\sim ms$), and formation of concentration distribution with mass

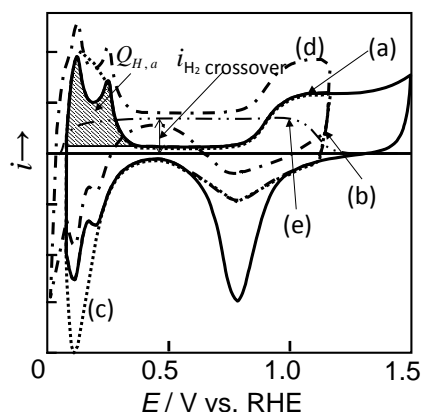


Fig. 9 Schematic image of cyclic voltammograms for (a) polycrystalline Pt in $1M H_2SO_4$, (b) Pt/C, (c) Pt/C with N_2 flow, (d) Pt/C with H_2 crossover, and (e) baseline of (d) for MEA.

transportation processes ($> s$). Figure 10 shows the typical AC impedance spectroscopy for fast reaction that has proportional region between overpotential and current. There is double layer at the interface between electrode and electrolyte, and it behaves like capacitor. Therefore, an equivalent circuit of the electrochemical system is expressed with Fig. 10 – b). Here, the C_d , R_{ct} , and R_s are capacitance of the double layer, charge transfer resistance, and ionic resistance of electrolyte, respectively. This equivalent circuit gives an arc in Cole-Cole plot that is imaginary part of the impedance $-Z_{Im}$ as a function of real part of the impedance Z_{Re} . An intercept to the real part at higher frequency side corresponds to the R_s , and another intercept to the real part at lower frequency side correspond to the $R_{ct} + R_s$. The maximum value of the $-Z_{Im}$ is equal to the $1/(R_{ct} C_d)$. Therefore, kinetic parameters of an electrochemical system can be evaluated with AC impedance spectroscopy. Detail of this treatment is explained in basic textbooks of electrochemistry [1].

The impedance spectroscopy of PEFCs is different from basic one. Typical electrochemical AC impedance spectroscopy for slow reaction with porous electrode such as oxygen gas diffusion electrode is shown in Fig. 11. Major differences are that the current is proportional to the exponential of overpotential, which is in Tafel region, and the

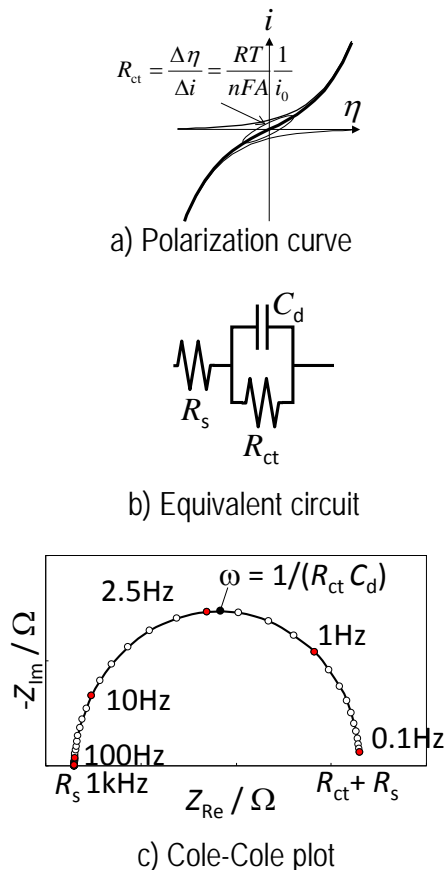


Fig. 10 Typical electrochemical AC impedance spectroscopy for fast reaction.

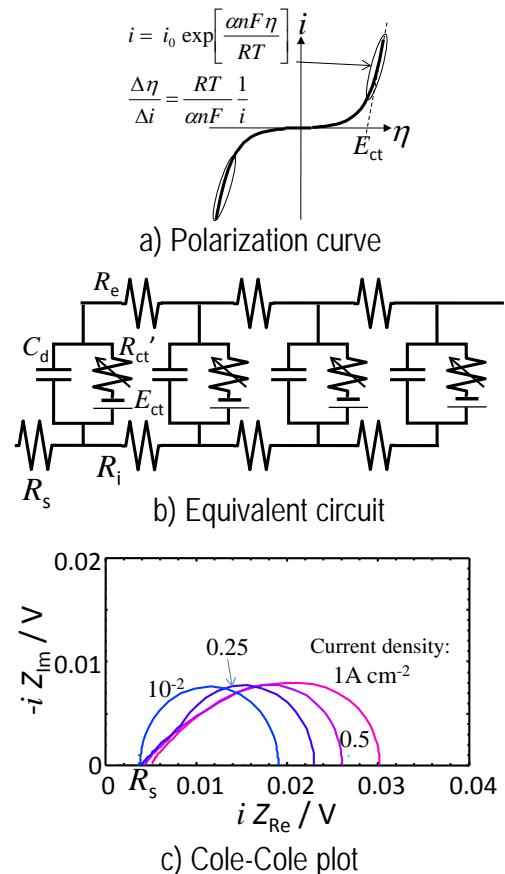


Fig. 11 Typical electrochemical AC impedance spectroscopy for slow reaction with porous electrode such as oxygen gas diffusion electrode.

porous electrode has thickness. As shown in Fig. 11 – a), the inverse of the slope of polarization curve $\Delta\eta/\Delta i$ decreases with increase of current i ; therefore, this value shall not be called “charge transfer re resistance” which is proportional to the inverse of exchange current density. Figure 11 – b) shows an equivalent circuit for these electrodes. Here, R_e , R_i , R_{ct}' , and E_{CT} are electronic resistance of thickness direction for porous electrode, ionic resistance of thickness direction for porous electrode, variable resistance correspond to the slop of the polarization curve, and apparent electromotive force as shown in Fig. 11 – a). This type of equivalent circuit is called a transmission line model. The vertical and horizontal axes of Fig. 11 –c) are product of $-Z_{Im}$ and i , and Z_{Re} and i , respectively. The arc is got with bias direct current. Otherwise, large amplitude of alternative current is needed because of large apparent resistance for charge transfer. In this plot, the sizes of arcs are almost same for all current density. The intercept of the higher frequency side is almost independent of current density in both experimental and numerical analysis; therefore, the intercept of the higher frequency side corresponds to ionic and electronic resistance. The aspect ratio of the arc increases with current density, because the R_{ct}' decreased with current density, so relative value of the R_i and R_e increase. The shape of the arc corresponds to the current distribution, but analytical method does not be standardized, yet.

CONCLUSION

In order to evaluate performance and property of fuel cell and its materials, electrochemical methods are strong tool. In the evaluation, correct equipments and selection of technique. Most of techniques are same to general electrochemical methods. However, some techniques are optimized for fuel cell evaluation based on the properties of the materials. Therefore, fundamentals of electrochemistry with basic assumption for the analysis shall be understood. Correct evaluation will be selected with correct understanding of the nature of materials.

Based on above, activity of electrocatalyst is usually evaluated with anodic sweep of slow scan linear sweep voltammetry. In order to determine kinetic current, rotating disk electrode is usually used to correct mass transfer. Chronoamperometry evaluates catalytic activity with poison or degradation behavior. Cyclic voltammetry analyzes electrochemical surface area (ECSA), hydrogen crossover behavior and others. In the evaluation of electrode membrane assembly (MEA), characteristics of the MEA must be understood. When the cyclic voltammetry, flow rate of nitrogen must be slow enough to determine the ECSA, and ac impedance spectroscopy gives ionic and electronic resistance with small bias direct current.

REFERENCES

- [1] A. J. Bard, L. R. Faulkner, “Electrochemical Methods – Fundamentals and Applications – Second edition, John Wiley & Sons, Inc. (2001).
- [2] A. J. Bard Ed., “Electroanalytical Chemistry A Series of Advance”, Marcel Dekker, vol. 9, p.54 (1976).

The quest of Hydrogen

*Once the electrons are gone
the protons start the ride
to find their friend the Oxygen
at membrane's other side.*

MODELING OF FUEL CELLS

Uwe Reimer

Institute of Energy and Climate Research / IEK-3: Electrochemical Process
Engineering / FZ Jülich GmbH

52425 Jülich / Germany / u.reimer@fz-juelich.de

Keywords: polarization curve, Nernst-Equation, Butler-Volmer-Equation, Tafel-Equation, efficiency, degradation

INTRODUCTION

The current-voltage curve, also called the polarization curve, describes the essential performance of a fuel cell or electrolyzer. In principle, the polarization curve can be represented by a great variety of mathematical equations. The choice of the 'right' set of equations depends strongly on the modeling task. For system simulation it is common to focus on the overall performance. Therefore, simple equations and look-up tables are used preferably which can be calculated very fast. In this talk a common model for the polarization curve is discussed, which is presumably the most simple model available with a clear physical meaning of the parameters. With the help of this basic approach the general response of a fuel cell with respect to the following topics is examined.

- efficiency and heat production
- influence of gas composition (using hydrogen versus reformat gas)
- aspects of degradation

The example polarization curve represents a high temperature PEFC (PBI/H₃PO₄ at 160 °C) but the principle applies to all fuel cell types and also to PEM electrolyzers. Therefore, the emphasis lies on the physical meaning of the model parameters. During the lesson it should become clear that the polarization curve is a powerful diagnostic tool in the development process of fuel cells, electrolyzer cells and systems. Because the model is quite simple, it is equally important to know its limitations.

The starting point for the derivation of the model equation is the calculation of the Nernst voltage. This is equal to the open cell voltage (OCV) of a fuel cell, also named *theoretical voltage* or *thermodynamic voltage*. The calculation of the Nernst voltage is discussed in more detail, because the equation depends strongly on the underlying physical assumptions of the electrode system. Starting from the commonly used notation in textbooks [1,2,3] the fundamental meaning is explained and the obvious deviation of experimental OCV values [4] is discussed. An extension of the Nernst equation is presented, which resolves this discrepancy between theory and experiment. Finally, different practical modeling approaches are explored that range from treating the Nernst equation as a constant value to the explicit incorporation of gas solubility and effective activity coefficients.

THE NERNST EQUATION

The Nernst voltage describes the cell voltage at thermodynamic equilibrium. It should therefore be equal to the open cell voltage (OCV) of a fuel cell. For the system oxygen/ hydrogen/ water the Nernst voltage is given by equation (1), where it is assumed that the electrodes are in contact with gases (no liquid water).

$$E_{Nernst}(T) = E^{\circ}(T) - \frac{RT}{2F} \ln \frac{P_{H_2O}}{P_{H_2} (P_{O_2})^{0.5}} \quad (1)$$

It must be noted that the logarithm in equation (1) must not have units. Therefore, the reduced partial pressure must be used, which is equal to the mole fraction X_i .

$$X_i = \frac{p_i}{p^0} \quad (2)$$

The term p_i in equation (2) is the partial pressure and p^0 the total pressure. By combining equations (1) and (2) the following equation (3) is obtained.

$$E_{Nernst}(T) = E^{\circ}(T) - \frac{RT}{2F} (\ln X_{H_2O} - \ln X_{H_2} - 0.5 \ln X_{O_2}) \quad (3)$$

In experiments usually a significantly lower OCV value is measured compared to the calculated Nernst voltage [4]. It is argued that several effects such as internal gas crossover and the different state of the catalyst at anode (Pt) and cathode (PtOx) lead to this deviation [4]. Additionally, the catalyst layer may be flooded with liquid water – a condition which is most obvious for electrolyzers and also holds for PEM fuel cells. It is very difficult to exactly calculate the influence of all of the above mentioned effects on the OCV value. In the following a simple formulation is discussed which allows at least to estimate the observed deviation.

Formally, in thermodynamics the activity must be used instead of partial pressure or concentrations. The term activity also recognizes deviations which are observed in systems under high pressure or concentrated salt solutions, i. e. liquids with high ionic

strength, which may also be present in thin liquid films within fuel cell electrodes. These deviations are commonly expressed by activity coefficients f_i as shown by equation (4).

$$f_i X_i = \frac{f_i' p_i}{p^0} \quad (4)$$

Thus, we yield the following notation of the Nernst equation.

$$E_{Nernst}(T) = E^\circ(T) - \frac{RT}{2F} (\ln f_{H_2O} X_{H_2O} - \ln f_{H_2} X_{H_2} - 0.5 \ln f_{O_2} X_{O_2}) \quad (5)$$

Since each single f_i is not known, it is advisable to collect the sum of all $\ln f_i$ into one summary parameter A' .

$$E_{Nernst}(T) = E^\circ(T) - \frac{RT}{2F} (\ln X_{H_2O} - \ln X_{H_2} - 0.5 \ln X_{O_2} - A') \quad (6)$$

During the lecture it is shown that based on equation (6) the OCV value of fuel cells can be calculated in agreement with experimental values. For interpretation of the values the most common physical models, namely the assumption of pure gas electrodes, gas electrodes with liquid water drop and electrodes covered by thin liquid films are discussed. The last model is also referred to as the model of flooded electrodes, which requires the incorporation of gas solubilities for the values of X_i . With this approach it is possible to estimate a theoretical range of possible OCV values for PEFC as function of temperature, which also depend strongly on the water content in the electrode layers.

THE POLARIZATION CURVE MODEL

The so called polarization curve describes the cell voltage as a function of current or current density. In the case of PEM fuel cells and PEM electrolyzers this is a nonlinear function, which is commonly described by equation (7) [1,2,3].

$$E_{cell} = E_{Nernst} - R_\Omega j - \eta_{act} - \eta_{trans} \quad (7)$$

For fuel cells loss terms lead to a decrease of cell voltage, as shown in equation (7), while for electrolyzers the cell voltage increases. The major influences on the cell voltage are:

- E_{Nernst} : Nernst voltage (dependence on feed gas composition)
- R_Ω : ohmic resistance (the major contribution is protonic conductivity of the membrane)
- η_{act} : activation losses (electrode processes, also called 'polarization')
- η_{trans} : mass transport losses (mass transport limitation in MEA/ GDL, also called diffusion overpotential)

In the most simple approach both the anode and cathode are combined into one effective electrode. For PEM fuel cells operated with hydrogen/ air this assumption is justified, because the overall contributions of the anode are very small. The advantage of this model is that it contains only a small number of parameters, whose physical meaning can be easily understood. The underlying assumptions and simplifications will be discussed in the lecture. The polarization curve model is used to explore the response of a PEM fuel cell to different operating conditions. The resulting ratio of heat and electricity generated is computed, which is the basis for the layout of cooling systems. The efficiency as a function of current density and stoichiometry is discussed and the impact of using reformat gas instead of pure hydrogen is shown.

Another important application is the general estimation of degradation effects. The final formulation of the polarization curve model in equation (8) contains three parameters, which are suitable to describe degradation.

$$E_{cell}(T) = E_{Nernst}(T) - R_{\Omega}(T)j - \frac{RT}{\alpha F} \ln \frac{j}{j_0(T)} - \frac{RT}{\alpha F} \ln \frac{j_{lim}}{j_{lim} - j} \quad (8)$$

The three parameters are:

- R_{Ω} - mean resistance of the MEA (ohmic resistance)
- j_0 - exchange current density
- j_{lim} - limiting current density

As first example the degradation of a PEM electrolyzer under constant load is discussed. In a second example the time dependend degradation of a high temperature PEFC with different load cycles is addressed and possible ways to extend the model are presented [5].

REFERENCES

- [1] O'Hayre, R. P., Cha, S.-W., Colella, W. G. and Prinz, F. B. *Fuel Cell Fundamentals*. Wiley, 2nd edition, 2009.
- [2] EG&G Technical Services, Inc. *Fuel Cell Handbook*. National Technical Information Service, U.S. Department of Commerce, Springfield, 7 edition, 2004.
- [3] Barbir, Frano. *PEM Fuel Cells: Theory and Practice*. Elsevier Academic Press, Amsterdam, Boston, Heidelberg, London, New York, 1 edition, 2005.
- [4] J. Zhang, Y. Tang, C. Song, J. Zhang, H. Wang, PEM fuel cell open circuit voltage (OCV) in the temperature range of 23 °C to 120 °C, *Journal of Power Sources* 163 (2006) 532.
- [5] U. Reimer, B. Schumacher, W. Lehnert, Accelerated Degradation of High-Temperature Polymer Electrolyte Fuel Cells: Discussion and Empirical Modeling, *Journal of The Electrochemical Society* 162 (2015) F153.

Summary: Thermodynamics

'standard' voltage:

$$E^\circ = -\frac{\Delta G}{zF}$$

'enthalpy' voltage:

$$E^H = -\frac{\Delta H}{zF}$$

efficiency:

$$\epsilon_{\text{th}} = \frac{\Delta G}{\Delta H}$$

$$\epsilon_{\text{cell}} = \frac{E_{\text{cell}}}{E^H}$$

- ΔG depends upon temperature and pressure

Nernst equation:

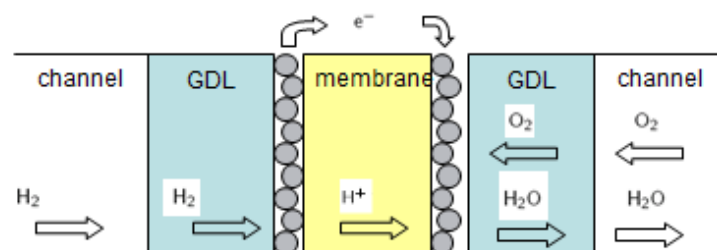
$$E = E^\circ - \frac{RT}{2F} (\ln x_{\text{H}_2\text{O}} - \ln x_{\text{H}_2} - 0.5 \ln x_{\text{O}_2})$$

- solubility of gases in liquid films can be accounted for

Electrode kinetics: Butler-Volmer equation

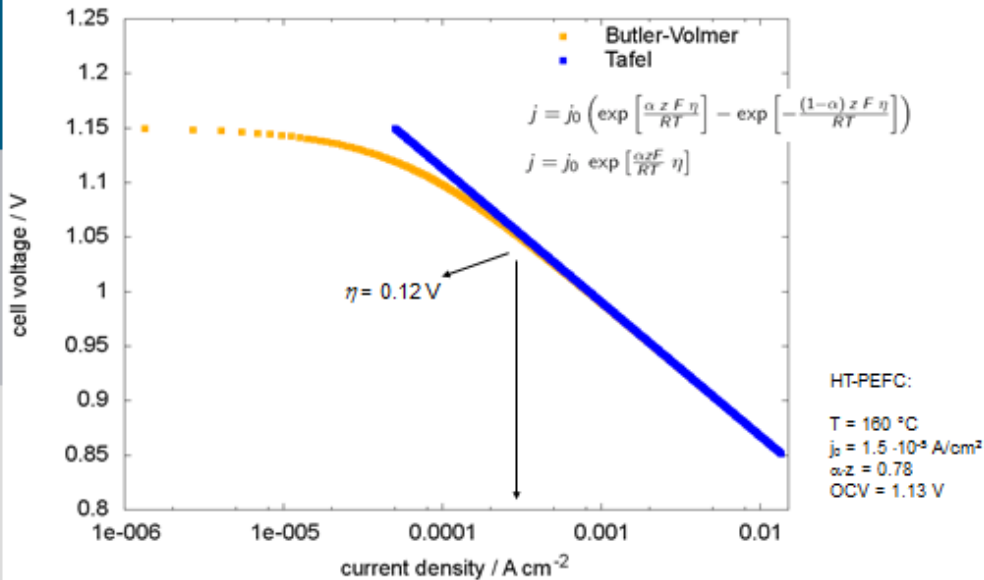
Butler-Volmer:
$$j = j_0 \left(\exp \left[\frac{\alpha z F \eta}{RT} \right] - \exp \left[-\frac{(1-\alpha) z F \eta}{RT} \right] \right)$$

Tafel:
$$j = j_0 \exp \left[\frac{\alpha z F}{RT} \eta \right]$$



Simplification: - anode and cathode are combined ("effective electrode")
 - Tafel equation is an approx.

Butler-Volmer → Tafel equation



Institute of Energy and Climate Research – Electrochemical Process Engineering (IEK-3)

3

Butler-Volmer / Tafel equation (2)

Meaning of the parameters

$$j = j_0 \exp \left[\frac{\alpha z F}{RT} \eta \right] \quad \rightarrow \quad \eta(j) = \frac{RT}{\alpha z F} \ln j - \frac{RT}{\alpha z F} \ln j_0 \quad \rightarrow \quad \eta(j) = A \ln j - B$$

j_0 exchange current density
 - number of active sites
 - total area of catalyst

α symmetry factor
 - seems to be a material property
 $\alpha \rightarrow [0 \dots 1.0]$

z number of electrons in slowest step
 - depends on the assumed mechanism

→ use an effective $\alpha' = \alpha \cdot z$

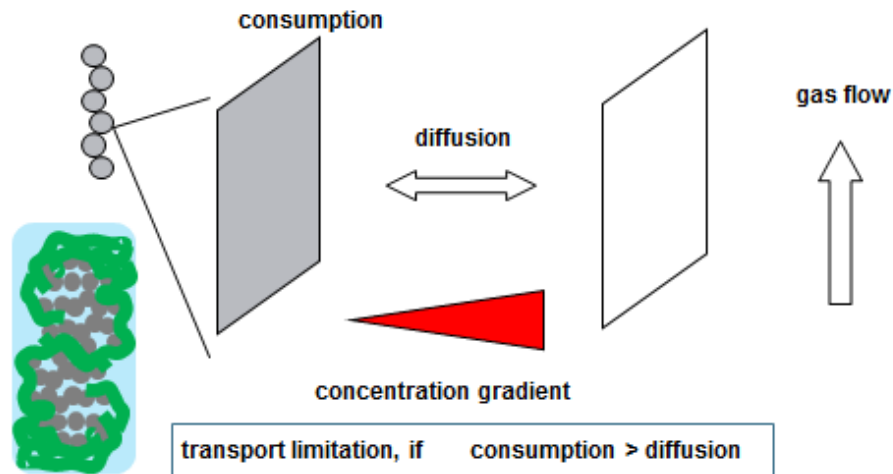
Institute of Energy and Climate Research – Electrochemical Process Engineering (IEK-3)

4

Transport limitation: diffusion

catalyst surface

gas channel



Institute of Energy and Climate Research – Electrochemical Process Engineering (IEK-3)

5

Transport limitation: diffusion

Ficks law:
$$j = \frac{z F D (c_{\text{bulk}} - c_{\text{surf}})}{\delta}$$

limit (maximum current) if $c_{\text{surf}} = 0$
$$j_{\text{lim}} = \frac{z F D c_{\text{bulk}}}{\delta}$$

⇒
$$\frac{j}{j_{\text{lim}}} = 1 - \frac{c_{\text{surf}}}{c_{\text{bulk}}}$$

How to relate $\frac{c_{\text{surf}}}{c_{\text{bulk}}}$ to a voltage?

Nernst:

Tafel:

$$\eta_{\text{trans}} = \frac{R T}{z F} \ln \left(\frac{j_{\text{lim}}}{j_{\text{lim}} - j} \right) \quad \eta_{\text{trans}} = \frac{R T}{\alpha F} \ln \left(\frac{j_{\text{lim}}}{j_{\text{lim}} - j} \right)$$

Attention: the value of j_{lim} will be different!!!

Institute of Energy and Climate Research – Electrochemical Process Engineering (IEK-3)

6

Short summary: polarization curve

$$E_{\text{cell}} = E_{\text{Nernst}} - R_{\Omega} j - \eta_{\text{act}} - \eta_{\text{trans}}$$

$$E_{\text{cell}} = E^{\circ} - \frac{RT}{2F} \ln \frac{x_{\text{H}_2\text{O}}}{x_{\text{H}_2} x_{\text{O}_2}^{0.5}} - R_{\Omega} j - \frac{RT}{\alpha F} \ln \left(\frac{j}{j_0} \right) - \frac{RT}{\alpha F} \ln \left(\frac{j_{\text{lim}}}{j_{\text{lim}} - j} \right)$$

j_0 exchange current density

j_{lim} limiting current density

α effective symmetry factor

R_{Ω} ohmic resistance of membrane

These parameters have to be obtained!

Polarization curve: fitting procedure

- obtain value for R_{Ω} e.g. from impedance (EIS)
- subtract $j \cdot R_{\Omega}$ from the polarization curve ('iR-free plot')
- use low current region to fit Tafel equation ($j < 0.2 \text{ A cm}^{-2}$)
- fit j_{lim}

Attention:

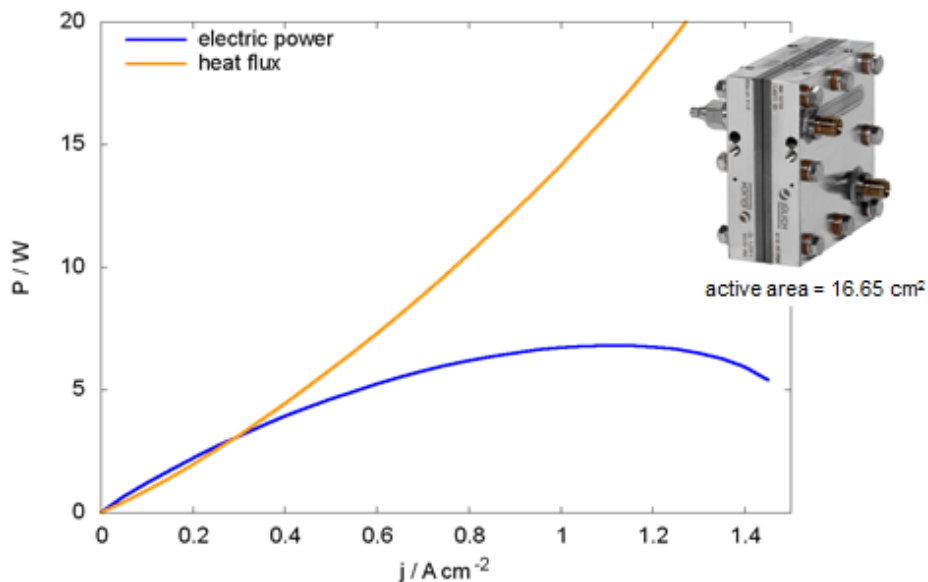


The experiment is 3D but the model is 0D (no spatial resolution).

Flow field size and geometry will have influence on the parameters.

Be aware what you compare!

Efficiency - heat and electricity

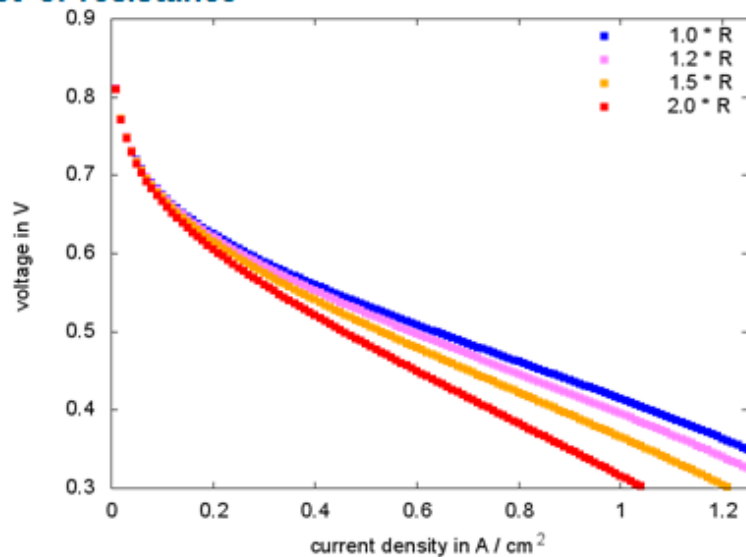


Institute of Energy and Climate Research – Electrochemical Process Engineering (IEK-3)

9

Effect of resistance

R_0 increases



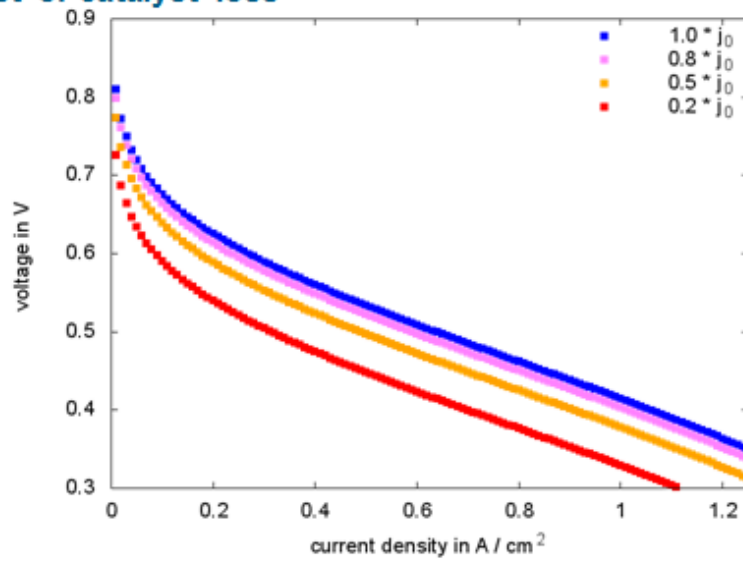
› drying of membrane

Institute of Energy and Climate Research – Electrochemical Process Engineering (IEK-3)

10

Effect of catalyst loss

j_0 decreases



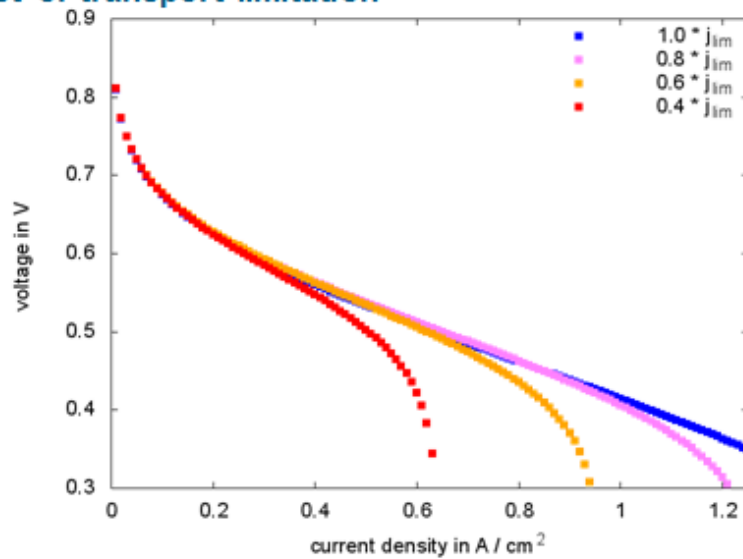
› number of cycles of the fuel cell (j_{lim} might also be affected)

Institute of Energy and Climate Research – Electrochemical Process Engineering (IEK-3)

11

Effect of transport limitation

j_{lim} decreases



› flooding (NT-PEFC) or total catalyst loss

Institute of Energy and Climate Research – Electrochemical Process Engineering (IEK-3)

12

ELECTROCHEMICAL IMPEDANCE SPECTROSCOPY AND HARMONIC DISTORTION ANALYSIS

Bernd Eichberger

Graz University of Technology, Inffeldgasse 10, A-8010 Graz, Austria
 Bernd.Eichberger@TUGraz.at

Keywords: Fuel Cell, Impedance Spectroscopy, Nyquist Diagram, Bode Plot, Total Harmonic Distortion

INTRODUCTION

Impedance Spectroscopy is a non-invasive method of analysing various frequency dependent phenomena of electrochemical components, especially batteries, fuel cells and electrochemical capacitors. It can be used for single cell testing in the laboratory and also for online stack monitoring.

It is an enhancement to impedance analysis where the cell impedance is plotted versus frequency. The (complex) electrical impedance Z of a test object is measured at several frequencies within a frequency range (spectrum) of interest. Voltage and current and their phase shift are measured while exciting the system using a sinusoidal voltage or current source. Sophisticated measurement systems can simultaneously apply several different frequencies and so reduce the test time.

The impedance of a fuel cell mainly consists of ohmic losses, anode activation losses, cathode activation losses and mass transfer effects. These phenomena occur at specific frequencies which allow distinguishing between them and investigating them separately by measuring within the appropriate frequency range (Figure 1). [1, 2]

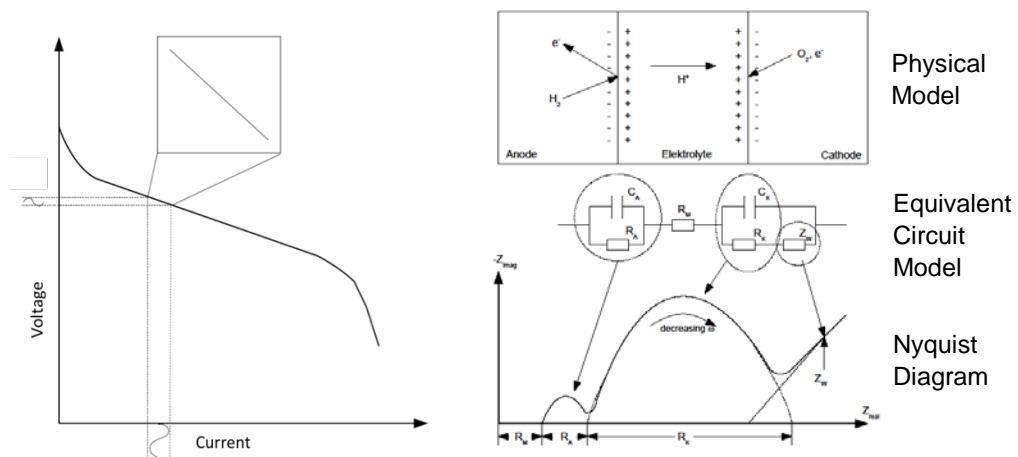


Figure 1: Fuel Cell Voltage / Current and Impedance Characteristic

IMPEDANCE BASICS

The electrical impedance \underline{Z} , also called alternating-current resistance, is the measure of alternating sinusoidal voltage applied to a passive two-pole circuit to the alternating current flowing through it and their phase shift. In mathematical terms it is represented as a complex number in Cartesian form $Z = R + jX$ or in polar form $Z = |Z|e^{j\arg[Z]}$ (Figure 2). The presentation as a complex number is a convenient method of handling amplitude and phase angle in case of harmonic (sine wave) signals.

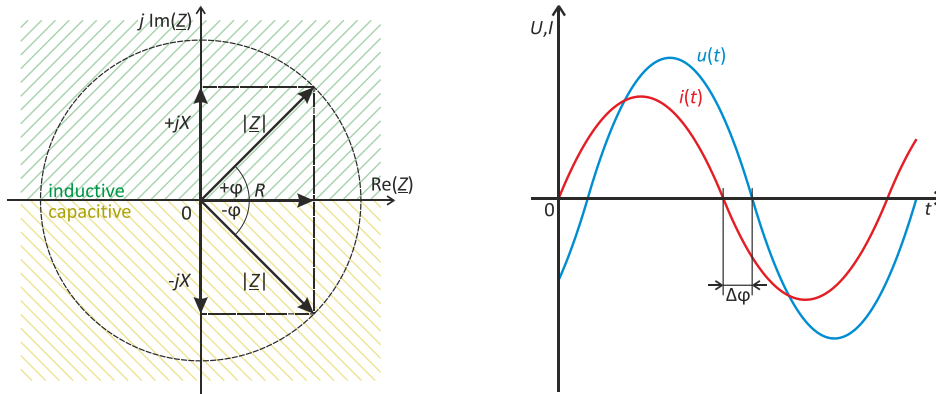
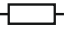




Figure 2: Representation of \underline{Z} in the complex plane, Phase shift $u(t)$ vs. $i(t)$

	Resistor: $Z = R$	(1)	Impedance $Z = (Re) + j(Im)$	(4)
	Capacitor: $Z = 1/j\omega C$	(2)	Magnitude $ Z = \sqrt{(Re)^2 + (Im)^2}$	(5)
	Inductor: $Z = j\omega L$	(3)	Phase $\varphi = \arctan(Im)/(Re)$	(6)

In a linear system, which is assumed here, the impedance \underline{Z} does not depend on the amplitude of voltage or current. This means that the network does not comprise nonlinear voltage/current characteristic such as PN-junctions (Diodes, Transistors). Moreover, it is time invariant and thus does not change its characteristics over time nor has it any kind of memory effect. The basic formulas are given in (1) to (6).

Such an impedance \underline{Z} can be made up of any combination of resistor, capacitor or inductor in various series and parallel connections. If the structure of the network and the values of all its components are known, the impedance \underline{Z} can be calculated at any desired frequency.

An equivalent circuit diagram of the battery or fuel cell is required for correlating the results of impedance spectroscopy measurements with the assumed chemical and physical processes inside the test object. Such an equivalent circuit mainly consists of mixed series/parallel connections of resistors and capacitors. Inductive behaviour can, in most cases, be neglected at low frequencies. [3, 4, 5]

Ideally the impedance spectrum of the test object and of the equivalent circuit matches. The degree of matching depends on the accuracy of the equivalent circuit and the fitting of the parts values. The interconnection of the components (R, C) and their values should closely represent the real chemical and physical properties, yet be as simple as possible.

MEASUREMENT TECHNIQUES

A straightforward approach for impedance measurement is by connecting the device under test to a constant AC current source and measuring voltage, current and phase angle (see

Figure 3a). Another approach is connecting an AC voltage source to a voltage divider consisting of the unknown impedance Z and a precision reference resistor R . (Figure 3b)

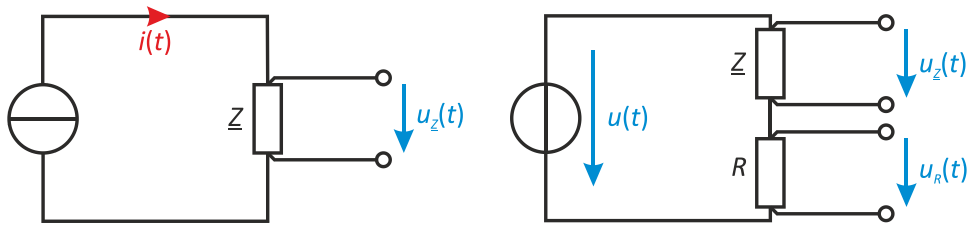


Figure 3a, 3b: Impedance measurement principles

In case of a fuel cell or battery it may be necessary to keep the DC cell voltage of the electrochemical element away from the excitation source and the measuring equipment. This can be accomplished using capacitors in a serial connection, as depicted in figure 4.

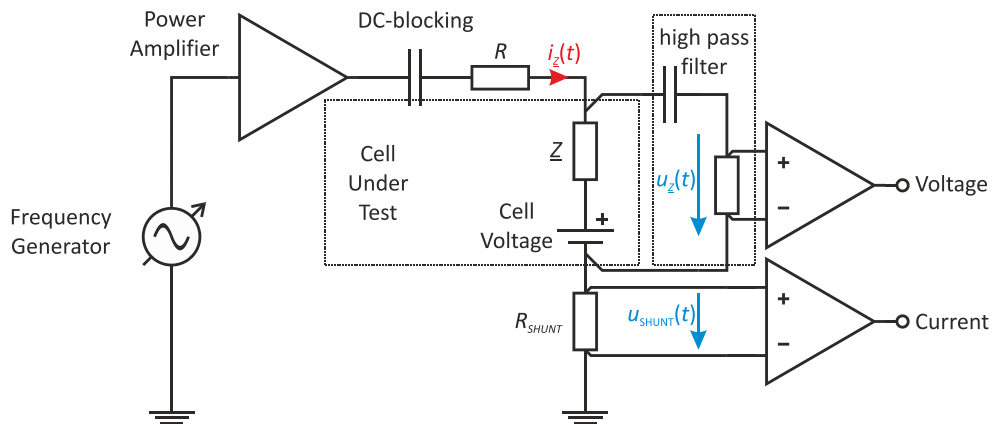


Figure 4: Impedance measurement, taking account of cell voltage

These straightforward setups are good for laboratory measurements using just a few different frequencies. Figure 5 shows a more advanced test arrangement. A microprocessor controls a frequency variable oscillator, which generates a sinusoidal voltage for the voltage controlled current source (VCCS) and in phase / quadrature phase digital signals for two synchronous rectifiers. The current from the VCCS causes a voltage drop across the impedance Z , which is amplified and split up by synchronous rectification into an in phase (real term) and quadrature phase (imaginary term) part. Further signal processing includes low-pass filtering and analogue-digital conversion. Finally, the microprocessor calculates the magnitude $|Z|$ and phase angle φ .

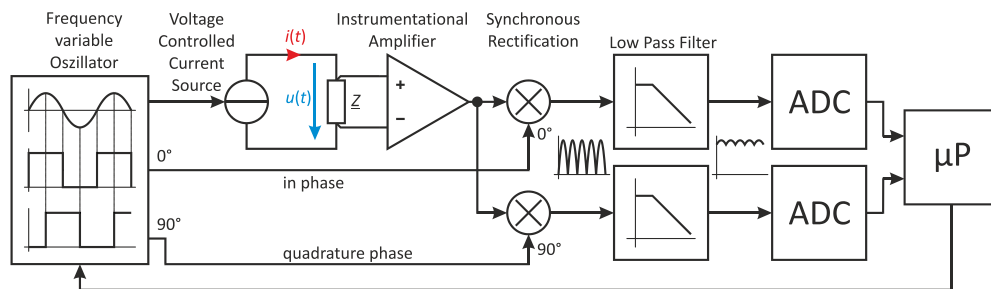


Figure 5: Signal generator, VCCS, quadrature synchronous rectification, A/D converters

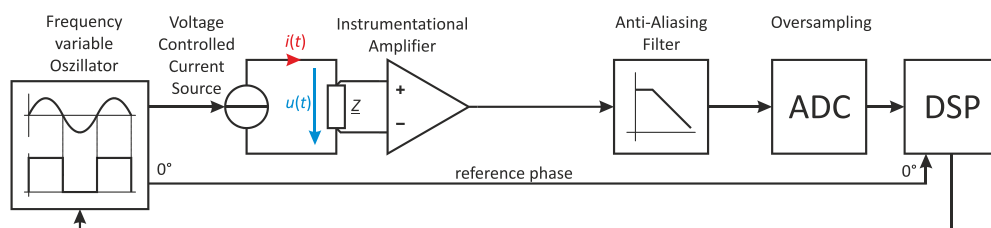


Figure 6: Impedance spectrum measurement with digital signal processing (DSP)

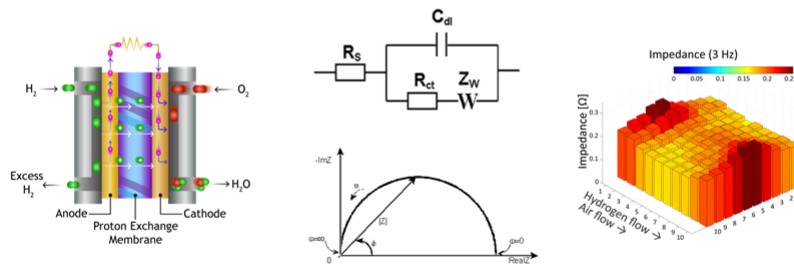
AC coupling between current source, device under test and input of instrumentation amplifier is not shown for reasons of clarity.

Digital signal processing (DSP) can handle synchronous rectification and low-pass filtering by software algorithms. An instrumentation amplifier fits the low level of the AC voltage signal across the impedance Z to the input range of the analogue-digital converter (ADC). The Nyquist-Shannon sampling theorem is met by an anti-aliasing higher order low-pass filter in combination with an oversampling ADC and further digital low-pass filtering, including sample rate reduction. Consequently, the frequency variable oscillator consists of a direct digital synthesizer (DDS) with an additional zero phase digital reference output.

REFERENCES

- [1] M.E. Orazem, B. Tribollet: Electrochemical Impedance Spectroscopy, Wiley, ISBN 978-0-470-04140-6 (2008)
- [2] V. Hacker, H. Brandstaetter, St. Weinberger: Real Time Diagnosis of the Operating State of Fuel Cells by Electrochemical Impedance Spectroscopy, 9th International Symposium on Electrochemical Impedance Spectroscopy, Okinawa (2013)
- [3] K. J. Runtz, M.D. Lyster: Fuel cell equivalent circuit models for passive mode-testing and dynamic mode design, Canadian Conference on Electrical and Computer Engineering, (2005), p. 794-797
- [4] S.C. Page, A.H. Anbuky, S.P. Krumbieck, J. Brouwer: Test Method and Equivalent Circuit Modelling of a PEM Fuel Cell in a Passive State (IEEE Transactions on Energy Conversion, volume 22, issue 3, pp. 764-773 (2007)
- [5] Electrochemical Impedance Spectroscopy (EIS): A Powerful and Cost-Effective Tool for Fuel Cell Diagnostics, Information on <http://www.scribner.com>

Electrochemical Impedance Spectroscopy and Harmonic Distortion Analysis



Bernd Eichberger, Institute of Electronic Sensor Systems, University of Technology, Graz, Austria
bernd.eichberger@TUGraz.at

B. Eichberger 10th International Summer School on Advanced Studies of Polymer Electrolyte Fuel Cells, Yokohama National University, Japan, Aug. 20th – Aug. 25th, 2017

1



Table of Content

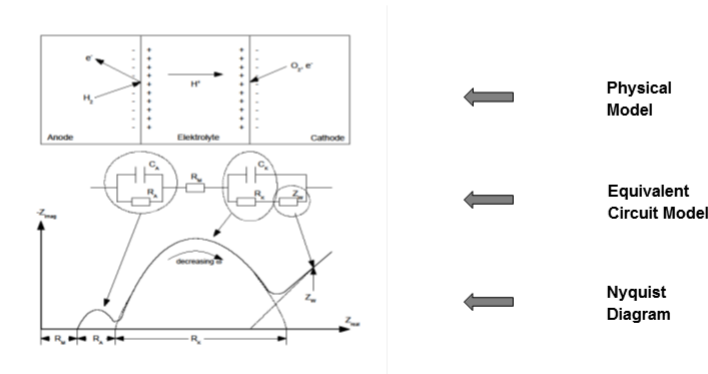
- Introduction
- Impedance and Impedance Spectroscopy
- Equivalent Circuits
- EIS Measurement Setup
- EIS Graphical Presentation
- Non-Linearity, Distortion Analysis

B. Eichberger 10th International Summer School on Advanced Studies of Polymer Electrolyte Fuel Cells, Yokohama National University, Japan, Aug. 20th – Aug. 25th, 2017

2

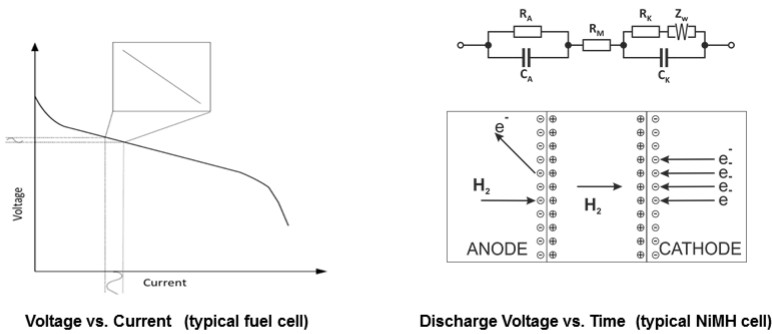
Electrochemical Impedance Spectroscopy

- **Non-invasive Method of Measuring Fuel Cell AC Characteristics**
- **Physical Model** ⇨ **Equivalent Circuit** ⇨ **EIS, Nyquist Diagram**



Electrochemical Impedance Spectroscopy

- **Voltage / Current Characteristics**, (complex) Impedance
- **Linearization:** Small Signal Sinusoidal Current Excitation
- **Operating Point** at the Steady State Curve



Voltage vs. Current (typical fuel cell)

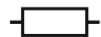
Discharge Voltage vs. Time (typical NIMH cell)

Impedance Basics

- Introduction
- **Electrical Impedance Basics**
- Equivalent Circuits
- EIS Measurement Setup
- EIS Graphical Presentation
- Non-Linearity, Distortion Analysis

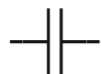
Electrical Impedances: Z - R, C, L

- **Components, Equations**



Resistor: $Z = R$

Impedance $Z = (Re) + j(Im)$



Capacitor: $Z = 1/j\omega C$

Magnitude $|Z| = \sqrt{(Re)^2 + (Im)^2}$



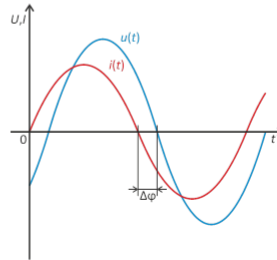
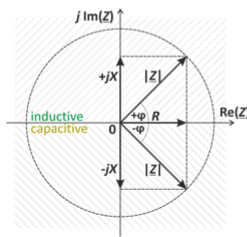
Inductor: $Z = j\omega L$

Phase $\varphi = \arctan [(Im)/(Re)]$

Angular Frequency: $\omega = 2\pi f$

Impedance: Magnitude and Phase

- **Sinusoidal Voltage, Current** $v_t = \hat{v}\sin(\omega t)$
 - magnitude of the complex impedance: ratio of the voltage amplitude to the current amplitude
 - Phase shift between Voltage $v(t)$ and Current $i(t)$
 - Phase angle $\Delta\varphi$: phase shift by which the current lags the voltage



Impedance Z

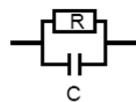
- **Mathematical Description of Voltage / Current Ratio**
- **Impedance** $Z = v(t)/i(t)$
- **Note: Resistance** $R = v/i$, no time dependency (t)
 - Sinusoidal Voltage $v(t)$ and Current $i(t)$
 - Time invariant and linear characteristics
 - Phase angle $\Delta\varphi$ does not depend on the amplitude
 - Z can be any combination of R, L, C : simple \Leftrightarrow complex !
 - The equivalent circuit of a fuel cell impedance includes elements with special phase characteristic: Warburg Impedance Z_w
 - Nonlinear elements cause distortions \Leftrightarrow harmonics analysis !

Equivalent Circuits

- Introduction
- Impedance Basics
- **Equivalent Circuits**
- EIS Measurement Setup
- EIS Graphical Presentation
- Non-Linearity, Distortion Analysis

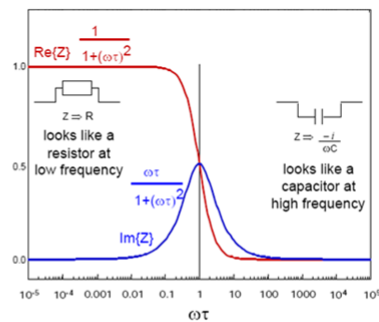
Equivalent Circuit Networks

- **Simplified Model**
 - Resistor and Capacitor in parallel (Voigt Network)
 - Electrical Layer, Capacitance with Isolation resistance



$$Z = R / (1 + j\omega C)$$

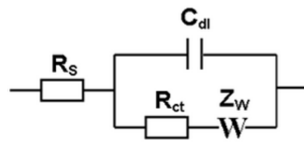
$$\tau = RC \text{ Time Constant}$$



Equivalent Circuit Networks

- **Basic Equivalent Circuit Model for Electrochemical Cells**
- **“Randles” Circuit: Mixed Kinetic and Diffusion Model**

- Electrolyte Resistance R_s
- Double Layer Capacitance C_{dl}
- Charge Transfer Resistance R_{ct}
- Warburg Impedance Z_w : Constant Phase Element, $\Delta\varphi = -45^\circ$



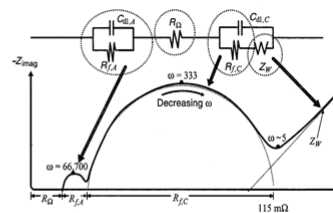
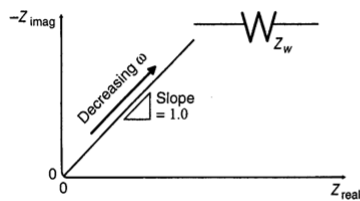
$$Z_w = \sigma / \sqrt{\omega} - j \sigma / \sqrt{\omega}$$

$$|Z_w| = \sqrt{2} \sigma / \sqrt{\omega}$$

Warburg Element

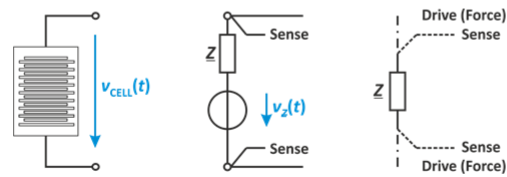
- **Warburg Element Z_w** $Z_w = \frac{A_w}{\sqrt{\omega}} + \frac{j A_w}{\sqrt{\omega}}$ $Z_w = \sigma / \sqrt{\omega} - j \sigma / \sqrt{\omega}$
- **Model for diffusion processes**
- **Significant at (very) low frequencies** $|Z_w| = \sqrt{2} \sigma / \sqrt{\omega}$
- **Porous bounded Warburg model :**

$$Z = \frac{\sigma_i}{\sqrt{w}} (1 - j) \tanh \left(\delta \sqrt{\frac{j\omega}{D_i}} \right)$$



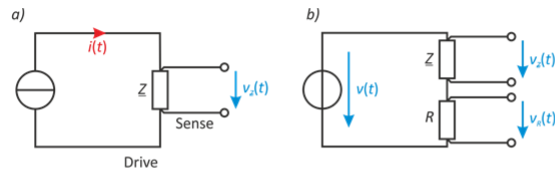
Impedance Measurement – Fuel Cell Equivalent Circuit

- **Fuel Cell and Equivalent Circuit Diagram**
 - Ideal Voltage Source and Series Impedance Z -> $V_{cell}(t)$
- **Four-Terminal Measurement**
 - Minimize Errors due to wiring resistance / voltage drops
 - Separate Drive and Sense connections, close to the fuel cell



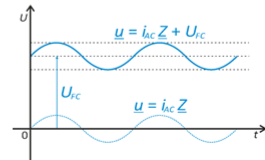
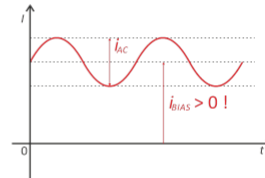
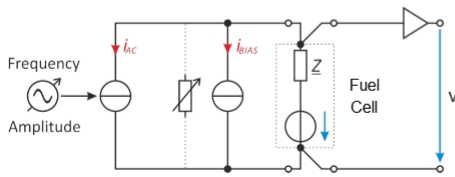
Impedance Measurement Principles (1)

- **AC Current Source (a)**
 - Ohm's Law, Precision AC Current Source
- **AC Voltage Source (b)**
 - Voltage Divider, Reference Resistor R for Current Measurement
 - Ratio metric Measurement



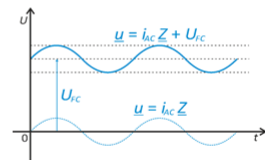
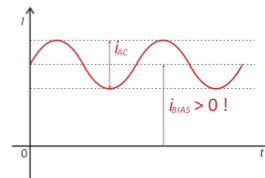
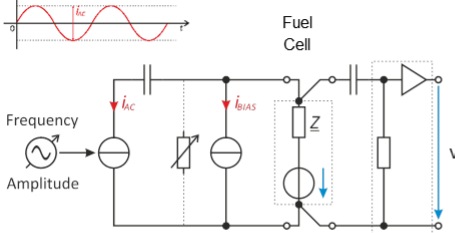
Impedance Measurement Principles (2)

- **AC Current Source, Bias Load**
 - No Current Flow into Fuel Cell, Bias Load
 - Full Bandwidth including DC
 - Fuel Cell Voltage is Offset Voltage for AC Measurement, Limits Dynamic Range !
 - Best for single (few) Cell Testing



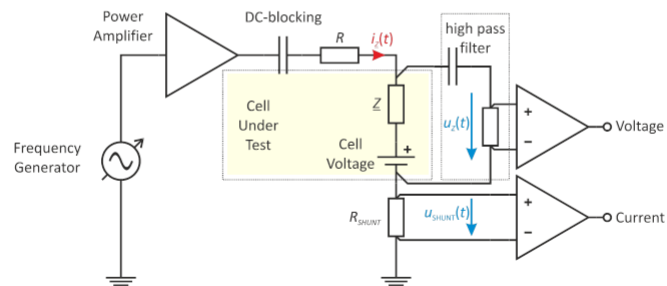
Impedance Measurement Principles (3)

- **AC Current Source, Bias Load, Coupling Capacitors**
 - No Current Flow into Fuel Cell, Bias Load
 - Limited Lower Bandwidth ($\tau=RC$)
 - Suited for Testing Large Stacks (HV)
 - Requires Sophisticated Protection



Impedance Measurement (1)

- **Practical Measurement Set-up**
 - AC coupling / DC blocking with capacitors

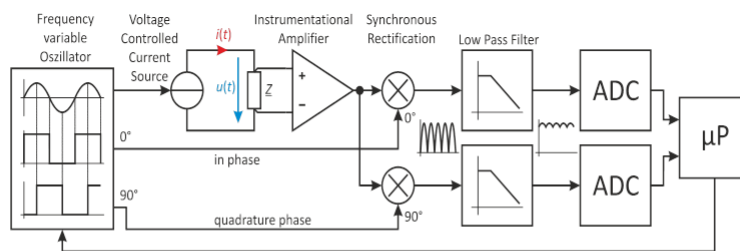


B. Eichberger 10th International Summer School on Advanced Studies of Polymer Electrolyte Fuel Cells, Yokohama National University, Japan, Aug. 20th – Aug. 25th, 2017

17

Impedance Measurement (2)

- **A more sophisticated Measurement Set-up**
 - Direct Digital Synthesizer, Synchronous Rectification
 - Analogue - Digital Converters, μ P Control

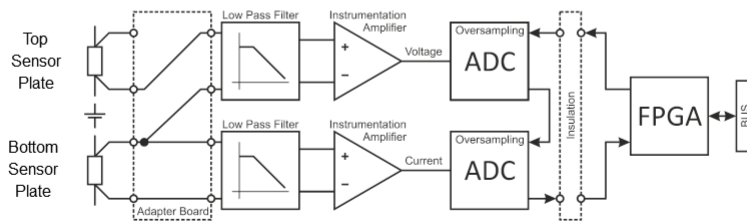


B. Eichberger 10th International Summer School on Advanced Studies of Polymer Electrolyte Fuel Cells, Yokohama National University, Japan, Aug. 20th – Aug. 25th, 2017

18

Impedance Measurement (3)

- **Measuring Voltage and Current, Fully Digital (Post) Processing**
 - Analog Filter, High Resolution Analog-to-Digital Conversion
 - Digital FIR Low Pass Filter with Sample Rate Reduction
 - Strictly preserves Phase Relation between Voltage and Current
 - Minimum Adjustments required

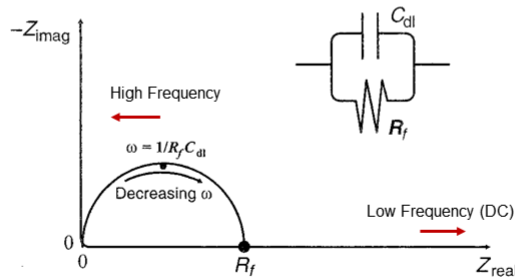


Graphical Presentation

- Introduction
- Impedance Basics
- Equivalent Circuits
- EIS Measurement Setup
- **EIS Graphical Presentation**
- Non-Linearity, Distortion Analysis

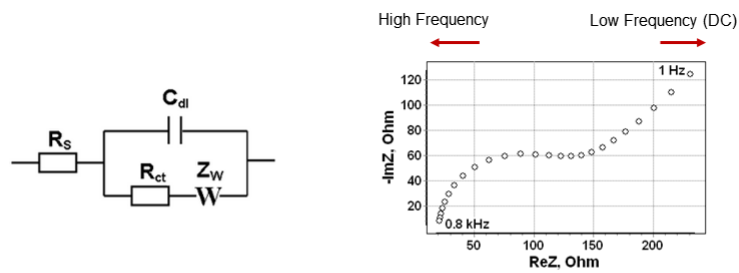
Nyquist Diagram

- **Complex Impedance Z over frequency range (2—dimensional)**
- **Z_{imag} and Z_{real}**
- **Missing frequency information**



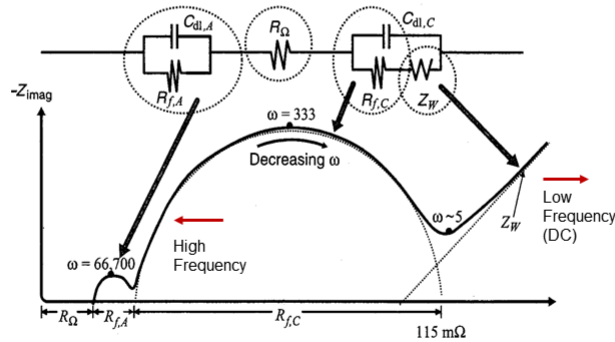
Nyquist Diagram (2)

- **Equivalent Circuit Diagram including Warburg Impedance**
- **Z_{imag} and Z_{real} from 1 Hz to 800 Hz**
- **Typical Nyquist Plot**



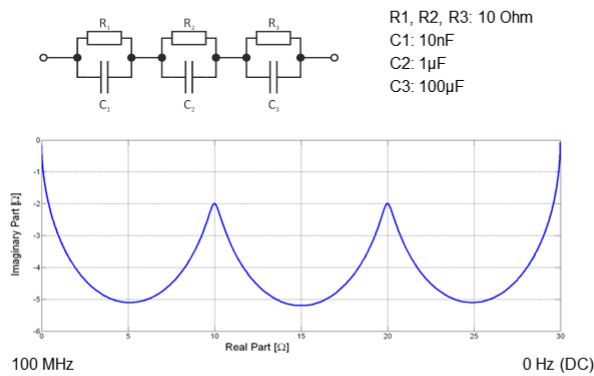
Nyquist Diagram (3)

- Series / Parallel Combination of R, C, Z_w (Warburg)
- Double Layer Capacitance (Anode, Cathode), Resistances



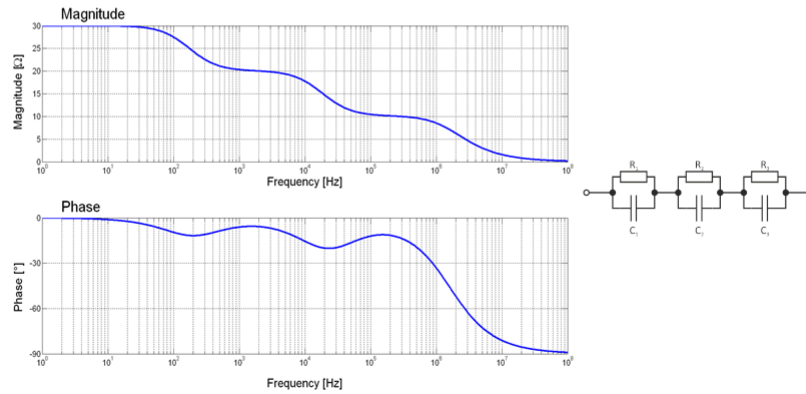
Nyquist Diagram (4)

- Example Circuit and calculated impedance vs. frequency
- RC parallel / series connections, different time constants



Bode Diagram

- **Magnitude / Phase vs. (log) Frequency**



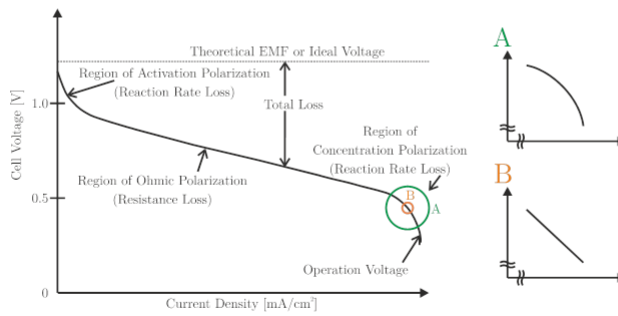
Enhanced Measurement Techniques

- Introduction
- Impedance Basics
- Equivalent Circuits
- EIS Measurement Techniques
- EIS Graphical Presentation
- **Non-Linearity and Distortion Analysis, Intermodulation**

Harmonic / Intermodulation Distortion Analysis

- **Fuel Cell Voltage vs. Current Density**

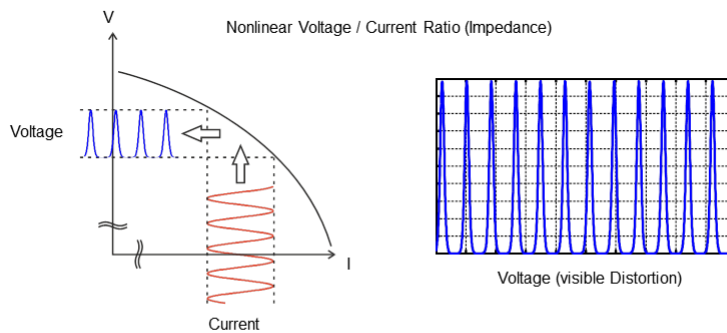
- Partly Non-Linear Transfer Function
- Depending on Operating Point and Amplitude/ Excitation Level



Harmonic Distortion Analysis

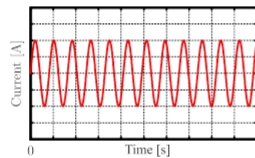
- **Exploiting non-linear Voltage/Current Characteristics**

- Additional information about internal state of a fuel cell (FC)
- Total Harmonic Distortion Analysis (THDA)

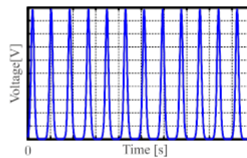


Harmonic Distortion Analysis

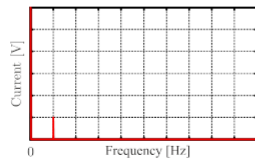
- **Harmonics Analysis (single frequency excitation)**
 - Amplitude Ratio: Fundamental Frequency vs. Harmonics
 - Fast Fourier Transformation (FFT)



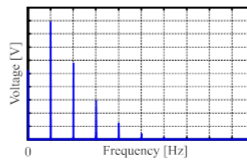
Sinusoidal Current Drive



Distorted Voltage across Nonlinear Impedance



Single Frequency (100 Hz)



Fundamental Frequency + Harmonics

Harmonic Distortion Analysis

- **Math Example**

$$u(t) = a_0 \cdot i(t) + a_1 \cdot i(t)^2$$

$$\omega = 2 \cdot \pi \cdot f$$

$$i(t) = \hat{i} \cdot \sin(\omega \cdot t)$$

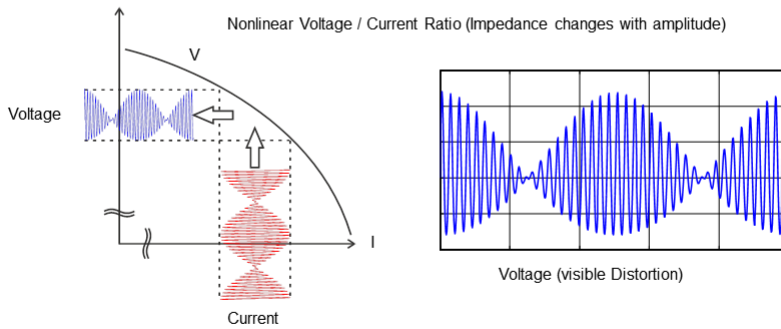
$$u(t) = a_0 \cdot \hat{i} \cdot \sin(\omega \cdot t) + a_1 \cdot \hat{i}^2 \cdot \sin^2(\omega \cdot t)$$

$$\sin^2(x) = \frac{1}{2} (1 - \cos(2x))$$

$$u(t) = \overbrace{a_0 \cdot \hat{i} \cdot \sin(\omega \cdot t)}^{\omega} + \overbrace{a_1 \cdot \frac{\hat{i}^2}{2} (1 - \cos(2 \cdot \omega \cdot t))}^{2 \cdot \omega}$$

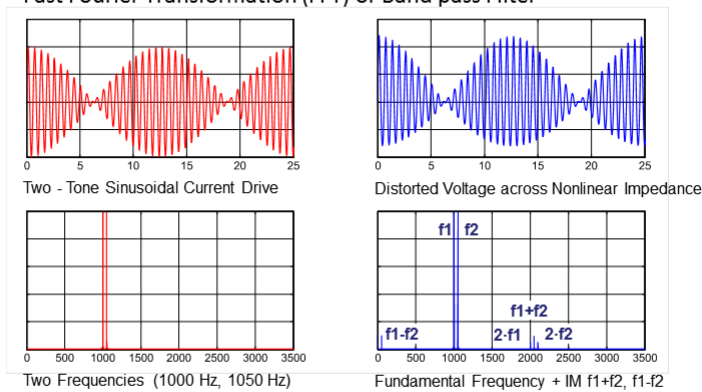
Intermodulation Distortion Analysis

- **Exploiting non-linear Voltage/Current Characteristics**
 - Additional information about internal state of a fuel cell (FC)
 - Second Order Intermodulation Frequencies f_1+f_1 , f_1-f_2



Intermodulation Distortion Analysis

- **Intermodulation, two (or more) frequencies excitation**
 - Output Spectrum contains $f_1 + f_2$, $f_1 - f_2$, $2 \cdot f_1$, $2 \cdot f_2$, ...
 - Fast Fourier Transformation (FFT) or Band pass Filter



Intermodulation Analysis

▪ **A Math Example**

$$u(t) = a_0 \cdot i(t) + a_1 \cdot i(t)^2$$

$$i(t) = \hat{i} \cdot \sin(\omega_1 \cdot t) + \hat{i} \cdot \sin(\omega_2 t)$$

$$u(t) = a_0 \cdot \hat{i} (\sin(\omega_1 t) + \sin(\omega_2 t)) + a_1 (\hat{i} \cdot \sin(\omega_1 t) + \hat{i} \cdot \sin(\omega_2 t))^2$$

$$u(t) = a + a_1 (\hat{i}^2 \cdot \sin^2(\omega_1 t) + 2 \cdot \hat{i}^2 \cdot \sin(\omega_1 t) \cdot \sin(\omega_2 t) + \hat{i}^2 \cdot \sin^2(\omega_2 t))$$

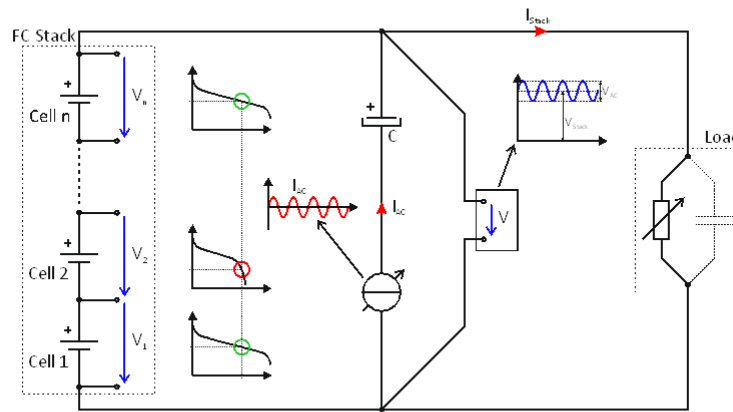
$$\sin(\alpha) \cdot \sin(\beta) = \frac{1}{2} (\cos(\alpha - \beta) - \cos(\alpha + \beta))$$

$$u(t) = a + a_1 (\hat{i}^2 \cdot \sin^2(\omega_1 t) + \hat{i}^2 (\cos(\omega_1 t - \omega_2 t) - \cos(\omega_1 t + \omega_2 t)) + \hat{i}^2 \cdot \sin^2(\omega_2 t))$$

$$\vdots$$

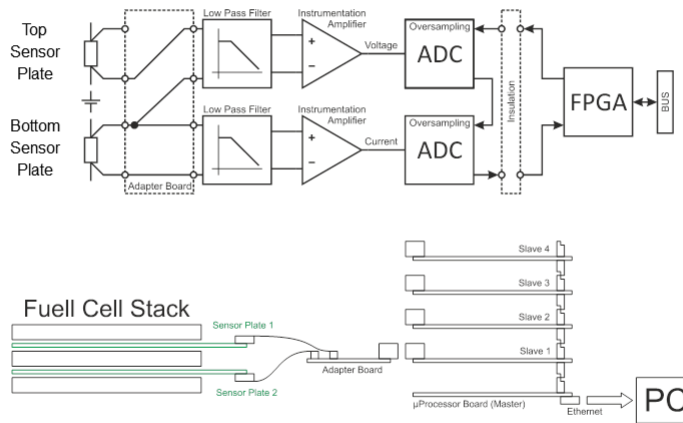
$$u(t) = a_0 \cdot \hat{i} \left(\overbrace{\sin(\omega_1 t)}^{\omega_1} + \overbrace{\sin(\omega_2 t)}^{\omega_2} \right) + a_1 \cdot \hat{i}^2 \left(1 - \frac{1}{2} \cdot \overbrace{\cos(2\omega_1 t)}^{2\omega_1} - \frac{1}{2} \cdot \overbrace{\cos(2\omega_2 t)}^{2\omega_2} + \overbrace{\cos(\omega_1 t - \omega_2 t)}^{\omega_1 - \omega_2} - \overbrace{\cos(\omega_1 t + \omega_2 t)}^{\omega_1 + \omega_2} \right)$$

Distortion and Intermodulation Analysis

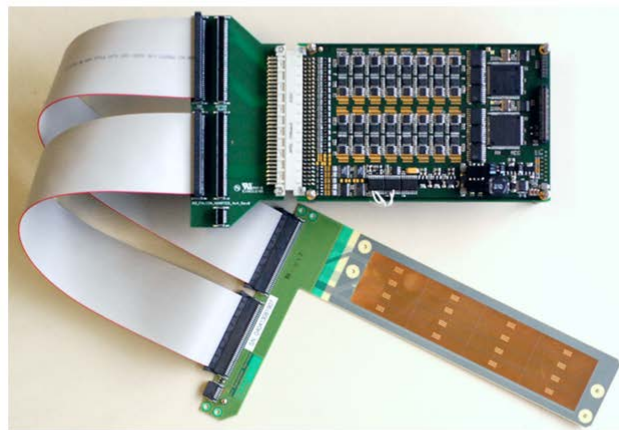


Typical Distortion Analysis Measurement Setup (also suitable for EIS)

Multi-Channel EIS / Distortion Measurement



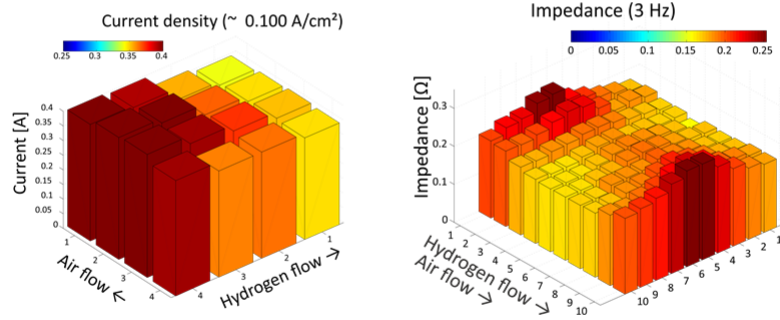
Multi-Channel EIS / Distortion Measurement



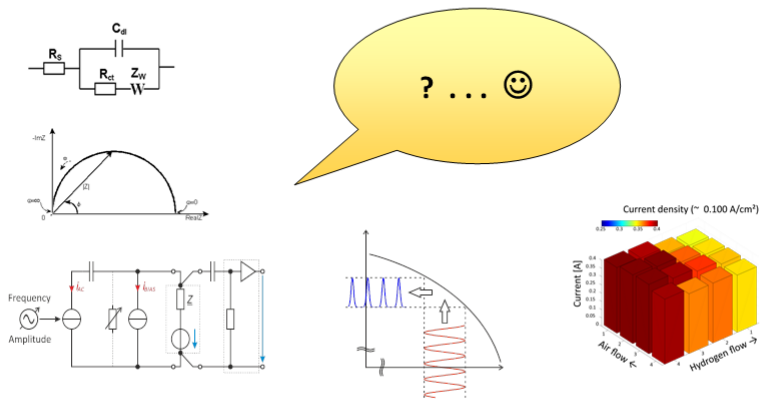
16 Channel Sensor Plate (courtesy of S++) and
16 Channel Voltage / Current / Temperature Sensor Interface Board

Multi – Channel EIS / Distortion Measurement

- 2-Dimensional View of Current Density and Impedance



Electrochemical Impedance Spectroscopy and Harmonic Distortion Analysis



HEAT AND MASS TRANSPORT INSIDE PEFC

Takuto Araki

Yokohama National University, 79-5 Tokiwadai, Hodogaya-ku, Yokohama, 240-8501 Japan, taraki@ynu.ac.jp

Keywords: Polymer electrolyte fuel cell, Heat transport, Mass transport, Oxygen diffusivity.

INTRODUCTION

In PEFCs, the water plays a significant role in proton conductivity of polymer electrolyte membrane (PEM), then water transports and distributions strongly affect PEFC performance. However, water transport phenomena inside PEMFC are so complicated as summarized in Fig.1. For instance, (1) the water is transported from the anode to cathode by electro-osmotic drag, (2) generated water at the cathode is diffused back toward the anode, (3) there are transport resistances at any boundaries between layers, (4) accumulated water droplet moves by surface tension and coalesces with each other and sometimes evaporates etc..

Oxygen is also key chemical species, because the activation overpotential at in cathode catalyst layer (CCL), which is a strong function of oxygen concentration, is the biggest cause of PEFC energy loss. Then, oxygen should be managed to be supplied uniformly to the catalyst particles in CCL.

To manage water transport, temperature distribution should be also controlled at the same time, because saturated vapor pressure shift much by the temperature change. Concretely, saturated vapor pressure increase 22% only by 5 °C rise in temperature (from 80 °C to 85 °C).

Formerly, cell geometries and materials have been designed and developed mainly by empirically, however, for further improvement of PEFC performance, optimal design based on systematic physical laws and numerical simulations is desired. However, even basic parameters such as mass transport and thermal characteristics through layers are not all cleared. Then, we and many researchers are trying to realize the heat and mass transport characteristics.

In this lecture, the basis and assessing methods of transport characteristics are mentioned firstly. Then, some practical instances how mass transports phenomena observed and how they affect cell performance are presented.

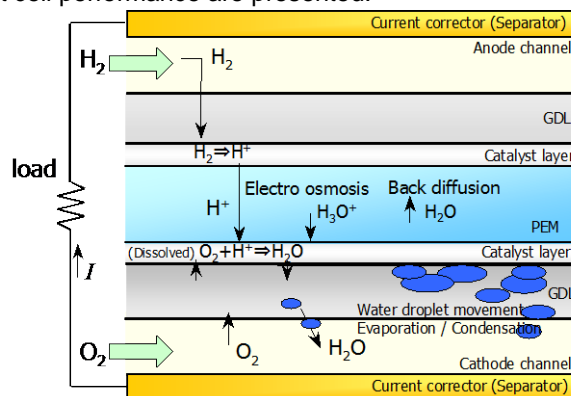


Fig.1: General factors of water transport inside PEFC

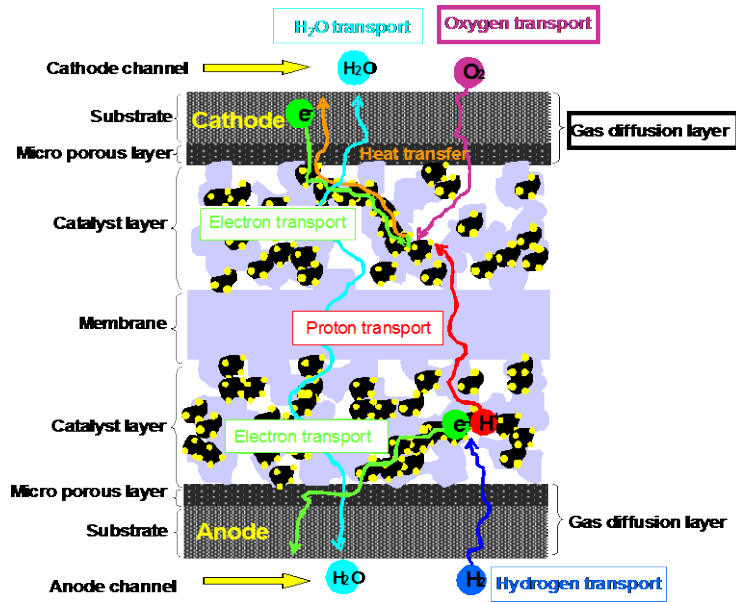


Fig.2: Mass transport factors around cathode catalyst layer

MEASUREMENTS OF HEAT AND MASS TRANSPORT CHARACTERISTICS

Diffusivity

There are some methods to measure diffusivity through GDL such as limiting current (sometimes with diluted oxygen) method, Galvanic battery method, concentration difference method and so on. The galvanic method has advantages of measurements speed and device simplicity. Thus, we have tried simultaneous measurements of oxygen diffusivity and liquid water visualization by synchro-tron X-ray CT. The results are shown on Fig.3.

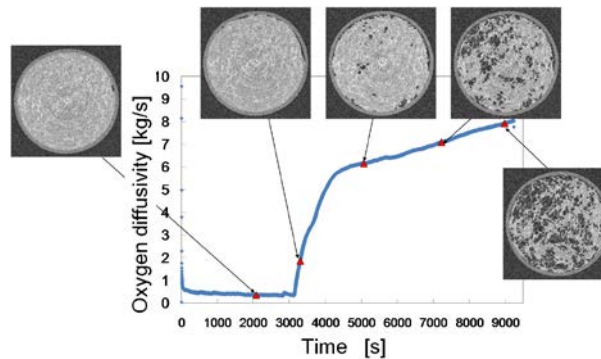


Fig. 3: Simultaneous measurements of oxygen diffusivity and water visualization by X-ray CT

Thermal conductivity

Measured thermal resistances as a function of compression pressure are shown in Fig. 4. The contact resistance at GDL surface was measured as big as the resistance of inside GDL, on the other hand, the contact resistance became extremely small when GDL contained much water.

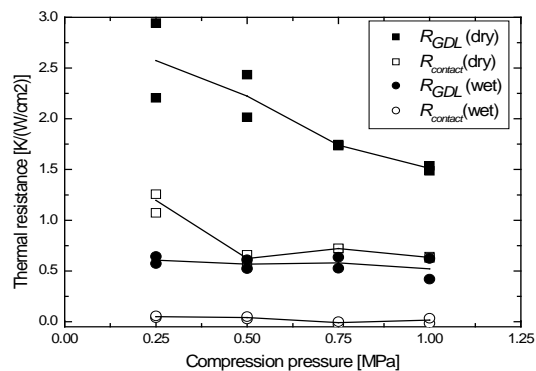


Fig. 4: Thermal resistance of GDL and its boundary

EFFECTS OF MASS TRANSPORT CONDITIONS ON POWER GENERATING CHARACTERISTICS

Flow configuration

Measured and calculated current densities are compared in Fig.5. Despite the difference in current density distribution, most conditions are all the same such as low supplied gas humidity (dew point 30°C), medium oxygen utilization ratio (50%), and cell temperature (70°C) and so on. The only difference is the supplied gas flow direction, and the reason of the difference is water distribution. In co-flow configuration, PEM near inlet tends to dry by relatively dry inlet gas and current decreased. On the contrary, produced water in counter flow configuration circulates and keeps overall PEM water content moderate. The efficiency of counter flow configuration is better than that of co-flow, and this is an instance why water (mass) transport management is important for PEFC.

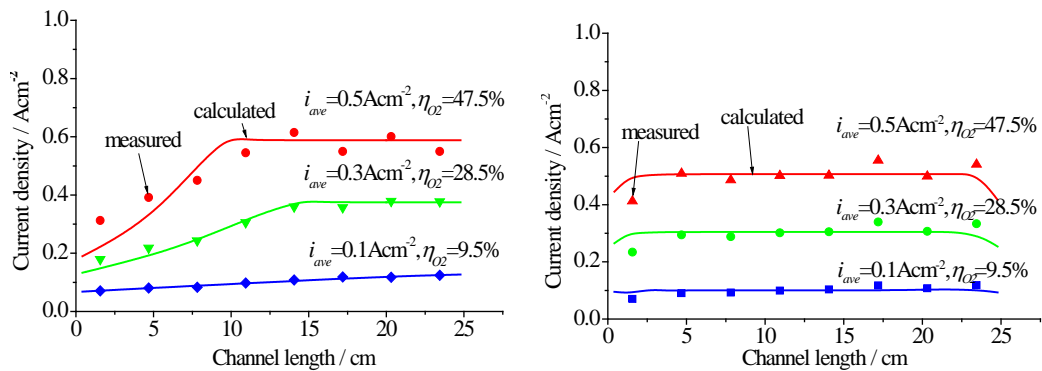


Fig. 5: Measured and calculated current distributions (left: co-flow, right: counter flow)

Heat and Mass transport inside PEFC

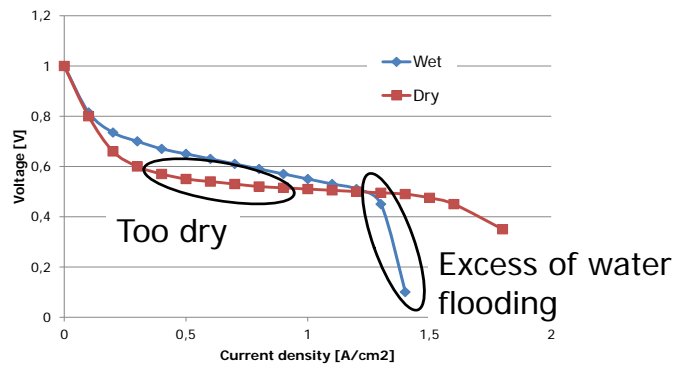


Takuto Araki
Department of Mechanical Engineering
Yokohama National University

<http://www.trans.me.ynu.ac.jp>

Advanced Studies of PEFC 5th International Summer School

Effects of Supplying gas humidity



Wet gas supply → Better performance in middle current density region
Flooding in high current density region
due to generated water

Dry gas supply → Better in high current region

4th International Summer School on Advanced Studies of PEFC

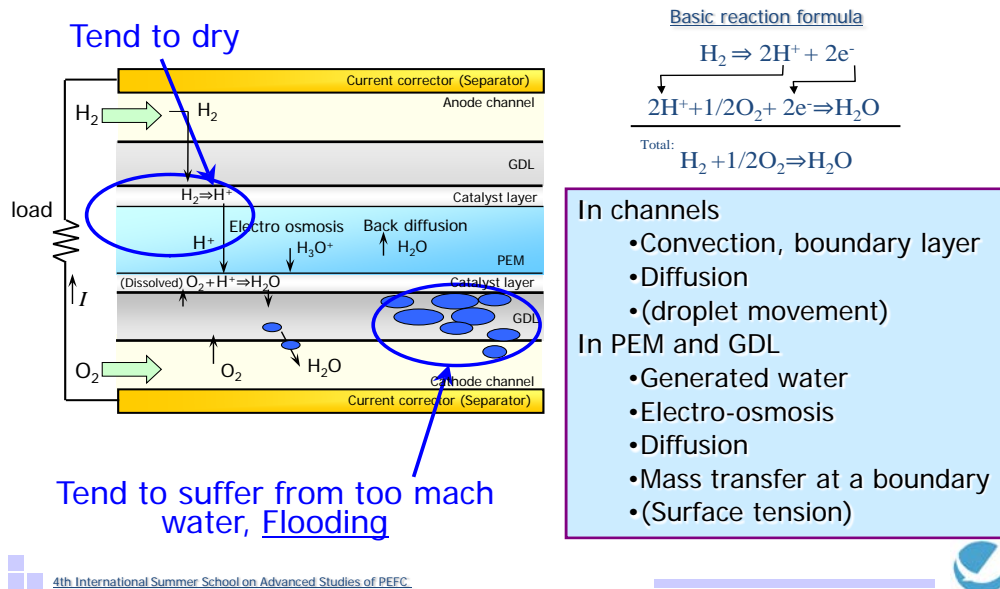
(Macroscopic) 2D water transport model



Considering averaged value is not enough.
Let's consider more detail

Advanced Studies of PEFC 5th International Summer School

Schematic view of 2D Water transport



4th International Summer School on Advanced Studies of PEFC

Generated water

$$J_{\text{H}_2\text{O}} = -\frac{\eta_e}{2F} i$$

role)

electrons of

Normally in PEFC,
we can assume current

Exception :

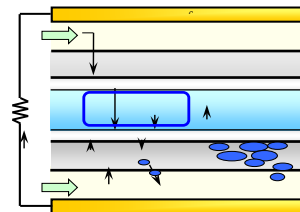


Electro osmosis Mechanism

$$n_{osm} = M_{OSM} \frac{F}{i}$$

many water molecules
moves with a proton (H⁺)

sorted



(Back) diffusion

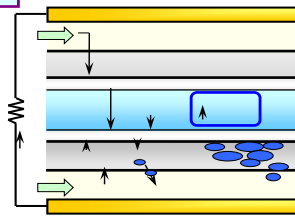
$$J_{diff} = -D \frac{\partial c}{\partial x} = -D \frac{\Delta c}{\Delta x}$$

D : Diffusion coefficient

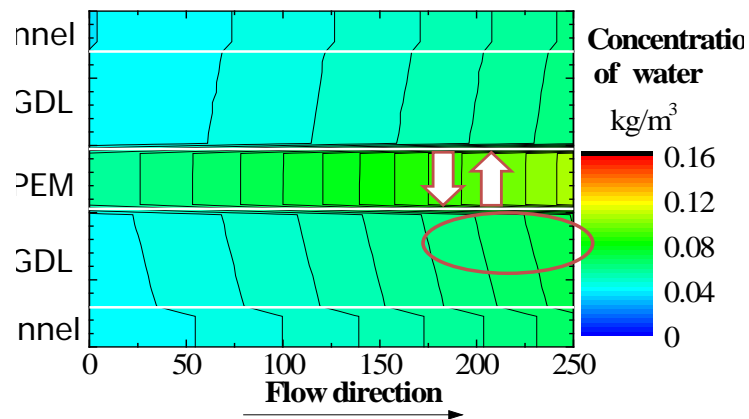
Diffusivity (cm^2/s)

J : Mole(or mass) flux by

$$\frac{\partial C}{\partial t} = D \frac{\partial^2 C}{\partial y^2} + D \frac{\partial^2 C}{\partial z^2} + S$$



A sample of calculated water distribution



Effect of water conditions on reaction distributions

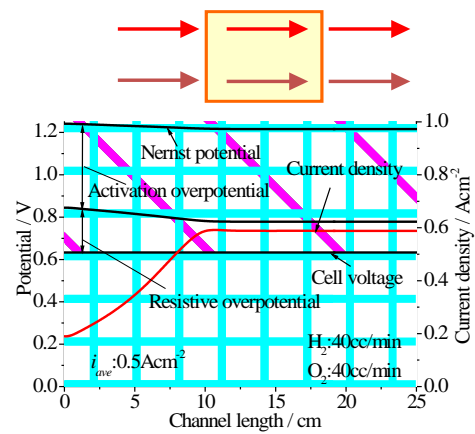
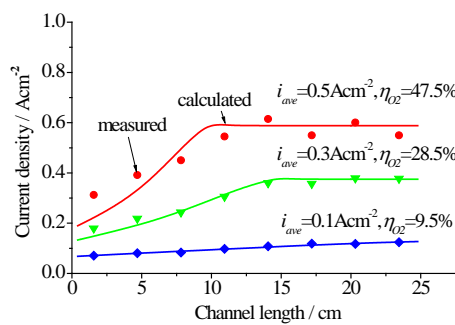
Reaction distribution
= Current distribution



Advanced Studies of PEFC 5th International Summer School

Dry gas but lower amount

($T_{cell}=60, T_{DPa}=T_{DPC}=30[^\circ\text{C}]$ $\text{H}_2=40, \text{O}_2=40[\text{cc}/\text{min}]$)

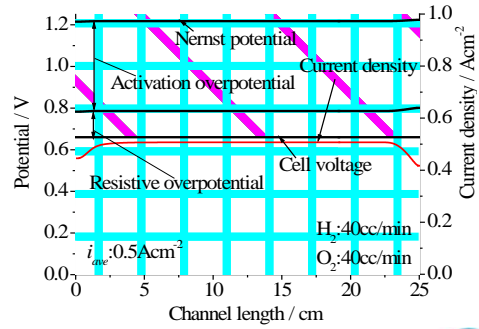
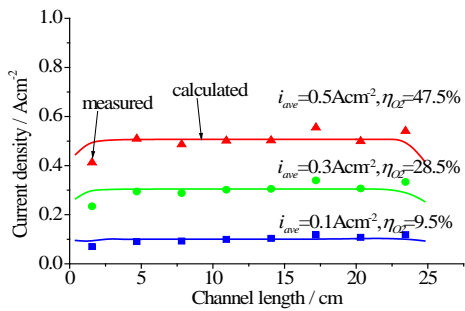
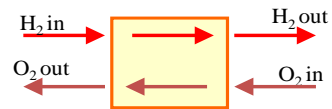


4th International Summer School on Advanced Studies of PEFC

Lower amount gas, counter flow

Low dew point temp. , Middle O₂ utilization rate (~47.5%) : case 2

($T_{cell}=60, T_{DPA}=T_{DPC}=30[^\circ\text{C}]$ H₂=40、O₂=40[cc/min])



BASIC OF THERMODYNAMICS FOR HYDROGEN PRODUCTION USING TRADITIONAL AND MEMBRANE REACTORS

Angelo Basile

Institute on Membrane Technology, Italian National Research Council, c/o University of Calabria, Cube 17/C, 87030 Rende (Cs), Italy. E-mail: a.basile@itm.cnr.it

Keywords: Membrane Reactors, Equilibrium Limited Reactions, Maximum Conversion.

INTRODUCTION

The most power-consuming operation in most chemical production is connected with the separation of multi-component mixtures. Today, separation technology in general, and membrane operations in particular, offer a good opportunity for energy savings; in fact, the thermodynamic efficiency of a separation process can have a profound impact on the overall cost of a chemical process. In view of reduction of energy-costs in thermal process engineering, the realization of well-integrated processes is something which chemical engineers are working with increasing intensity in recent years. In this context, thermodynamics provides, in addition to energy balances and strategies of optimum energy utilization, a general set of relationships for both phase and reaction *equilibria*. In these processes, the maximum performances of conventional reactors are evaluated with regard to the efficiency of energy conversion under the laws of thermodynamics: conservation of energy (first law) as well as the quality of energy (second law).

Most of the chemical reactions carried out on Traditional Reactors (TRs) are reversible and the conversion is necessarily limited by thermodynamic equilibrium. The exit conversion of such reversible reactions can be increased by using a Membrane Reactor (MR), where a selective removal of (almost) one of the products increases conversion beyond the maximum one that it is possible to obtain in the TR. In other words, the maximum conversion that is possible to have in a TR, in which a generic chemical reaction is carried out, corresponds to the equilibrium conversion, whereas in a MR a *supra-equilibrium* conversion is obtained.

In this lecture, the limiting conversions of chemical reactions carried out in a MR are discussed and compared with those in a TR.

EQUILIBRIUM OF A TR

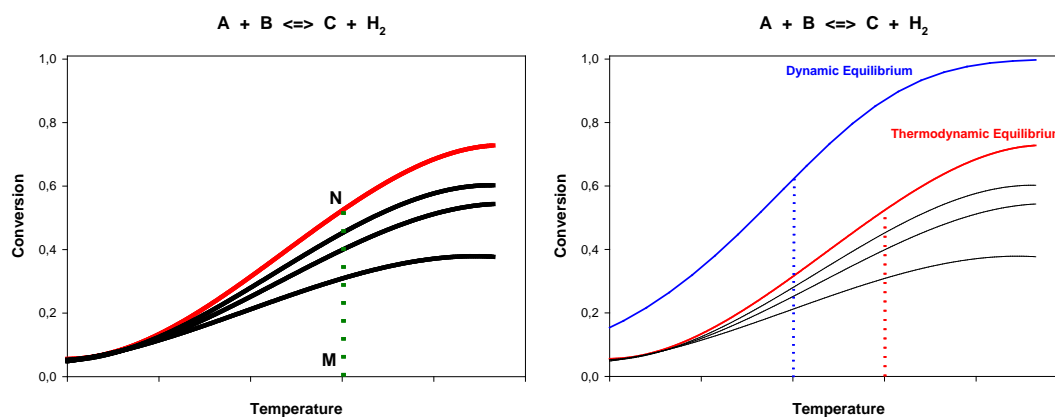
As it is well known, any change occurring in a *closed* (homogeneous or heterogeneous) pVT system of uniform T and p and also in thermal and mechanical equilibrium with its surroundings, but not initially at internal equilibrium with respect to chemical reaction, is irreversible, and must necessarily bring the system closer to an equilibrium state. The first and second laws of thermodynamic permit to predict the behaviour (*i.e.* the composition at equilibrium) of the system via the minimization of the total *Gibbs free energy*.

EQUILIBRIUM OF A MR

The thermodynamic equilibrium of a chemical reaction, a scientifically well accepted concept, is a constrain of the TRs. So it is clear that the effective conversion for a single passage of the reactant can never be higher than the equilibrium conversion. In order to overcome the equilibrium conversion, some other systems have to be used, such as a separation unit after the reactor or a recycle of the reactants. A MR is able to give a conversion higher than the corresponding equilibrium conversion of a TR. This sentence is

not in contrast with the laws of thermodynamic. In fact, the conversion of a MR is compared with the equilibrium conversion related to a TR, which indeed is a different reaction system.

Let's considering a generic equilibrium reaction " $A + B \rightleftharpoons C + H_2$ " carried out in both a MR and a TR. It is possible to demonstrate that the calculation of the maximum conversion for the MR can be easily done by using two conditions: the chemical equilibrium in the reaction zone and the permeation equilibrium between the reaction and permeation zones. The set of non-linear equations can be solved either using a Newton-Raphson algorithm or numerical commercial software. The equations can be solved, for example, using the Solver procedure in Matlab. A conceptual comparison between the results obtained for TR and MR (the feed gas is assumed to be continuously at equilibrium inside the MR) is given in the following figures [1] where the *Thermodynamic Equilibrium* curve represent the equilibrium conversion for a TR, whereas the *Dynamic Equilibrium* curve is related to only a (dense palladium-based) MR and represents the reaction not limited by chemical kinetics.



To resume, MRs offer a potentially new approach to solving a long standing problem – overcoming the thermodynamic limitations of chemical reversible reactions. This phenomenon is called “equilibrium shifting”. It should be noted that the equilibrium considered in MRs is the *hypothetical* equilibrium of the *closed* system formed by a fixed mass of the reaction side feed only. It is not the equilibrium of the actual MR system, which would include both the feeds to the reaction and permeate sides. However, it must be also stressed that Thermodynamics provides only one aspect: the selective and continuous removal of hydrogen is a *necessary* condition to achieve a conversion higher than equilibrium does, but it is not *sufficient* [2].

REFERENCES

- [1] A. Basile, F. Gallucci, M. De Falco, A. Ersoz and S. Tosti: Thermodynamic Approach of Membrane Reactors, ch. 2 - pagg. 35-62, in Simulation of Membrane Reactors, A. Basile & F. Gallucci Eds., Nova Sci. Pub., 2009.
- [2] B.A. Raich and H.C. Foley: Supra-equilibrium conversion in palladium membrane reactors: kinetic sensitivity and time dependence, Appl. Catal. A, 129 (1995) 167-188.

Basic of thermodynamics for hydrogen production II using traditional and membrane reactors

Angelo Basile

*Institute on Membrane Technology
(ITM-CNR), Rende (CS) - Italy*

a.basile@itm.cnr.it

EXAMPLE 1. WATER GAS SHIFT REACTION.

- Consider a system composed by the following gaseous species: CO, H₂O, CO₂ and H₂. The initial (*i.e.* before reaction) composition is: 1 mol CO, 3 mol H₂O, 0 mol CO₂ and 0 mol H₂. Calculate the equilibrium composition at 1000 K and 1 bar. Values of $\Delta G_f^\circ(1000\text{ K})$ are:

$$\Delta G_f^\circ(\text{CO}) = - 200.58 \text{ kJ/mol}$$

$$\Delta G_f^\circ(\text{H}_2\text{O}) = - 192.59 \text{ kJ/mol}$$

$$\Delta G_f^\circ(\text{CO}_2) = - 395.85 \text{ kJ/mol}$$

$$\Delta G_f^\circ(\text{H}_2) = 0.0 \text{ kJ/mol}$$

Solution

The general equation to be used is:

$$\Delta G_f^\circ + RT \ln (\phi_i x_i p/p^\circ) + \lambda_k a_{ik} = 0 \quad (i = 1, 2, \dots, n)$$

In this case, there are 4 chemical species (CO, H₂O, CO₂ and H₂, $n = 4$) and 3 different atomic masses (C, O, H, $k = 3$) in the system; the equation to be solved becomes:

$$\Delta G_f^\circ + RT (\ln \phi_i + \ln x_i + \ln p/p^\circ) + \lambda_k a_{ik} = 0 \quad (i = 1, 2, 3, 4)$$

Being $p = p^\circ = 1$ bar, it follows

$$\Delta G_f^\circ + RT (\ln \phi_i + \ln x_i) + \lambda_k a_{ik} = 0 \quad (i = 1, 2, 3, 4)$$



- Values of A_k are determined from initial moles:
- Carbon: $A_C (1 \text{ mol CO}) = 1 \times 1 = 1$
- Oxygen: $A_O (1 \text{ mol CO} + 3 \text{ mol H}_2\text{O}) = 1 \times 1 + 3 \times 1 = 4$
- Hydrogen: $A_H (3 \text{ mol H}_2\text{O}) = 3 \times 2 = 6$
- Values a_{ik} are determined from the chemical formulas of the species.



	Element k		
	Carbon	Oxygen	Hydrogen
	$A_k = \text{number of atomic masses of } k \text{ in the system}$		
Species i	$A_C = 1$	$A_O = 4$	$A_H = 6$
CO	$a_{CO,C} = 1$	$a_{CO,O} = 1$	$a_{CO,H} = 0$
H ₂ O	$a_{H_2O,C} = 0$	$a_{H_2O,O} = 1$	$a_{H_2O,H} = 2$
CO ₂	$a_{CO_2,C} = 1$	$a_{CO_2,O} = 2$	$a_{CO_2,H} = 0$
H ₂	$a_{H_2,C} = 0$	$a_{H_2,O} = 0$	$a_{H_2,H} = 2$



Being the system at 1000 K, the hypothesis of perfect gas is justified and so the term ϕ_i is zero. Then:

$$\Delta G_f^\circ + RT (\ln x_i) + \lambda_k a_{ik} = 0 \quad (i = 1, 2, 3, 4)$$

Moreover, considering $RT = 8.31 \text{ kJ/mol}$

$$\Delta G_f^\circ + 8.31 (\ln x_i) + l_k a_{ik} = 0 \quad (i = 1, 2, 3, 4)$$



Then, the corresponding 4 equations related to the 4 species are:

$$\text{CO:} \quad -200.58 + 8.31 (\ln x_{\text{CO}}) \quad + l_C \quad + \quad l_O \quad = 0$$

$$\text{H}_2\text{O:} \quad -192.59 + 8.31 (\ln x_{\text{H}_2\text{O}}) \quad + \quad l_O \quad + \quad 2l_H \quad = 0$$

$$\text{CO}_2: \quad -395.85 + 8.31 (\ln x_{\text{CO}_2}) \quad + l_C \quad + \quad 2l_O \quad = 0$$

$$\text{H}_2: \quad 0.0 + 8.31 (\ln x_{\text{H}_2}) \quad + \quad 2l_H \quad = 0$$

Using the equation

$$\text{SUM}_{i=1,n} n_i a_{ik} = A_k$$

dividing both members by n , it follows:

$$\text{SUM}_{i=1,n} (n_i a_{ik})/n = (A_k)/n$$

and, being also $x_i = n_i/n$ and $n = n_p$, we have:

$$\text{SUM}_{i=1,n} x_i a_{ik} = (A_k)/n_i$$

Then, the mass balance equations corresponding to the 3 elements are:

$$\text{Carbon:} \quad x_{CO} + x_{CO_2} = 1 / n_i$$

$$\text{Oxygen :} \quad x_{CO} + x_{CO_2} = 4 / n_i$$

$$\text{Hydrogen:} \quad x_{H_2O} + x_{H_2} = 6 / n_i$$

Moreover, it is also always valid:

$$x_{CO} + x_{CO_2} + x_{H_2O} + x_{H_2} = 1$$



Finally, we have:

$4 + 3 + 1 = 8$ non-linear equations, and

8 unknowns: x_{CO} , x_{CO_2} , x_{H_2O} , x_{H_2} , n_i , λ_C , λ_O , λ_H .

Simultaneous computer solution will give the equilibrium composition requested by the exercise. To be observed that the 3 Lagrange multipliers (λ_C , λ_O , λ_H) do not have any physical meaning but were useful for the calculation procedure



ULTRA PURE HYDROGEN PRODUCTION USING MEMBRANE REACTOR TECHNOLOGY

Angelo Basile, Adolfo Iulianelli

Institute on Membrane Technology of the Italian National Research Council (ITM-CNR),
Via P. Bucci Cubo 17/Cc/o University of Calabria, Rende (CS), 87036 – Italy, Ph.: +39
0984 492013/1, Fax: +39 0984 402103,
e-mail: a.basile@itm.cnr.it, a.iulianelli@itm.cnr.it

OUTLOOK

Today, hydrogen represents a convenient energy carrier for many applications. In the last decades, several studies address the production of hydrogen coming from reforming reactions performed in membrane reactors and this field of research represents the scope of this chapter, reviewing the recent findings about hydrogen generation from reforming processes of renewable sources combined with membrane reactor technology. Furthermore, a discussion about the general classification of the membranes is given and discussed.

INTRODUCTION

The climate change and air pollution related to the emissions due to the exploitation of fossil fuels is pushing towards the utilization of alternative technologies and the exploitation of renewable sources. Among other solutions, proton exchange membrane fuel cells (PEMFCs) represent a viable energy solution, since they have zero greenhouse gas emission. Nevertheless, PEMFCs supplying imposes the purification of hydrogen, which currently takes place in second stage processes, namely water gas shift (WGS) reaction performed in two reactors operating in series at high and low temperatures, partial oxidation (PROX) and pressure swing adsorption (PSA). In particular, Figure 1 represents most of the processes used for hydrogen generation coming from both renewable sources and derived of fossil fuels.

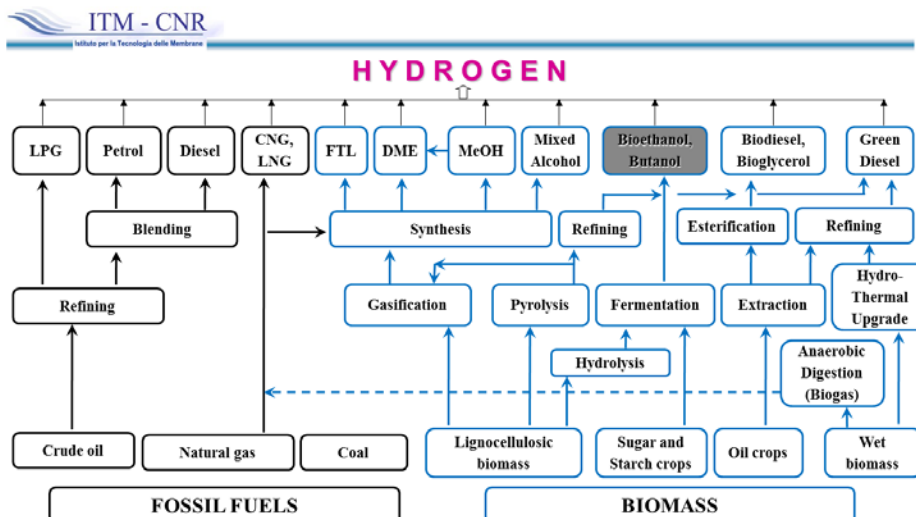


Figure 1. Hydrogen production from several processes and different feedstocks

The hydrogen purification affects negatively such reforming process in terms of costs and efficiency. Thus, much attention has been devoted to the development of alternative technologies to generate high grade hydrogen, particularly the membrane reactor (MR) technology, which plays an important role as an alternative solution to the conventional reactors (CRs), Figure 2.

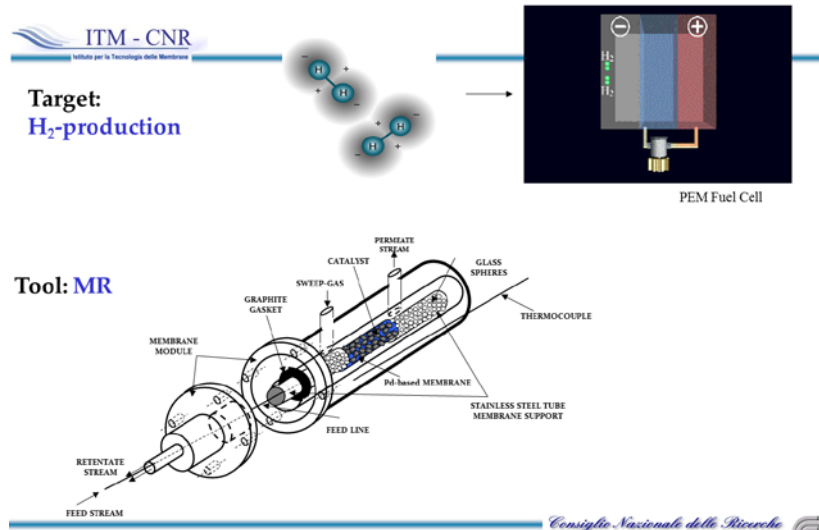


Figure 2. Hydrogen generation from membrane reactors for PEMFCs supplying

The main advantage of MR utilization consists of combining in a single stage the reforming reaction for generating hydrogen and its purification without needing any further processing [1,2].

However, the concept of MRs has been introduced since the 1950s, associated with the utilization of new inorganic materials and the development of high-temperature membrane processes.

Membrane	ϕ_{pore} (nm)	Diffusion mechanism	$\alpha_{H_2/other\ gas}$	Permeability	Reactant loss
macroporous	> 50	Poiseuille	1	very high	high
mesoporous	2 – 50	Knudsen	$H_2/N_2=3.74$	high	average
microporous	< 2	Activated process	high	average	low
dense Pd	-	Fick	infinite	very low	-

Some characteristics of porous and dense membranes.

- According to the IUPAC definition, porous membranes with average pore diameter larger than 50 nm are classified as macroporous, and those with average pore diameters in the intermediate range between 2 and 50 nm as mesoporous; microporous membranes have average pore diameters smaller than 2 nm.
- Macroporous membranes show no selectivity towards the gas permeating through the pores.
- Mesoporous membranes suffer from poor membrane selectivity, since the permeation is mainly based on a Knudsen diffusion mechanism, and separation is only affected by molecular size only.

Figure 3. Inorganic membranes subdivision

Generally, the MRs are subdivided as follows:

- a) Dense and porous inorganic membrane reactors.
- b) Electrochemical membrane reactors (fuel cells, electrolytic cells, etc.)
- c) Zeolite membrane reactors.
- d) Photo-catalytic membrane reactors.
- e) Polymeric membrane reactors.
- f) Bio-medical membrane reactors or membrane bio-reactors.

The combination of membranes using chemical and biochemical reactions makes it possible to intensify the whole process.

Generally, membranes are categorized by their material or structure and are defined as a layer of material, acting as a selective barrier between two phases, remaining impermeable to specific particles, molecules, or substances under a specific driving force.

Inorganic membranes are further subdivided as in Figure 3.

Of great relevance, the performance of a generic membrane is evaluated by:

- 1) the permeating flux through the membrane;
- 2) its perm-selectivity.

The permeating flux through a membrane can be expressed as flux or permeation rate (J) and it is defined as the volume flowing through the membrane per unit area and time. Since the transport through the membrane takes place as a result of a driving force acting on the components in the feed, the permeation rate through the membrane is proportional to this driving force as in eq. (1):

$$J = -A \frac{dY}{dx} \quad (1)$$

Where, A represents the phenomenological coefficient and dY/dx the driving force, expressed as the gradient of Y as a variable indicating temperature, concentration, pressure along with a coordinate x perpendicular to the transport barrier.

The separation factor (α), normally adopted for gas mixtures, can be defined for a mixture consisting of two components as in Eq. (2) reported below:

$$\alpha_{A/B} = \frac{y_A / y_B}{x_A / x_B} \quad (2)$$

where y_A and y_B are the concentrations of the mixture components A and B in the permeate and x_A and x_B their concentrations in the feed. If the permeation rate of component A through the membrane is larger than that of component B, the separation factor is represented by the ratio $\alpha_{A/B}$; if component B permeates preferentially, then the separation factor is represented by $\alpha_{B/A}$. If $\alpha_{A/B} = \alpha_{B/A} = 1$, no separation occurs.

HYDROGEN TRANSPORT IN PALLADIUM-BASED MEMBRANES


Various inorganic materials can be used for preparing membranes such as ceramic, carbon, silica, zeolite, oxides (alumina, titania, zirconia) as well as palladium, silver etc. and their alloys. Concerning the metallic membranes, they have high cost and can suffer from embrittlement phenomenon, particularly in the case of palladium membranes.

Furthermore, they possess low permeability when showing high hydrogen perm-selectivity at moderate temperatures.

However, it is worth of noting that much literature exists on palladium-based membranes, especially in the field of high grade hydrogen generation due to their high hydrogen solubility and perm-selectivity [3].

Palladium absorbs about 600 times its volume of hydrogen at ambient temperature, although some palladium alloys show higher hydrogen permeability than pure palladium. Furthermore, palladium alloys show higher resistance to the hydrogen embrittlement than pristine palladium. Indeed, if pure palladium membranes are exposed to a hydrogen flux, the amount of hydrogen absorbed into the membrane lattice can be responsible of a phase transition from α to β palladium hydride. This is the so-called "hydrogen embrittlement phenomenon" and it is due to the dissolved hydrogen that makes several elongations of the metallic film (involving in the α - β hydride transformations), causing fractures after repeated thermal cycles. Regarding the palladium-silver alloy, the membrane lattice is expanded by the silver atoms, making the alloy less influenced by the hydrogen permeation and, thus, less brittle than the pure palladium [3]. In dense self-supported Pd-based membranes, the molecular transport takes place via solution-diffusion mechanism, which involves the following activated steps, Figure 4:

- 1) dissociation of molecular hydrogen at the gas/metal interface,
- 2) adsorption of the atomic hydrogen on the membrane surface,
- 3) dissolution of atomic hydrogen into the palladium matrix,
- 4) diffusion of atomic hydrogen towards the opposite side,
- 5) re-combination from atomic to molecular hydrogen at the gas/metal interface,
- 6) molecular hydrogen desorption.

 ITM - CNR
Istituto per la Tecnologia delle Membrane

Generally, the permeation (at constant temperature) through a dense palladium membrane is described by the following expressions

$C_{H_2} = K_S \cdot p_{H_2}^{0.5}$ **Sieverts law**

$P_{H_2, Sievert} = D_{H_2} \cdot K_S$

$J_{H_2} = P_{H_2} (p_{H_2, ret}^n - p_{H_2, perm}^n) / t$ $(n = 0.5 \div 1)$

$J_{H_2, Sievert} = D_{H_2} \cdot K_S (p_{H_2, ret}^{0.5} - p_{H_2, perm}^{0.5}) / t$ $(n = 0.5)$

$J_{H_2} = P_{H_2, linear} (p_{H_2, ret} - p_{H_2, perm}) / t$ $(n = 1)$

Figure 4. Equation relating the hydrogen transport in Pd-based membranes

Each one of the aforementioned steps can be responsible for hydrogen permeation through the dense palladium membrane, all of which also depend on variables such as temperature, pressure, gas mixture composition and thickness of the membrane.

The hydrogen transport through a generic membrane can be expressed as the hydrogen permeating flux, as follows:

$$J_{H_2} = Pe_{H_2} (p_{H_2,retentate}^n - p_{H_2,permeate}^n) / \delta \quad (3)$$

where J_{H_2} represents the hydrogen flux permeating through the membrane, Pe_{H_2} the hydrogen permeability, δ the membrane thickness, $p_{H_2,retentate}$ and $p_{H_2,permeate}$ the hydrogen partial pressures in the retentate (reaction side) and permeate (side in which hydrogen permeating through the membrane is collected) zones, respectively, n (variable in the range 0.5 - 1) the dependence factor of the hydrogen flux on the hydrogen partial pressure. For membranes having a thickness higher than 5 μm , equation (4) becomes the *Sieverts-Fick* law (5):

$$J_{H_2, Sieverts-Fick} = Pe_{H_2} \cdot (p_{H_2,retentate}^{0.5} - p_{H_2,permeate}^{0.5}) / \delta \quad (4)$$

At high pressures, the hydrogen-hydrogen interactions in the palladium bulk are not negligible, so that n becomes equal to 1:

$$J_{H_2} = Pe_{H_2} \cdot (p_{H_2,retentate} - p_{H_2,permeate}) / \delta \quad (5)$$

Furthermore, if the hydrogen permeability is expressed as an *Arrhenius*-like equation, the *Sieverts-Fick* law becomes *Richardson's* equation (7):

$$J_{H_2} = Pe_{H_2}^0 [\exp(-E_0/RT)] \cdot (p_{H_2,retentate}^{0.5} - p_{H_2,permeate}^{0.5}) / \delta \quad (6)$$

Such contaminants as hydrogen sulfide, SO_2 , Hg vapor, thiophene, arsenic, unsaturated hydrocarbons, or chlorine carbon can irreversibly poison dense Pd-based membranes. Furthermore, the presence of CO affects a lot the hydrogen permeating flux through the membrane, particularly below 150 $^\circ\text{C}$ or at high CO feed concentrations. This is due to the effect of adsorbed CO, displacing the adsorbed hydrogen, covering the hydrogen adsorption sites. Also steam can be responsible of a negative influence on the hydrogen permeation through dense Pd-membranes. Indeed, the water vapor dissociation/recombinative desorption makes possible the contamination of the palladium surface with adsorbed oxygen.

During the last years, special attention has been paid to composite Pd-based membranes with the intent of reducing the amount of palladium and, consequently, lowering the cost. In detail, composite membranes can be constituted by a thin dense layer of palladium or its alloy deposited onto a porous support among porous Vycor glass (silica gel), SiO_2 , Al_2O_3 , and B_2O_3 or porous stainless steel (PSS) and pencil [4]. In particular, a thermal expansion coefficient of the aforementioned supports close to palladium makes the composite membrane durable and resistant to cracks due to the thermal cycles, simplifying the gas sealing. Sometimes, at relatively high temperatures PSS supports alloy the palladium, lowering the hydrogen permeability. Then, as a consequence, a PSS-supported Pd-based membrane can offer an optimal compromise among moderate cost, high H_2 permeability and perm-selectivity and good mechanical resistance. Nevertheless, thin selective Pd-layers can be fulfilled directly onto the specific support and, depending on the membrane preparation process, a threshold about the minimum thickness obtainable by the deposition method can be encountered. This limits the performance of a composite membrane and it is more emphasized at higher support pore sizes. However, the reduction of the palladium layer involves two opposing effects. On one hand, thin Pd-layers can induce an atomic H diffusion time reduction with a consequent enhancement of the

membrane permeance, meanwhile decreasing the cost due to a lower Pd content. On the other hand, the hydrogen diffusion resistance can be increased owing to the need of reducing the pores size of the support. Another important issue associated to the deposition of palladium on a support (porous or dense) is the entire membrane stability. For example, owing to different thermal expansion coefficients within the Pd-layer and the selective layer volume variation due to the hydrogen diffusion in the palladium lattice, the membrane support could show an instability at the interface Pd-layer/support in terms of adherence loss, flaking-off and cracking.

Furthermore, the interaction between the selective Pd-layer with the support and the gaseous environment can introduce other forms of instability due to the Pd-layer microstructure. Therefore, thin Pd-layers, small grains and high density of grain borders are related to grain size growth, impurity dissolution, grain borders diffusion and alloy segregation. All of the aforementioned issues on instability can result in a reduction of the membrane performance, particularly evident at higher temperatures.

The general difference between dense self-supported and composite Pd-based membranes is related to the hydrogen perm-selectivity with respect to all other gases. Indeed, for dense Pd-membranes it is full, while for the composite Pd-membranes it can vary depending on many parameters such as: Pd-layer, preparation technique, support, and support preparation. The composite Pd-based membranes are commonly not fully hydrogen perm-selective and the hydrogen permeating flux can be determined by using Eq. (4), as given earlier in this chapter.

In this case, the n value, variable from 0.5 (used for indicating *Sieverts-Fick* law and applied for dense Pd-membranes) to 1 (used when, at high pressures, the hydrogen-hydrogen interactions in the palladium bulk are not negligible) is calculated for a supported Pd-based membrane. A linear regression equation can be used with experimental points obtained by considering the experimental hydrogen permeating flux against transmembrane pressure at different “ n ”, with the associated response factor R^2 . The most coherent “ n ” factor is, then, the one associated with the linear regression and the maximum R^2 factor.

However, housing whatever Pd-based membrane in a MR, its effect on a such reforming reaction can make it possible to overcome the thermodynamic restrictions of equilibrium limited reactions due to the removal of hydrogen from the reaction side for the selective permeation through the membrane (“shift effect”). In fact, owing to *Le Chatelier’s* principle, the reaction can be shifted towards the reaction products, with a consequent enhancement of the conversion and with the further benefit of collecting high grade hydrogen on the permeate side of the MR. Therefore, dense self-supported Pd-based MRs seem to be more adequate to generate PEMFC grade hydrogen due to the full hydrogen perm-selectivity of the membrane (Figure 5), while – depending on the finite value of hydrogen perm-selectivity of the composite membrane – the purified hydrogen can be supplied to other kinds of fuel cells or to high temperature PEMFCs, whose CO content can be up to 20000 ppm.



Figure 5. Dense Pd-based MR at bench scale – ITM-CNR laboratories.

HIGH-GRADE HYDROGEN GENERATION FOR FUEL CELLS FROM REFORMING OF RENEWABLES IN MRS

In the last years, MRs technology has been applied to reforming reactions of renewable sources to generate high-grade hydrogen. Among a number of renewable sources, ethanol and methanol seem to be the most promising because directly producible from biomass. In the following the most recent advances about hydrogen production from ethanol and methanol steam reforming reaction through MRs utilization are presented and discussed.

ETHANOL STEAM REFORMING IN MRS

Ethanol steam reforming (ESR) reaction for hydrogen production has been mostly studied in conventional fixed bed reactors even though more recently a number of researchers has spent their efforts to perform this reaction in MRs. Table 1 shows some representative studies about ESR reaction performed in different MRs, providing the most important and up-dated results in terms of high-grade hydrogen generation, as recently published by Basile et al. [5].

Table 1 is split in two parts i) dense self-supported and ii) composite supported Pd-based membranes in MRs. As requested by the scientific community, the need of decreasing the Pd-content in Pd-based membranes has strongly emerged for reducing the membrane cost. As shown in the aforementioned table, the purity of hydrogen produced during the reaction is ~ 100% in the case of dense Pd-membranes utilization and between 90 and 100% in case of composite Pd-membranes.

Our group at CNR-ITM has been involved in several studies about ESR reaction, paying special attention to both dense and composite Pd-based MRs, obtaining a variety of results, depending on the operating conditions adopted as well as the catalysts used.

As summarized in the table, Borgognoni et al. (see ref. [5]) used a 150 μm thick dense Pd-Ag hydrogen full perm-selective membrane in a MR at 450 °C and 5.0 bar to obtain a 70% hydrogen yield and more than 90% hydrogen recovery with a hydrogen purity of 100%.

Mironova et al. (see ref. [5]) used a Pd-Ru dense membrane 50 μm thick in an MR, reaching around 50% hydrogen yield with the hydrogen recovered being 100% pure at 450 °C and 1.0 bar.

In the last few years, much attention has been paid to developing composite Pd-based MRs. As an example, Papadias et al. (see ref. [5]) carried out the ESR reaction in a MR allocating a composite Pd-Ag based membrane having a Pd-Ag layer of around 30 μm , reaching 75% hydrogen yield at 700 °C and around 7.0 bar.

Lin et al. developed a MR housing a supported Ni-Pd-Ag membrane with an active layer < 8 μm , allowing a hydrogen recovery of about 70% with a purity > 90%, while reaching 80% ethanol conversion at 450 °C and 3.0 bar.

More recently, Hedayati et al. (see ref. [5]) prepared a composite Pd-membrane with a dense layer of around 30 μm deposited via electroless plating technique onto a porous stainless steel support, globally obtaining at 650 °C and 4.0 bar, complete ethanol conversion and a hydrogen yield around 35%.

Murmura et al. (see ref. [5]) developed a MR housing a really thin Pd-layer supported on alumina, produced by ECN. In this case, 100% ethanol conversion, 80% hydrogen yield and 100% hydrogen purity were obtained with this technological solution.

Table 1. Literature studies about ethanol steam reforming reaction in MRs (adapted from Basile et al. [5]).

Membrane in the MR	Pd/Pd-alloy layer [μm]	T [°C]	p [bar]	Conversion [%]	H ₂ recovery [%]	H ₂ purity [%]	Reference
dense Pd-Ag	50	400	1.5	95	30	≈ 100	Lulianelli & Basile [43]
dense Pd-Ag	50	400	3.0	~ 100	90	≈ 100	Lulianelli et al. [44]
dense Pd-Ag	50	400	1.0	50	< 10	≈ 100	Lulianelli et al. [45]
dense Pd-Ag	50	400	1.3	~ 100	15	≈ 100	Basile et al. [46]
dense Pd-Ag	50	500	3.5	99	~ 27	≈ 100	Basile et al. [47]
dense Pd-Ag	150	450	5.0	-	93	≈ 100	Borgognoni et al. [48]
dense Pd-Ru	50	450	1.0	-	-	≈ 100	Mironova et al. [72]
composite Pd-Ag	30	700	~ 7.0	-	-	-	Papadias et al. [49]
composite Ni-Pd-Ag	< 8	450	3.0	81	-	>	Lin et al. [50]
composite Pd on Al ₂ O ₃	8	400	3.0	98	67	≈ 97	Lulianelli et al. [51]
composite Pd on PSS	25	400	8.0	100	55	≈ 95	Basile et al. [52]
composite Pd on PSS	25	400	12.0	87	12	≈ 95	Seelam et al. [53]
composite Pd-Ag on PSS	30	650	4.0	100	-	-	Hedayati et al. [73]
composite Pd on Al ₂ O ₃	4-5	480	10	100	-	≈ 100	Murmura et al. [74]

¹ calculated.

METHANOL STEAM REFORMING IN MRS

Methanol can be also produced renewably and useful for producing hydrogen in a steam reforming process. Methanol steam reforming (MSR) reaction is commonly performed in conventional reformers in the range between 240 and 260 °C.

Table 2. Literature studies about methanol steam reforming reaction in MRs (adapted from Basile et al. [5]).

Membrane	Pd/Pd-alloy layer [μm]	T [$^{\circ}\text{C}$]	p [bar]	Conversion [%]	H ₂ recovery [%]	H ₂ purity [%]	Reference
Dense Pd-Ag	50	300	3	-	80	\approx 100	Iulianelli et al. [56]
Dense Pd-Ru-In	200	200	7	\approx 90	\approx 24	\approx 100	Itoh et al. [63]
Dense Pd-Cu	25	300	10	> 90	\approx 38	\approx 100	Wieland et al. [64]
Composite Pd-Ag/Al ₂ O ₃	7	330	3.0	85	40	\approx 100	Liguori et al. [55]
Composite Pd-Ag/ α -Al ₂ O ₃	3.9	250	10	100	95	\approx 100	Israni & Harold [65]
Composite Pd-Ag/PSS	20/25	240	10	< 40	18	-	Rei et al. [66]

When carried out in MRs, CO can be formed as a byproduct of hydrogen production, representing the main drawback of this reaction because acting as a poison on the Pd-surface. Table 2 summarizes some recent representative results coming from Basile et al. [5] about MSR reaction in MRs, summarizing a number of results from the open literature about both dense and composite Pd-based MRs. As in the case of the ESR reaction, our group at CNR-ITM spent much attention about MSR in Pd-based MRs, paying much attention to different kinds of MRs, analyzing the influence of such parameters as reaction temperature, pressure, residence time, feed molar ratio, sweep gas flow rate and oxygen addition. In all of the investigated cases, it was found that Pd-based MRs showed clear superiority in terms of methanol conversion, selectivity and productivity over the CRs, operating at the same experimental conditions. As our best result regarding a dense self-supported Pd-Ag MR, 80% hydrogen recovery with a purity of about 100% was reached at 300 °C and 3.0 bar. On the contrary, by using a composite Pd-based MR 85% methanol conversion and 40% hydrogen recovery were reached with around 100% of purity and a CO content lower than 10 ppm, as required by low temperature PEMFCs.

However, regarding dense membranes, other researchers developed MRs (housing dense and unsupported Pd-membranes at different thickness) to carry out MSR reaction by optimizing the experimental conditions, achieving complete methanol conversion, high hydrogen recovery with around 100% of hydrogen purity. As a general comment about the data summarized in Table 2, it is possible to observe that, by reducing the palladium thickness in the composite Pd-based membranes, the high H₂/other gas perm-selectivity is maintained sometimes at the same level of the dense ones showing high performance during MSR reaction in terms of methanol conversion and hydrogen recovery.

For example, Israni and Harold obtained 100% of methanol conversion with a correspondent hydrogen recovery of 95% at a purity of around 100%, at 250 °C and 10 bar.

On the contrary, in the work of Rei et al., low performance was achieved (less than 40% of methanol conversion and 20% of hydrogen recovery at 200 °C and 10 bar), confirming that the solution of thin Pd-layers deposited onto porous supports is not really effective.

CONCLUSION

PEMFC-grade hydrogen can be produced alternatively from reforming processes of renewables such as ethanol and methanol by utilizing MRs technology. With respect to the conventional processes, this option alternative choice can make possible the integration of MRs with the PEMFCs. Indeed, an important issue, not commonly addressed in the specialized literature, takes into account that natural gas, or other derived of fossil fuels, is essentially used for stationary applications, generating high-impact products for the ambient. On the other hand, it would be expected that renewable sources such as methanol and ethanol could drive the production of hydrogen by taking care the ambient and harmful emissions. Nevertheless, the development of MR technology demonstrates that efforts are still needed to solve some deficiencies related to its utilization on a larger industrial scale.

ACRONYMS

PPS	Porous stainless steel
PEMFC	Proton exchange membrane fuel cell
MSR	Methanol steam reforming
MR	Membrane reactor
ESR	Ethanol steam reforming
CR	Conventional reactor

SYMBOLS

α	Separation factor
δ	Membrane thickness
y_A, y_B	concentrations of the mixture components <i>A</i> and <i>B</i> in the permeate
<i>Y</i>	Variable indicating temperature, concentration, pressure, etc.,
x_A, x_B	concentrations of the mixture components <i>A</i> and <i>B</i> in the feed
<i>X</i>	Coordinate
<i>T</i>	Absolute temperature
<i>r</i>	Reaction rate
<i>R</i>	Universal gas constant
$p_{H_2-retentate}$	Hydrogen partial pressures in the retentate side
$p_{H_2-permeate}$	Hydrogen partial pressures in the permeate side
$P_{\Theta H_2}$	Hydrogen permeability
P_{e_0}	Pre-exponential factor
p	Partial pressure
<i>n</i>	Dependence factor of the hydrogen flux to the hydrogen partial pressure
K_{eq}	Equilibrium constant of reactions
<i>k</i>	Rate coefficient of reactions
<i>K</i>	Adsorption constant
J_{H_2}	Hydrogen flux permeating through the membrane
<i>H</i>	Permeation rate
E_a	Apparent activation energy

REFERENCES

- [1] A. Iulianelli, S. Liguori, T. Longo, A Basile, Inorganic membrane and membrane reactor technologies for hydrogen production, in "Hydrogen Production: Prospects and Processes", Damon Robert Honery and Patrick Moriarty (Eds.) (Victoria, Australia), Nova Science Publishers, Series: Energy Science, Engineering and Technology, Ch. 12, pp. 377-398, (2012), ISBN: 978-1-62100-246-8.
- [2] S. Wieland, T. Melin, A. Lamm, Membrane reactors for hydrogen production, Chem. Eng. Sci., 57 (2002) 1571-1576.

- [3] A. Basile, A. Iulianelli, T. Longo, S. Liguori, M. De Falco, Pd-based selective membrane state-of-the-art, Ch. 2 pp. 21-55 in "Membrane Reactors for Hydrogen Production Processes", L. Marrelli, M. De Falco & G. Iaquaniello Editors, Springer London Dordrecht Heidelberg New York, 2011, ISBN 978-0-85729-150-9, DOI 10.1007/978-0-85729-151-6.
- [4] S. Liguori, A. Iulianelli, F. Dalena, P. Pinacci, F. Drago, M. Broglia, Y. Huang, A. Basile, Performance and long-term stability of Pd/PSS and Pd/Al₂O₃ for hydrogen separation, *Membranes*, 4 (2014) 143-162.
- [5] A. Basile A. Iulianelli, G. Bagnato, F. Dalena, Hydrogen production for PEM fuel cells, Ch. 13, In: Production of hydrogen from renewable resources, Z. Fang, R.L. Smith, X. Qi (Eds.), in press (2015) Springer Netherlands, DOI: 10.1007/978-94-017-7330-0, Series ISSN: 2214-1537.

FUNDAMENTALS OF ELECTRODE PROCESSES

Bernhard Gollas

Graz University of Technology, Stremayrgasse 9, 8010 Graz, Austria
bernhard.gollas@tugraz.at,

Keywords: electrochemical double layer, electrochemical reactions, thermodynamics, kinetics, electrode reaction mechanisms.

INTRODUCTION

Fuel cells convert chemical energy into electrical energy through spontaneous electrochemical reactions. In order to understand the performance and limitations of fuel cells, a minimum knowledge of the basics of electrode processes is required. It is the purpose of this lecture to provide the necessary information. The most important terms and concepts will be introduced. The peculiarities of electrochemical in comparison to chemical reactions are discussed, i.e. the reaction site and the elemental steps of electrochemical reactions. It is explained, how these peculiarities affect the kinetics of electrode reactions. The following topics will be covered:

EXAMPLES OF ELECTRODE PROCESSES

Electrochemistry in and outside of equilibrium

Electron transfer

- Exchange current density
- Rate constant
- Overpotential
- Butler-Volmer model
- Tafel equation
- Microscopic models

Mass transport

- Diffusion
- Migration
- Convection

Interplay of electron transfer and mass transport

- Slow electron transfer
- Reversible systems

The electrochemical double layer

- Models
- Capacitance

Adsorption

- Adsorption equilibria in the absence of electron transfer
- Adsorption in the absence and presence of electron transfer
- Dissociative adsorption

Electrocatalysis

- The hydrogen evolution reaction
- The oxygen reduction reaction
- Electrocatalytic electrodes

Phase formation

- Nucleation
- Growth

Coupled chemical reactions

- Reaction mechanisms

REFERENCES

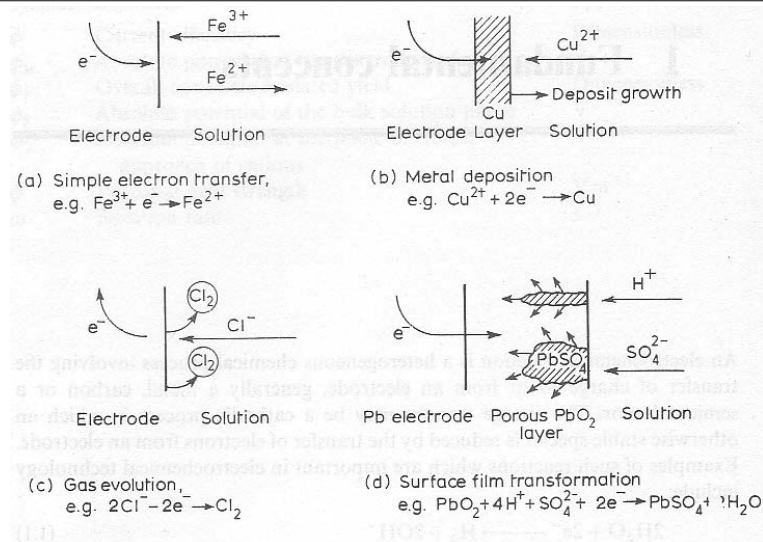
- [1] Derek Pletcher, A First Course in Electrode Processes, Electrosynthesis Company, Inc. 1991.
- [2] Derek Pletcher, Frank C. Walsh, Industrial Electrochemistry, 2nd edition, Chapman & Hall, 1993.
- [3] Derek Pletcher, Southampton Electrochemistry Group, Instrumental Methods in Electrochemistry, Ellis Horwood, 2001.
- [4] Allen J. Bard, Larry R. Faulkner, Electrochemical Methods: Fundamentals and Applications, Wiley; 2nd edition, 2000.
- [5] Fritz Beck, Elektroorganische Chemie: Grundlagen und Anwendungen, Weinheim 1974.
- [6] Volkmar M. Schmidt, Elektrochemische Verfahrenstechnik, Wiley-VCH, 2003.
- [7] Keith B. Oldham, Jan C. Myland, Alan M. Bond, Electrochemical Science and Technology: Fundamentals and Applications, Wiley, Chichester, 2012.

Fundamentals of Electrode Processes

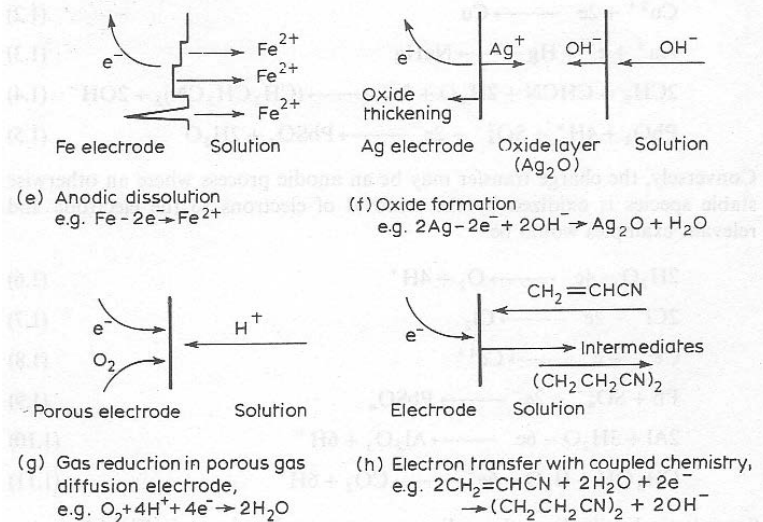
Overview

1. Introduction
2. The electrochemical double layer
3. Electron transfer
4. Mass transport
5. Adsorption
6. Electrocatalysis
7. Phase formation
8. Coupled chemical reactions

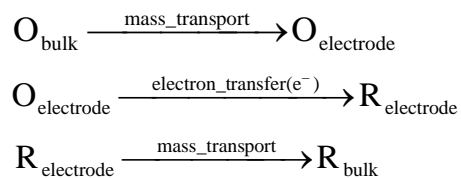
Introduction



Introduction



Simple electrode reactions: $\text{O} + \text{e}^- = \text{R}$



change (current density, i)

Complications:

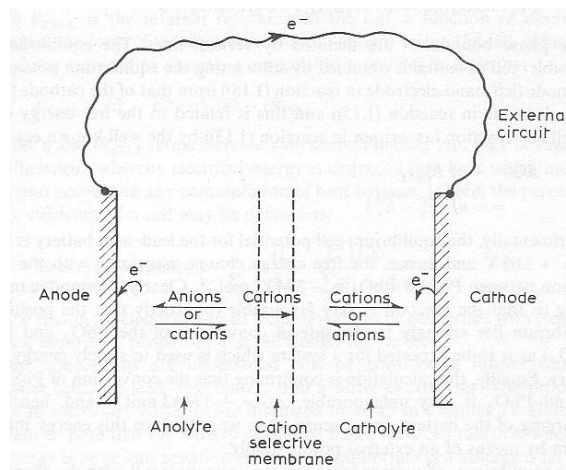
- Adsorption
- Coupled chemical reactions (in electrolyte or on electrode surface)
- Phase formation
- Multiple electron transfer

Note: For example, the complete anodic oxidation of benzene involves at least 30 electron transfer, 36 bond cleavage and 12 bond formation steps.

Introduction

1. **Reactant/product may be**
 - organic/inorganic/bio
 - charged/neutral
 - soluble/gas/solid
2. **Electrode reaction may be**
 - direct
 - indirect (mediated)
3. **Medium may be**
 - water
 - liquid, NH_3 , SO_2 , HF etc.
 - protic/aprotic organic solvent
 - molten salt (high/low temperature)
 - ion conducting solid
4. **Electrode may be**
 - metal
 - carbon
 - oxide
 - conducting ceramic
 - conducting polymer
 - semi conductor

Introduction



Charge transport processes in a cell having a cation selective membrane as separator

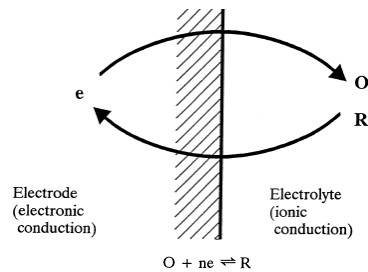
Introduction

Features of all electrochemical reactions:

Electrode as reducing or oxidising agent for molecules in solution (or gas phase, or solid).

1. Mass transport from 3-D solution space to 2-D electrode surface
 2. Current through solution and through outer circuit between the electrodes
- Difference to homogeneous (chemical) electron transfer (et) reactions
 - Charge balance = 0

Electron Transfer



'Electrodes'

metals
 semiconductors
 insulators

oxide covered metals
 conducting polymers
 modified electrodes
 bipolar electrodes
 metal powders/colloids

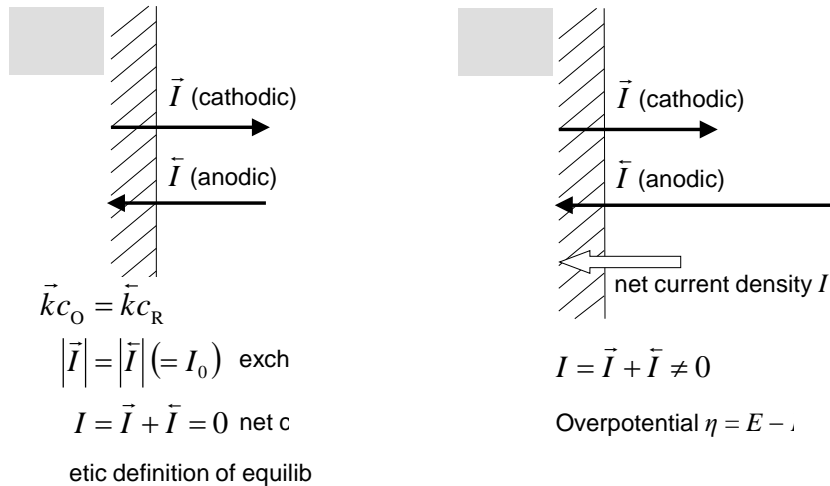
 etc.

'Electrolytes'

aqueous solutions
 non-aqueous solutions
 polyelectrolytes
 ionic liquids
 (molten salts)
 ionic conductors
 (beta alumina)

 etc.

Electron Transfer



Mass Transport

Three forms important in electrochemistry:

1. Diffusion (movement of species due to a concentration gradient)
2. Migration (movement of ions due to a potential gradient)
3. Forced/natural convection (movement of solution due to pressure gradient)

Note

1. Chemical change at electrode surface always leads to diffusion:
 - reactant to the electrode
 - product away from the electrode
2. In a cell there is always a potential gradient between anode and cathode.

Reactant and/or product is always a charged species

⇒ migration always occurs

⇒ minimised for reactant/product by addition of inert electrolyte
3. Flowing solution, moving electrode, gas sparging, etc. leads to convection.

Interplay of ET and MT

Complete I/E curve for a couple O/R having relatively low $I_0 \Rightarrow$ significant overpotential required to drive forward and backward reaction.

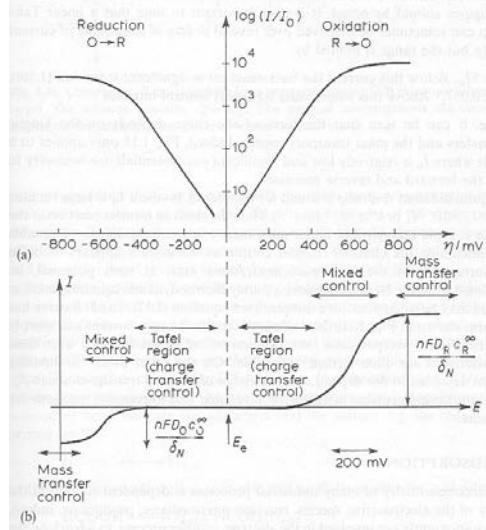
Linear Tafel region limited by:

1. $I > 5 I_0$

Below this current back-reaction is significant.

2. $I < 0,05 I_L$

Mass transport above this value.



The Electrochemical Double Layer

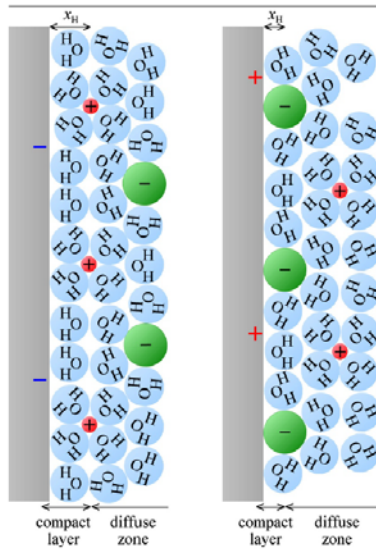


Figure 13.4 Cartoon of the supposed structure of the interfacial region of a double layer when the electronic conductor is charged negatively (left) or positively (right). Only a small portion of the diffuse zone is shown.

Keith B. Oldham, Jan C. Myland, Alan M. Bond, *Electrochemical Science and Technology: Fundamentals and Applications*, Wiley, Chichester, 2012.

DAFC, DBFC, HTPEM AND AFC

Viktor Hacker, Bernd Cermenek

Graz University of Technology, Inffeldgasse 25 C, A-8010 Graz, Austria
alexander.schenk@tugraz.at

Keywords: direct alcohol fuel cell, direct borohydride fuel cell, high-temperature PEFC, alkaline fuel cell

INTRODUCTION

Within the last decades, a wide range of possible applications for fuel cells were identified and thus, various types of fuel cells have been developed. These different types of fuel cells are most commonly distinguished either by their electrolyte, the used fuel or the working temperature. Naturally, much effort has been devoted to the development of fuel cell technologies, systems, components and materials. This abstract provides a short introduction into the fields of direct alcohol fuel cells (DAFCs), direct borohydride fuel cells (DBFCs), high-temperature polymer electrolyte fuel cells (HT-PEFCs) and alkaline fuel cells (AFCs).

DIRECT ALCOHOL FUEL CELLS

Fuel cells, which are capable of utilizing the chemical energy of liquid fuels directly, receive great attention for portable and mobile applications due to convenient, safe, and easy fuel storage. Naturally, alcohols are of high interest as such energy source due to widespread availability and their relatively high mass energy density, which is comparable to gasoline. Most widely investigated liquid as fuel for DAFCs are:

- methanol (CH_3OH),
- ethanol ($\text{C}_2\text{H}_6\text{O}$),
- 1-propanol ($\text{C}_3\text{H}_8\text{O}$),
- 2-propanol ($\text{C}_3\text{H}_8\text{O}$),
- ethylene glycol ($\text{C}_2\text{H}_6\text{O}_2$) and
- glycerol ($\text{C}_3\text{H}_8\text{O}_3$).

Low molecular weight alcohols, e.g. methanol, ethanol and ethylene glycol are especially interesting for fuel cell application and have been investigated extensively. The full direct oxidation of these alcohols yields besides electricity and heat only water and CO_2 as by-products. Currently, most DAFCs use acidic polymer electrolytes, facilitating the removal of CO_2 , generated at the anode. However, due to kinetic constraints of the alcohol oxidation acidic DAFCs show rather low performance. By switching to an alkaline reaction media the kinetics of the alcohol oxidation can be enhanced significantly [1].

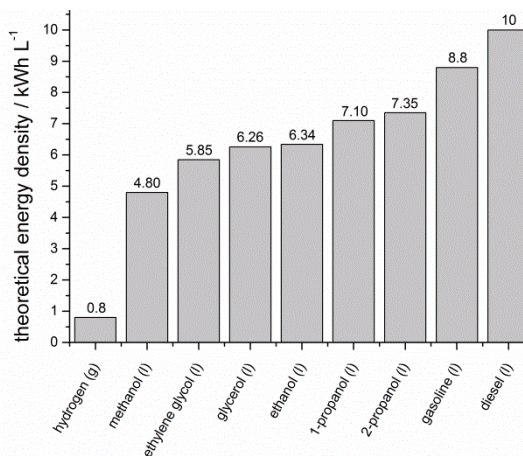
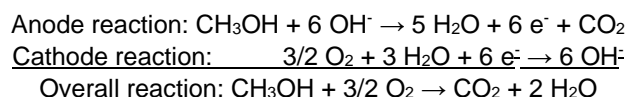


Fig.1. Energy density of various liquid fuels.

- *Direct methanol fuel cells*

Among the listed alcohols from above, so far only methanol has been commercialized as fuel for fuel cell application. Due to the absence of C-C bonds in its molecular structure, the oxidation of methanol is not hindered, resulting in comparably high DAFC performance. All other direct liquid fuel cell systems suffer from slow reaction kinetics at the anode, mainly due to complex C-C bond cleavage; necessary for complete oxidation.

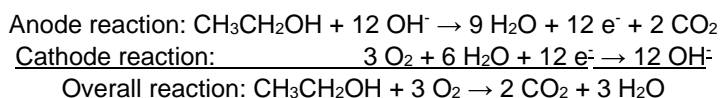
Platinum has the highest catalytic activity toward direct methanol oxidation in acidic and alkaline environment. Most available direct methanol fuel cell systems utilize acidic electrolytes, which were developed for PEFCs. Nevertheless, in alkaline media the activity of platinum toward methanol oxidation is increased due to two factors: the lack of specifically-adsorbing spectator ions in alkaline solutions and the high coverage of the platinum surface by hydroxide ions at low potentials, which is required for methanol oxidation [1].



- *Direct ethanol fuel cells*

The usage of methanol as fuel is subject to controversies, as methanol and its reaction intermediates (i.e. formaldehyde and formic acid) are highly toxic and the production of methanol from bio-based resources is rather complex. In this regard, the direct ethanol fuel cell can be seen as the advancement of the direct methanol fuel cell. In contrast to methanol, ethanol is already commercialized as fuel in several countries for conventional combustion engines, e.g. in Brazil or in the USA. Ethanol possesses high acceptance as fuel as it is non-toxic and typically produced from biomass, such as sugar cane, corn, and straw.

In its design, the direct ethanol fuel cell resembles the direct methanol fuel cell. Typically, conventional acidic polymers are used as electrolyte and platinum as electrocatalyst. In alkaline media, however palladium is the most active catalyst toward ethanol oxidation. Furthermore, the reaction kinetics are enhanced in alkaline environment, thus strong research interest has risen regarding the development of alkaline anion exchange membranes that possess high tolerance toward ethanol [1].

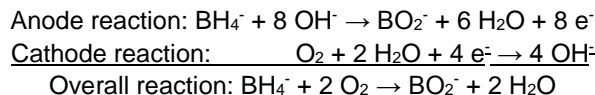


DIRECT BOROHYDRIDE FUEL CELLS

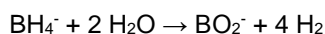
Apart from alcohols as liquid source of energy for fuel cells, solutions containing the borohydride anion BH_4^- (e.g. aqueous solutions of sodium borohydride NaBH_4) are of great interest. Sodium borohydride is a white crystalline solid with an energy density of 9.3 Wh g^{-1} , exhibits high solubility in water (55 g in 100 g of water) and a long-term half-life stability of 426 days in alkaline solutions at a pH value of 14.

The direct borohydride fuel cell converts the chemical energy of the BH_4^- anion into electrical energy. The complete oxidation of NaBH_4 is achievable with various

electrocatalysts, such as Pt, Au, Pd and Ru, at a theoretical potential of -1.24 V vs. SHE, resulting in the release of 8 electrons per molecule of BH_4^- [2].



One of the biggest challenges to overcome in the development of DBFCs is the major side reaction of the borohydride oxidation reaction, namely the borohydride hydrolysis reaction, as given below.



The borohydride hydrolysis reaction results in a reduced coulombic efficiency and can lead to mechanical stress inside the electrode due to hydrogen evolution. Besides the pH of the borohydride solution, the employed catalyst has a major influence on reaction pathway. In general, electrocatalysts can be divided into hydrolyzing and non-hydrolyzing materials, depending on their tendency toward hydrogen adsorption. For example platinum and palladium belong to the group of hydrolyzing catalysts [3].

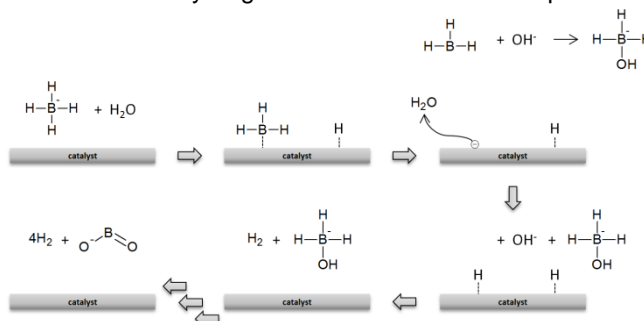


Fig.2. Proposed mechanism of catalytic borohydride hydrolysis.

- *DBFC approaches*

DBFCs can generally be divided into membrane based and non-membrane based systems.

Membrane based approaches allow the usage of anion as well as cation exchange membranes. However, the usage of cation exchange membranes is associated with drawbacks, such as the excessive need of hydroxide at the anode (at least eight equivalents to borohydride), the drop of pH in the fuel during operation and the formation of sodium hydroxide at the cathode. In contrast, anion exchange membranes do not show any of these disadvantages.

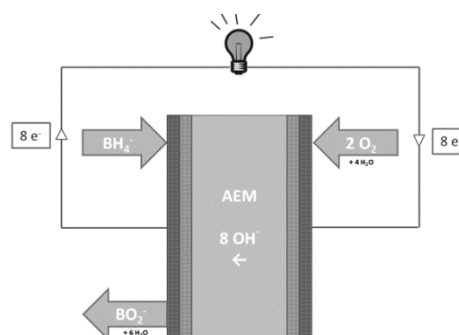


Fig.3. Anion exchange membrane (AEM) based DBFC.

Membrane-free DBFC systems offer several advantages, but require catalysts with very high selectivity. In so-called mixed reagent DBFCs, the electrodes and a separator are rolled similar to a conventional primary or secondary battery. Fuel, oxygen and electrolyte are supplied to the cell as a single solution.

A compromise of these approaches is the mixed electrolyte fuel cell, where oxygen is supplied separately. Since borohydride is stored in high alkaline aqueous media, the solution can act as electrolyte and fuel at the same time. Anode and cathode are sandwiched with a simple polyethylene separator, which is soaked with fuel. The fuel is pumped through the porous structure of the anode, also ensuring proper mass transport. The main advantage of this approach is that high selectivity is only required the cathode as no oxygen is present at the anode [4].

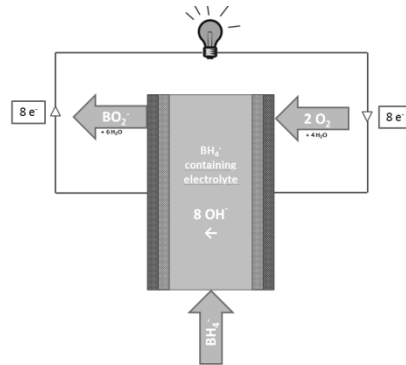


Fig.4. Non-membrane based mixed electrolyte

HIGH-TEMPERATURE PEFC

Typically polymer electrolyte fuel cells (PEFCs) operate in a temperature range below 90 °C. However, to overcome some of the limitations, which are related to the low temperature (LT-) operation of PEFCs, the development of high-temperature PEFCs has been pursued. The major disadvantages of LT-operation are the slow electrode kinetics, a rather low tolerance toward contamination of the fuel stream and a complicated water management and challenging heat management. Operating fuel cells at elevated temperatures (above 90 °C) can address these issues [5].

- *Improved reaction kinetics*

The temperature dependence of the exchange current densities, i.e. the reaction rates, for the hydrogen oxidation reaction and the oxygen reduction reaction in polymer electrolyte fuel cells follows the Arrhenius relationship

$$k = A e^{-E_a/(RT)}$$

Thus both exchange current densities will increase subsequently as the operating temperature increases [5].

- *Improved tolerance toward fuel contamination*

Usually the supplied gases, hydrogen and air, contain undesired impurities or contaminants. Contamination from the air stream varies with the environmental situation, e.g. city and country side. Whereas, contaminations in the hydrogen stream derives from the hydrogen production process itself.

Currently, hydrogen is generated by steam reforming of organic fuels, such as methane

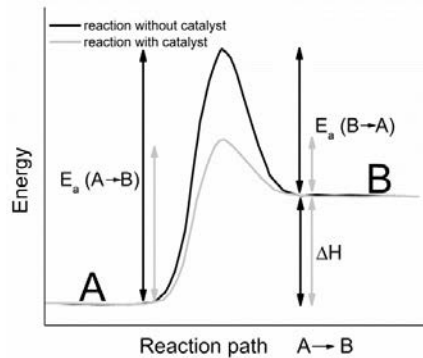


Fig.5. Activation energy of a reaction.

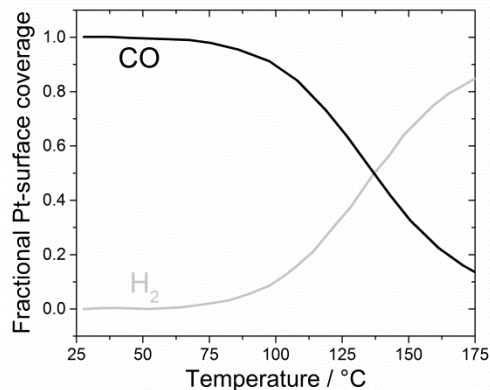


Fig.6. Adsorption of H₂ and CO on platinum as a function of the temperature. Adopted from [5].

(natural gas). Typically, the resulting hydrogen-rich gas contains 40-70% H₂, 10-25% CO₂, 1-5% CO and small quantities of inert gases, water vapor and sulfur compounds. Among the listed impurities, CO is the most critical with respect to catalyst activity. Even trace amounts of CO as low as 10ppm can lead to a significant loss in cell performance at LT-operation due to deactivation of active Pt catalyst sites for hydrogen oxidation. CO adsorption at platinum surfaces is favored at low temperatures, thus increasing the operation temperature of the fuel cell reduces the strength of CO adsorption, resulting in a higher tolerance towards contamination [5].

- *Simplified water and heat management*

Water management affects the overall power density and efficiency of LT-PEFC systems and therefore its technical design is of tremendous importance in order to maintain high proton conductivity. Typically, complex systems humidify the anode and cathode feed gases to ensure high water content inside the PEFC electrolytes. Nevertheless, too much water can lead to flooding, thus occupying the porous structure of the electrodes or blocking the gas transport channels of the flow fields [5,6].

In HT-PEFCs usually phosphoric acid doped polybenzimidazole (PBI) are employed as electrolyte instead of perfluorosulfonic acid polymers, like Nafion. Phosphoric acid doped PBI operates without any humidification and at temperatures in-between 150-200 °C. At such temperatures the design of a PEFC can be significantly simplified. Humidification of the electrolyte is not needed and flooding issues are less pronounced due to generation of gaseous product water. Furthermore, due to the absence of liquid water, less mass-transport limitation occurs in the catalyst and gas diffusion layers of the electrodes, meaning the flow field design can be simplified (e.g. into parallel channels). All in all, the high temperature operation of a PEFC enables a completely simplified water management. [5,6]

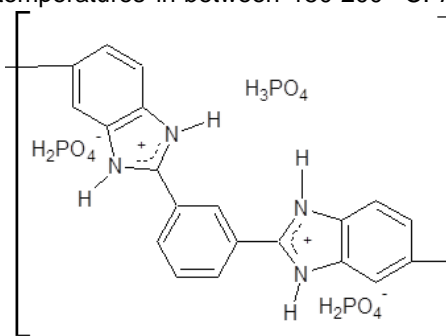


Fig.7. Structure of phosphoric acid-doped polybenzimidazole.

Additionally, the heat management in an HT-PEFC can also be simplified in comparison to a LT-PEFC. Due to the exothermic reaction of hydrogen and oxygen a fuel cell produces large amounts of heat during operation. This heat needs to be removed in order to keep the cell temperature at a reasonable value and maintain good performance and high efficiency. At low temperatures this is achieved by using water-, air- or oil-based cooling systems. At elevated temperatures excess heat can be removed much faster, due to the higher difference between environmental temperature and operating temperature. Therefore, an HT-PEFC cooling system can be reduced 3-4 times in size compared to LT-operation, increasing the overall mass-specific and volume-specific power density of the fuel cell system. Furthermore, the excess heat can be utilized, thus increasing the overall efficiency of the PEMFC system. [5-7].

ALKALINE FUEL CELLS

Alkaline fuel cells (AFCs) have a long history, starting in the 1950s with NASA's space program Gemini. In the 1960s this technology was also chosen to power the spacecraft for the Apollo missions to moon. Despite many spectacular milestones, including nine flights

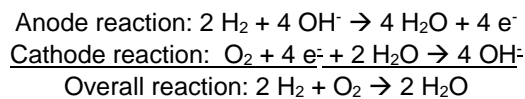
to the moon and three Skylab missions, the AFC technology was overtaken in the mid-1980 and 1990s due to the rise of solid acidic electrolytes, which resulted in more compact, lighter and more robust fuel cell systems, namely the PEFC [8].

The ongoing commercialization of fuel cells is taking place in the international well established field of acidic PEFCs, however new developments in the field of AFCs, like the demonstration of stable anion exchange membranes (AEMs), might soon bring Pt-free alkaline cells into an advantageous position. The alkaline environment enables the use of a broad range of less noble and certainly more cost-saving materials than platinum, which is state-of-the-art in acidic cells.



Fig.8. AFC powered Austin A40 hybrid city car of Prof. K. Kordesch [9]

The electrochemical half-cell reactions of H₂/O₂ alkaline fuel cells are as follows:



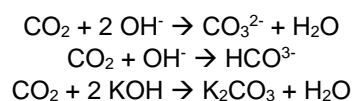
Typically, in AFCs an aqueous potassium hydroxide solution is used as electrolyte. Hydroxide anions (OH⁻) are formed at the cathode from oxygen and water, consuming 4 electrons per molecule of oxygen. The hydroxide ions migrate from the cathode to anode of the fuel cell and are there converted to water, consuming hydrogen and releasing 2 electrons per molecule of hydrogen. The electrons flow through the external current and are consumed in the cathode half-cell reaction [8].

- *Advantages of AFCs*

Due to the alkaline environment, advantages over acidic fuel cells arise. Firstly, the oxygen reduction reaction kinetics is enhanced as result of a simpler reaction mechanism. Secondly, many metals are thermodynamically stable in at the high pH of the electrolyte, thus other than platinum group metals, such as nickel, silver and manganese oxide, may be used as catalyst. Additionally, humidification of the reactant gases is not necessary for AFCs, thus reducing balance of plant utilities [8].

- *Disadvantages*

One of the major challenges associated with AFCs is significant sensitivity of alkaline electrolytes toward carbonation. Since air contains approx. 400ppm of carbon dioxide, carbonates can be formed when alkaline fuel cells are fed with ambient air, leading to serious cell degradation effects. The chemical reactions are given below:



The formed carbonates can block the porous structure of the electrodes, resulting in mass transport losses and loss of electrolyte in the catalyst layer. Furthermore, the precipitates can eventually mechanically separate the active layers from the electrodes [8]. In order to circumvent the precipitation of carbonates in the electrolyte and the electrodes, AFCs need to be supplied either with pure oxygen on the cathode or with pre-treated air from carbon dioxide removal or scrubbing.

Another disadvantage is that AFCs typically utilize liquid electrolytes, resulting in rather low mass-specific and volume-specific power densities of the fuel cell system [8].

- *Recent progress in AFC technology*

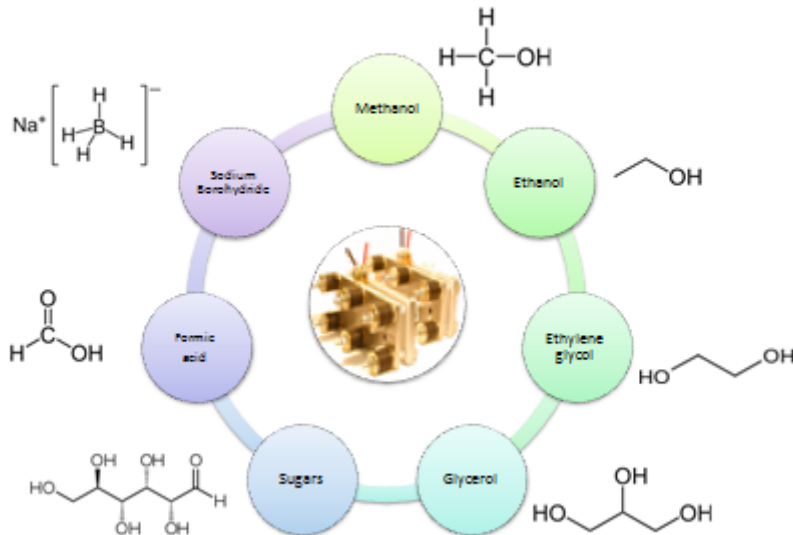
In recent years alkaline fuel cells regained ever more interest on an international level and significant progress could be achieved in the drawback areas mentioned above, such as solid alkaline electrolyte membranes. Based on comparable efforts in HT-PEFCs development, polybenzimidazole doped with potassium hydroxide were among the investigated membrane material for AFC application. However, carbonation cannot be resolved with this kind of heterogeneous polymer membranes. Today, research is driven by developing homogeneous polymer electrolytes with covalently bound positively charged groups. These polymers are theoretically immune to carbonate precipitation as mobile cations within the electrolyte are eliminated.

The advantages of having a membrane instead of liquid electrolytes are high reliability against reactant gas leaks, and the fact that membranes can be applied much thinner than liquid electrolytes, thus allow the design of very compact fuel cell stacks, which operate independent of the cell orientation and independent of acceleration forces that might be present if the stack is, for example, operated in vehicles [8]. Furthermore, traditional bipolar stack designs from PEFCs can be adopted, reducing development costs.

REFERENCES

- [1] E. Antolini, E.R. Gonzalez, *J. Power Sources*. **195** (2010), 3431.
- [2] C. Grimmer, R. Zacharias, M. Grandi, B. Cermenek, A. Schenk, S. Weinberger, F.A. Mautner, B. Bitschnau, V. Hacker, *J. Phys. Chem. C*. **119** (2015), 23839.
- [3] C. Grimmer, M. Grandi, R. Zacharias, B. Cermenek, H. Weber, C. Morais, T.W. Napporn, S. Weinberger, A. Schenk, V. Hacker, *Appl. Catal. B Environ.* **180** (2016), 614.
- [4] C. Grimmer, Energy and hydrogen storage in borohydride based ionic liquids, Graz University of Technology, 2016.
- [5] J. Zhang, H. Zhang, J. Wu, J. Zhang, High-Temperature PEM Fuel Cells, in: *Pem Fuel Cell Test. Diagnosis*, Elsevier B.V., Amsterdam, 2013: pp. 243.
- [6] J. Zhang, Z. Xie, J. Zhang, Y. Tang, C. Song, T. Navessin, Z. Shi, D. Song, H. Wang, D.P. Wilkinson, Z.-S. Liu, S. Holdcroft, *J. Power Sources*. **160** (2006), 872.
- [7] J. Jensen, Q. Li, C. Pan, A. Vestbo, K. Mortensen, H. Nybopetersen, C. Lausorensen, T. Nedergaardclausen, J. Schramm, N. Bjerrum, *Int. J. Hydrogen Energy*. **32** (2007), 1567.
- [8] V. Hacker, A. Schenk, S.D. Fraser, K. Kordesch, Cells and Stacks, in: J. Reedijk (Ed.), *Elsevier Ref. Modul. Chem. Mol. Sci. Chem. Eng.*, Elsevier, Waltham, MA, 2015.
- [9] K. Kordesch, J. Gsellmann, M. Cifrain, S. Voss, V. Hacker, R.R. Aronson, C. Fabjan, T. Hejze, J. Daniel-Ivad, *J. Power Sources*. **80** (1999), 190.

Direct Fuel Cells – Different Fuels

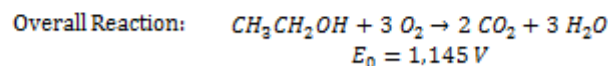
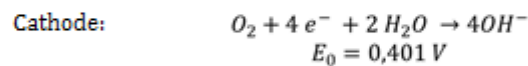
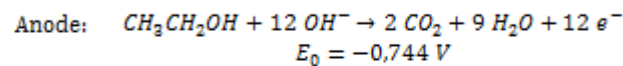
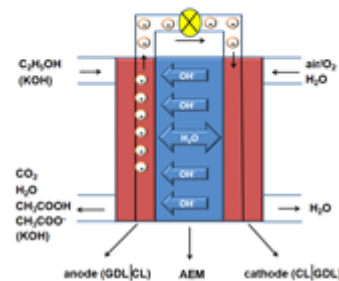


1

TU Graz | Institute of Chemical Engineering and Environmental Technology

Alkaline Direct Ethanol Fuel Cell

- Alkaline environment improves the ethanol oxidation reaction kinetics
- Direction change of the osmotic drag reduces cross over
- Non-noble metals can be used as catalyst

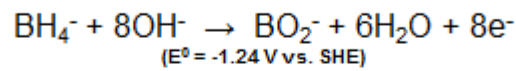


2

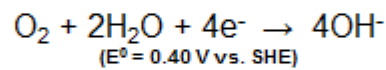
TU Graz | Institute of Chemical Engineering and Environmental Technology

Direct Borohydride Fuel Cell

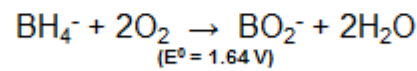
- Anode reaction



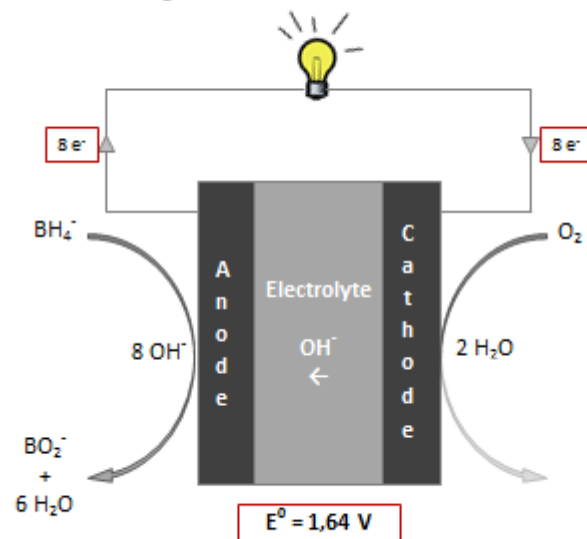
- Cathode reaction



- Overall

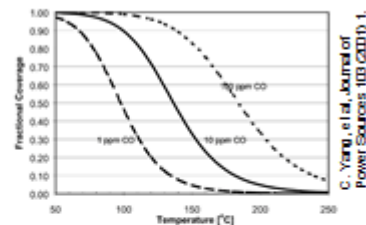


Direct Borohydride Fuel Cell

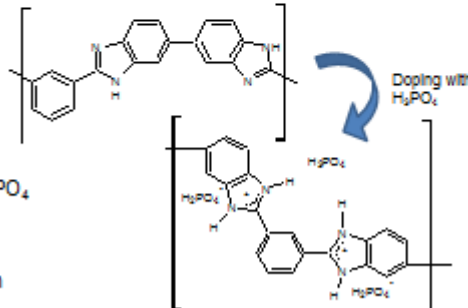


High temperature PEFC

- **Operating temperature:**
 - 150 - 200 °C
- **Advantages HT:**
 - Higher CO tolerance
 - Faster kinetics
 - Simpler cooling of stack
 - Easier water management
- **Disadvantages HT:**
 - Very corrosive
 - Dilution by product water
 - Bipolar plates of graphite
- **Electrolyte**
 - Polybenzimidazole doped with H_3PO_4
 - Acid base interaction
 - Independent of humidification
 - Conductivity comparable to Nafion



C. Yang, et al., Journal of Power Sources 163 (2001) 1.

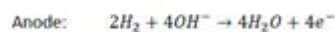
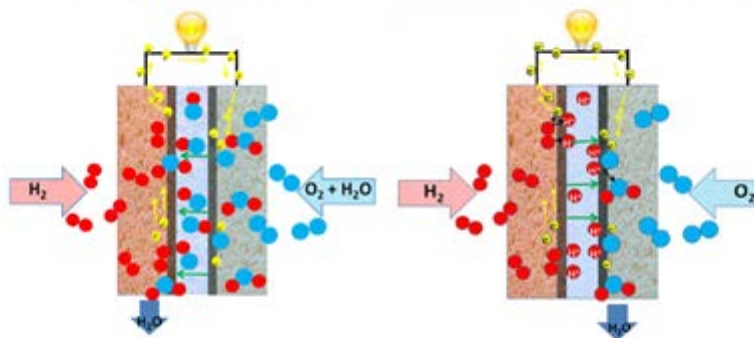


5

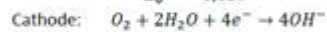
TU Graz | Institute of Chemical Engineering and Environmental Technology

CEET

Alkaline fuel cells vs. Acidic fuel cells

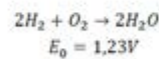


$$E_0 = -0,83V$$



$$E_0 = 0,4V$$

General:



$$E_0 = 0V$$



$$E_0 = 1,23V$$

6

TU Graz | Institute of Chemical Engineering and Environmental Technology

CEET

Operation conditions

Acidic Fuel Cell

- Temperature: up to 80°C
- Ionic species: H⁺
- Electrolyte: typically polymer electrolyte membrane
- Electrode material: almost always Pt

Alkaline Fuel Cell

- Temperature: up to 80°C
- Ionic species: OH⁻
- Electrolyte: typically liquid, others possible
- Electrode material: many possible, usually Ni

Kordesch's Austin A-40

- 1960
- H₂/air fuel cell and lead acid batteries hybrid
- Drove it three years on public roads
- CO₂ scrubber filled with 10 kg of soda lime
- No gas or electrolyte in the fuel cell during shut down prolongs the lifetime
- Six hydrogen bottles on the roof
- About 300 km range
- 2 min refilling time



3 Lecturers

Prof. Takuto Araki	Yokohama National University, Japan taraki@ynu.ac.jp
Prof. Angelo Basile	University of Calabria, Italy a.basile@itm.cnr.it
Prof. Bernd Eichberger	Graz University of Technology, Austria bernd.eichberger@tugraz.at
Prof. Bernhard Gollas	Graz University of Technology, Austria bernhard.gollas@tugraz.at
Prof. Viktor Hacker	Graz University of Technology, Austria viktor.hacker@tugraz.at
Prof. Yoshiyuki Kuroda	Yokohama National University, Japan kuroda-yoshiyuki-ph@ynu.ac.jp
Prof. Boniface Kokoh	Université de Poitiers, France boniface.kokoh@univ-poitiers.fr
Prof. Shigenori Mitsushima	Yokohama National University, Japan mitsushi@ynu.ac.jp
Dr. Têko W. Napporn	Université de Poitiers, France teko.napporn@univ-poitiers.fr
Prof. Ken-ichiro Ota	Yokohama National University, Japan ken-ota@ynu.ac.jp
Dr. Uwe Reimer	Jülich Research Centre, Germany u.reimer@fz-juelich.de
Dr. Cordellia Sita	University of the Western Cape, South Africa csita@uwc.ac.za
Gaetano Squadrito	CNR-ITAE, Italy gaetano.squadrito@itae.cnr.it

Verlag der Technischen Universität Graz

www.ub.tugraz.at/Verlag
